INFORMATION TO USERS

This material was produced from a microfilm copy of the original document. While the most advanced technological means to photograph and reproduce this document have been used, the quality is heavily dependent upon the quality of the original submitted.

The following explanation of techniques is provided to help you understand markings or patterns which may appear on this reproduction.

1. The sign or "target" for pages apparently lacking from the document photographed is "Missing Page(s)". If it was possible to obtain the missing page(s) or section, they are spliced into the film along with adjacent pages. This may have necessitated cutting thru an image and duplicating adjacent pages to insure you complete continuity.

2. When an image on the film is obliterated with a large round black mark, it is an indication that the photographer suspected that the copy may have moved during exposure and thus cause a blurred image. You will find a good image of the page in the adjacent frame.

3. When a map, drawing or chart, etc., was part of the material being photographed the photographer followed a definite method in "sectioning" the material. It is customary to begin photoing at the upper left hand corner of a large sheet and to continue photoing from left to right in equal sections with a small overlap. If necessary, sectioning is continued again — beginning below the first row and continuing on until complete.

4. The majority of users indicate that the textual content is of greatest value, however, a somewhat higher quality reproduction could be made from "photographs" if essential to the understanding of the dissertation. Silver prints of "photographs" may be ordered at additional charge by writing the Order Department, giving the catalog number, title, author and specific pages you wish reproduced.

5. PLEASE NOTE: Some pages may have indistinct print. Filmed as received.

Xerox University Microfilms
300 North Zeeb Road
Ann Arbor, Michigan 48106

76-27,432

ALFERNESS, Rodney Clifford, 1946-
OPTICAL PROPAGATION IN HOLOGRAPHIC GRATINGS.

The University of Michigan, Ph.D., 1976
Physics, optics

Xerox University Microfilms, Ann Arbor, Michigan 48106

OPTICAL PROPAGATION IN HOLOGRAPHIC GRATINGS

by

Rodney Clifford Alferness

A dissertation submitted in partial fulfillment
of the requirements for the degree of
Doctor of Philosophy
(Physics)
in The University of Michigan
1976

Doctoral Committee:

Professor Emmett N. Leith, Co-Chairman
Professor John F. Ward, Co-Chairman
Professor Donald I. Meyer
Professor C. Wilbur Peters
Associate Professor David N. Williams

DEDICATION

To my Wife

Deanna

ACKNOWLEDGEMENTS

It is with great pleasure that I express my gratitude to Professor Leith for his support, advice and encouragement during my thesis research. As both a teacher and researcher, his enthusiasm, keen physical intuition and vast knowledge set an example that few equal.

I thank the other members of my committee for giving of their valuable time. In particular, a special word of thanks to my Co-Chairman, Professor Ward. I am grateful to Professor Juris Upatnieks who has always given freely of his time and considerable knowledge of coherent optics.

Collaboration with colleague Steve Case on some of the experimental work has been very helpful. I thank Bruce Hansche for proofreading several manuscripts and for numerous useful discussions. I have also benefitted from conversations from B.J. Chang and W. Wang. I thank Dolores Clarke for her long hours spent typing the thesis.

The continued patience and understanding of my wife, Deanna, has been invaluable in my completion of this work.

The generous support of the National Science Foundation, Grant GK-42361, is gratefully acknowledged.

TABLE OF CONTENTS

	Page
DEDICATION	ii
ACKNOWLEDGEMENTS	iii
LIST OF ILLUSTRATIONS	vi
CHAPTER	
1. INTRODUCTION	1
2. THE THEORY OF THIN-GRATING DECOMPOSITION	6
2.1 Review of Prior Work	6
2.2 Thin-Grating Decomposition	8
2.2.1 Single Phase Sinusoidal Grating	9
2.2.2 Inclusion of Film Nonlinearities	19
2.2.3 Slanted Fringes	21
2.2.4 Differential Spatial Dispersion	22
2.3 Transition Between Thin and Thick Regimes	25
2.4 Analytical Results for a Thick, Sinusoidal Grating	29
2.5 Summary	35
3. SECOND-ORDER READOUT OF A SINGLE, THICK HOLOGRAPHIC GRATING	37
3.1 Readout at the Second-Order Bragg Angle	41
3.1.1 Pure Sinusoidal Grating, $n_2 = 0$	44
3.1.2 The General Case, $n_2 \neq 0$	48
3.1.3 Simplified Results for γ_1/ξ, γ_2/ξ, $<< 1$	52
3.2 Readout Angles Near the Second Bragg Angle	54
3.3 Transition Between Thin and Thick Regimes at the Second Bragg Angle	57
3.4 Experimental Verification	59
3.4.1 Readout at the Second Bragg Angle	61
3.4.2 Determination of the Film Nonlinearity	67
3.4.3 Angular Selectivity	67
3.5 Extension of Analytical Results for First-Order Readout	67
3.6 Summary and Conclusions	71

CHAPTER Page

4. PROPAGATION IN STRONGLY-COUPLED MULTIPLE THICK GRATINGS 73

4.1 Background 74
4.2 Incoherent Superposition Construction I 75

4.2.1 Direct Coupling 79
4.2.2 Cross Coupling 91
4.2.3 The Two Extremes of Double Diffraction 100

4.3 Incoherent Superposition Construction II 101

4.3.1 Direct Coupling 106
4.3.2 Cross Coupling 109

4.4 Coherent Superposition Construction 109
4.5 Experiments 117

4.5.1 Incoherent Superposition 118
4.5.2 Coherent Superposition 128

4.6 Summary and Conclusions 132

5. PROPAGATION IN NONUNIFORMLY MODULATED THICK GRATINGS 135

5.1 Background 135
5.2 Application of TGD to Nonuniform Gratings . . . 137

5.2.1 Fourier Transform Relation for Low DE 138
5.2.2 Sinc Function Modulation Profile 139
5.2.3 Fringe Shift 144

5.3 Construction of Gratings with Required Index Profiles 149

5.3.1 Grating Interferometer 149
5.3.2 Experiments 153

5.4 Summary and Conclusions 156

6. SUMMARY AND CONCLUSIONS 158

APPENDIX 161

REFERENCES 169

LIST OF ILLUSTRATIONS

Figure		Page
2-1a.	Construction of the holographic grating	10
2-1b.	Holographic grating	11
2-2.	Thin-grating decomposition	14
2-3.	Grating readout	14
2-4.	Differential dispersion versus readout spatial frequency	24
2-5.	Diffraction efficiency versus readout spatial frequency	26
2-6.	Transition between thin and thick regimes	28
2-7.	Readout of thick grating	32
2-8.	First order DE versus ξ	32
3-1.	Differential dispersion versus readout spatial frequency	38
3-2.	Readout at second Bragg angle	38
3-3.	Second-order DE versus fundamental grating strength, ($n_2 = 0$)	47
3-4.	First-order DE versus fundamental grating strength, ($n_2 = 0$)	47
3-5.	Second-order DE versus harmonic grating strength, ($\gamma_1 = 2.5$)	51
3-6.	Second-order DE versus negative harmonic grating strength, ($\gamma_1 = 2.5$)	51
3-7.	Angular selectivity for second-order readout, f = 850 1/mm	56
3-8.	Angular selectivity for second-order readout, f = 1000 1/mm	56
3-9.	Transition between thin and thick regimes for second-order readout	58
3-10.	Second-order DE: comparison of experiment and theory	63

Figure Page

3-11. First-order DE: comparison of experiment and theory 64

3-12. Experimental second-order DE versus determined n_1 66

3-13. Nonlinear film response of dichromated gelatin . . 68

3-14. Angular selectivity for second order readout: comparison of experiment and theory 68

4-1. Geometry for incoherent superposition I 76

4-2. Direct-coupling readout 80

4-3. Differential dispersion for direct-coupling readout 80

4-4. Angular selectivity for direct-coupling readout . . 85

4-5. Decoupling with offset: direct-coupling mode . . . 87

4-6. Modulation dependence of decoupling 90

4-7. Cross-coupling readout 93

4-8. Differential dispersion for cross-coupling readout 93

4-9. DE of first and cross-coupled orders 97

4-10. Angular selectivity of cross-coupled order 97

4-11. Decoupling with offset: cross-coupling mode . . . 99

4-12. Geometry for incoherent superposition II 102

4-13. Readout modes 103

4-14. Differential dispersion for type II geometry 103

4-15. Angular selectivity for direct-coupling readout . . 107

4-16. Decoupling with offset: direct-coupling mode . . . 108

4-17. Angular selectivity for cross-coupling readout . . 110

4-18. Decoupling with offset: cross-coupling mode . . . 111

4-19. Coherent superposition 113

4-20. Readout modes for coherently added gratings . . . 113

4-21. Angular selectivity for coherently added gratings 116

4-22. Three-beam experimental arrangement 119

Figure Page

4-23. Experimental DE for readout at noncommon BA, $\Delta\phi = 0$ 123

4-24. Comparison of experimental and theoretical angular selectivity for direct-coupling readout: variable $\Delta\phi$ 125

4-25. Comparison of experimental and theoretical angular selectivity for cross-coupling readout: variable $\Delta\phi$ 126

4-26. Experimental angular selectivity for high modulation, $n_2 \cong .017$, $\Delta\phi \cong 0$ 129

4-27. Experimental angular selectivity for coherent superposition, $n_1 \cong n_2 \cong n_3 \cong .01$ 131

5-1. Sinc function 141

5-2. Angular response for sinc function index modulation profile 143

5-3. Fringe shift 145

5-4. Angular response for π fringe shift at center of grating 145

5-5. Angular response for π fringe shift 148

5-6. Grating interferometer 150

5-7. Fringe visibility versus z', W = 1 mm, f = 330 1/mm. 155

5-8. HWHM of fringe visibility curve 155

CHAPTER 1
INTRODUCTION

The revival of holography by Leith and Upatnieks (1-3) has generated a host of interesting new phenomenon in optics. In Leith-Upatnieks off-axis holography, the total scalar information of an arbitrary object waveform is encoded by interferring it with a known reference wave. The information is encoded as the amplitude and phase modulation of a basic periodic fringe structure - the spatial carrier. This interference pattern is recorded on a photo-sensitive emulsion. The developed photographic plate is a hologram, which, when illuminated by a wave identical to the reference, produces a diffracted wave identical in all respects to the original object waveform.

The simplest hologram, indeed so simple that many would not call it a hologram, is formed when both the object and reference waves are uniform plane waves. In this case, the recorded "hologram" is simply the basic grating which is a spatial sinusoidal variation with period determined by the angle between the incident waves and the recording wavelength. This thesis is a theoretical and experimental study of optical propagation in holographically constructed gratings.

The properties of holographic gratings are strongly dependent upon the recording material. Those recorded in silver-based films are characterized by a spatially varying absorptivity and are called amplitude or absorption gratings. Such gratings are very lossy. Gratings recorded in materials in which, after development, only the index of refraction varies, are called pure phase or dielectric gratings. Dichromated gelatin (4-6), photopolymers (7-9)

and lithium niobate (10) are examples. In addition, there are mixed gratings in which both the absorptivity and index of refraction vary periodically. These result from recording in a silver-based material and then using a bleaching process after normal development. Bleaching converts the silver (but only partially) into a transparent silver compound, thus transforming the spatial modulation from absorptivity to index of refraction (11). Because they are essentially lossless, pure phase materials offer the greatest advantage in light usage and they will be our primary concern.

The relative emulsion thickness is also an important grating parameter. Gratings can be roughly divided into three classes: thin, intermediate, and thick, based upon the ratio of their thickness to spatial period. Thin gratings are well understood. When recorded in phase materials, they generate multiple-diffracted orders whose intensity is essentially independent of the angle of the incident wave (12). Gratings of intermediate thickness are perhaps the most difficult to understand and the least studied. They have several strong orders and moderate angular dependence. Thick or volume gratings are very interesting because of their ability (when recorded in phase materials) to diffract all of the incident light into a single first-diffracted order (13). In addition, they demonstrate strong angular selectivity in that significant diffraction occurs only when the incident wave is near the Bragg angle. (The first-order Bragg angles are identical to the angles of the construction beams if the readout wavelength is equal to the construction wavelength.) Thick gratings will be our primary concern. But we will also examine the transition from the thin to thick regimes to gain a better understanding of gratings that are just marginally thick. Such gratings are important in applications where a high diffraction efficiency over a broad region of incident angles is desired.

To analyze optical propagation in holographic gratings theoretically, we have developed a new approximate theory known as the method of thin-grating decomposition (14). The method views intermediate and thick gratings as simply a system of many thin gratings. The well-known properties of thin gratings can then be used to quantitatively predict the effects of their thicker counterparts. The principle advantages of this method are its intuitive simplicity - it is based upon the concepts of the amplitude transmittance and transfer functions that are common to other areas of coherent optics and holography; its general applicability; and its ease of implementation.

A great deal of work has previously been done on wave propagation in thick holographic gratings and in other periodic structures. However, in this thesis, we use the method of thin grating decomposition to derive new and rather interesting results concerning second-order readout (incident wave near second Bragg angle) of thick gratings, the properties of strongly-coupled multiple gratings and the effects of nonuniform modulation upon tailoring the angular selectivity of thick gratings. We examine in some detail double diffraction phenomenon in thick holographic gratings. We perform a general three-wave analysis (in the Appendix) to derive closed-form solutions for the diffraction efficiencies of three strongly-coupled waves in a thick grating structure. These results are very broadly applicable. They are applied to second-order readout of single gratings and to extending the results of first-order readout. They are also used in the study of multiple gratings. The derived analytical results are verified by numerous experiments performed with gratings constructed holographically in dichromated gelatin film.

This thesis is organized by chapter as follows. Chapter 2 gives a brief review of past work on holographic gratings. The

method of thin-grating decomposition (TGD) is developed for a single phase grating. The concept of spatial dispersion is discussed and the thickness criterion is examined.

In Chapter 3, the method of TGD is used to derive algebraic expressions for the diffraction efficiency (DE) of the first and second orders of a thick grating for readout angles near the second Bragg angle. Experimental results that support the theory are presented. The importance of double diffraction is shown both theoretically and experimentally.

Chapter 4 is a comprehensive investigation of the properties of strongly-coupled multiple gratings recorded in the same thick emulsion. The basic coupling mechanisms are examined. Two types of incoherently superimposed double gratings as well as the three grating structure made by simultaneously interferring three plane waves are studied. The general expressions derived in the Appendix are applied to predict the DE for arbitrary degrees of coupling and readout angles. Again, experimental results are presented that are in good agreement with the theoretical results. The possibility of 100% cross coupling of energy between two gratings, which I predicted (14), is demonstrated experimentally (15).

In Chapter 5, propagation in thick gratings that have a nonuniform modulation in depth is studied with the aim of increasing the width and the uniformity of the angular response of such structures. Methods are described for making gratings with desired index profiles. Experimental results that demonstrate the latter are given. A general summary and suggestions for further research are given in Chapter 6.

In the Appendix, the general algebraic expressions for the diffraction efficiencies of three strongly coupled waves are derived.

The analysis is general so that the results can be used directly in Chapters 3 and 4.

CHAPTER 2
THE THEORY OF THIN-GRATING DECOMPOSITION

In this chapter we begin by giving a brief background of previous work done with holographic gratings recorded in thick materials. The theory of thin-grating decomposition (TGD) is developed. The important concept of spatial dispersion is then discussed and used to review and clarify the classification of gratings according to their effective thickness. We then use TGD to demonstrate the transition from the thin to thick regimes for readout at the first Bragg angle. Finally, for readout near the first Bragg angle of a thick grating, we show that the expression for first-order diffraction efficiency determined by TGD is equivalent to Kogelnik's coupled-wave solution of Maxwell's equations.

2.1 Review of Prior Work

The theory of optical propagation in thick holographic gratings has previously been studied by several people (13, 16-20). Leith et al. used the scalar Kirchhoff diffraction integral to calculate the relative intensity of the strong diffracted order (16). Although it was a first-order analysis, limited to cases where the readout wave is not severely depleted, the analysis did predict such properties as strong angular and wavelength dependence (selectivity) of the diffraction efficiency. That is, in thick gratings the diffraction efficiency (DE) decreases rapidly to zero for readout angles or wavelengths different from their construction values. They also presented experimental angular selectivity results. Further, they made use of the angular selectivity property to store multiple superimposed but independently reconstructible holograms on the same plate by using different reference angles - a technique known as Bragg-angle multiplexing. Using

very thick materials, Friesem recorded more than 100 holograms by this method (21).

Burckhardt developed the rigorous solution of Maxwell's equations for the pure-phase sinusoidal grating (17). The method is strictly numerical and requires using a digital computer to find the eigenvalues and eigenvectors of an infinite matrix. The rigorous electromagnetic boundary conditions are applied. In practice the matrix is truncated with negligible error introduced. He considered only first-order readout for gratings whose fringe planes are perpendicular to the plane of the emulsion. However, the theory includes the energy exchange amongst higher orders so that no assumption of strong Bragg suppression of higher orders is required. The method can thus be used for gratings of arbitrary thickness. Kaspar extended this method to include gratings with an arbitrary periodic variation of both refractive index and absorptivity (20). Again the method was limited to single gratings and only first-order readout was considered. Despite its rigor this approach has not found widespread usage amongst the holography community perhaps because it is not so easily implemented on a digital computer.

Kogelnik has used a coupled-wave analysis to obtain analytic expressions for the first-order diffraction efficiency for a pure sinusoidal grating (13). The analysis is quite comprehensive in that it includes both transmission and reflection holograms that are recorded in phase, absorption or mixed materials. However, his solution is restricted to readout angles near the first Bragg angle and is valid only for gratings sufficiently thick such that a single diffracted order is significant. Using results from the theory of acoustic gratings, he uses $Q = 2\pi f^2 \lambda D/n_o$ (the parameters will be defined below), as a thickness parameter. He assumes that gratings with $Q > 10$ satisfy the above thickness criterion and are covered by his theory. When valid, this is the most useful theory for first-order readout. His results predict the possibility of 100% diffraction into the first order.

Bergstein and Kermisch have derived similar results for pure phase gratings (18). They also noted that the assumption of a single significant diffracted order requires a low index modulation in addition to a large Q factor.

Propagation in holographic gratings closely parallels that in other periodic structures such as crystals (22, 23) and acoustic gratings (24). The application of the dynamic theory of x ray diffraction in crystals to holographic gratings has been discussed (21, 25). A perturbation method has been used to analyze thick, weakly modulated acoustic gratings (24). An extensive bibliography on acoustic gratings is given in Ref. 13. Compared to crystals or acoustic gratings, the holographic gratings we investigate in this thesis are typically much more strongly modulated and comparatively thin.

2.2 Thin-Grating Decomposition

The method of thin-grating decomposition is a new, intuitively physical method for analyzing optical propagation in holographic gratings of arbitrary thickness. The approach is particularly appealing to workers in holography because it uses only well-known thin grating theory and is based upon the same principles commonly used to analyze systems of discrete holographic gratings as, for example, the grating interferometer (26, 27). The approach is also well suited and was originally developed to treat structures comprised of several strongly coupled gratings (14, 15) which is described in Chapter 4. Indeed, the conceptual simplicity, general applicability and ease of implementation of this approach offer advantage over the theory given by Burckhardt (17) and Kaspar (20) for the single grating case. Despite its nonrigorous origin, we shall see that the method of TGD gives accurate results. Very general applicability can be obtained because all that need be specified are the properties of the thin grating slabs which may be phase, absorption or mixed. The effects of higher

diffracted orders are included so gratings of arbitrary thickness can be considered. Multiple fringe structures can be considered by allowing each thin grating to have several basic spatial frequencies. It is a scalar theory and thus is valid for polarization along the grating fringes (14).

2.2.1 Single Phase Sinusoidal Grating

For simplicity, we describe the method for a single, pure-phase sinusoidal grating. The extension to gratings with higher order harmonic refractive index components (that result in holographically produced gratings because of a nonlinear film response) is then straightforward and will be discussed.

The grating is constructed interferometrically as shown in Fig. 2-1. The film emulsion of thickness D is perpendicular to the z axis and is assumed to be of infinite extent in the x and y directions. (Of course, in practice this is never the case. Zech (28) has experimentally found that the condition W/D > 5, where W is the actual lateral extent, is sufficient for the above assumption to be valid.) We limit the analysis to one lateral dimension. Monochromatic plane waves R of amplitude a_1 incident at angle θ_1 (angles measured inside the emulsion relative to the z axis) and S of amplitude a_2 at θ_2 interfere to produce fringes throughout the volume of the emulsion (Fig. 2-1b). The two beams are derived from the same laser source (Fig. 2-1a) and are assumed to be completely coherent. The interference pattern recorded by the emulsion (an intensity detector) can be written as

$$I(x, z) = \left| a_1 \exp\left[i \frac{2\pi n_o}{\lambda_c} (\sin \theta_1 x + \cos \theta_1 z) \right] + a_2 \exp\left[i \frac{2\pi n_o}{\lambda_c} (\sin \theta_2 x + \cos \theta_2 z) \right] \right|^2 \qquad 2.1$$

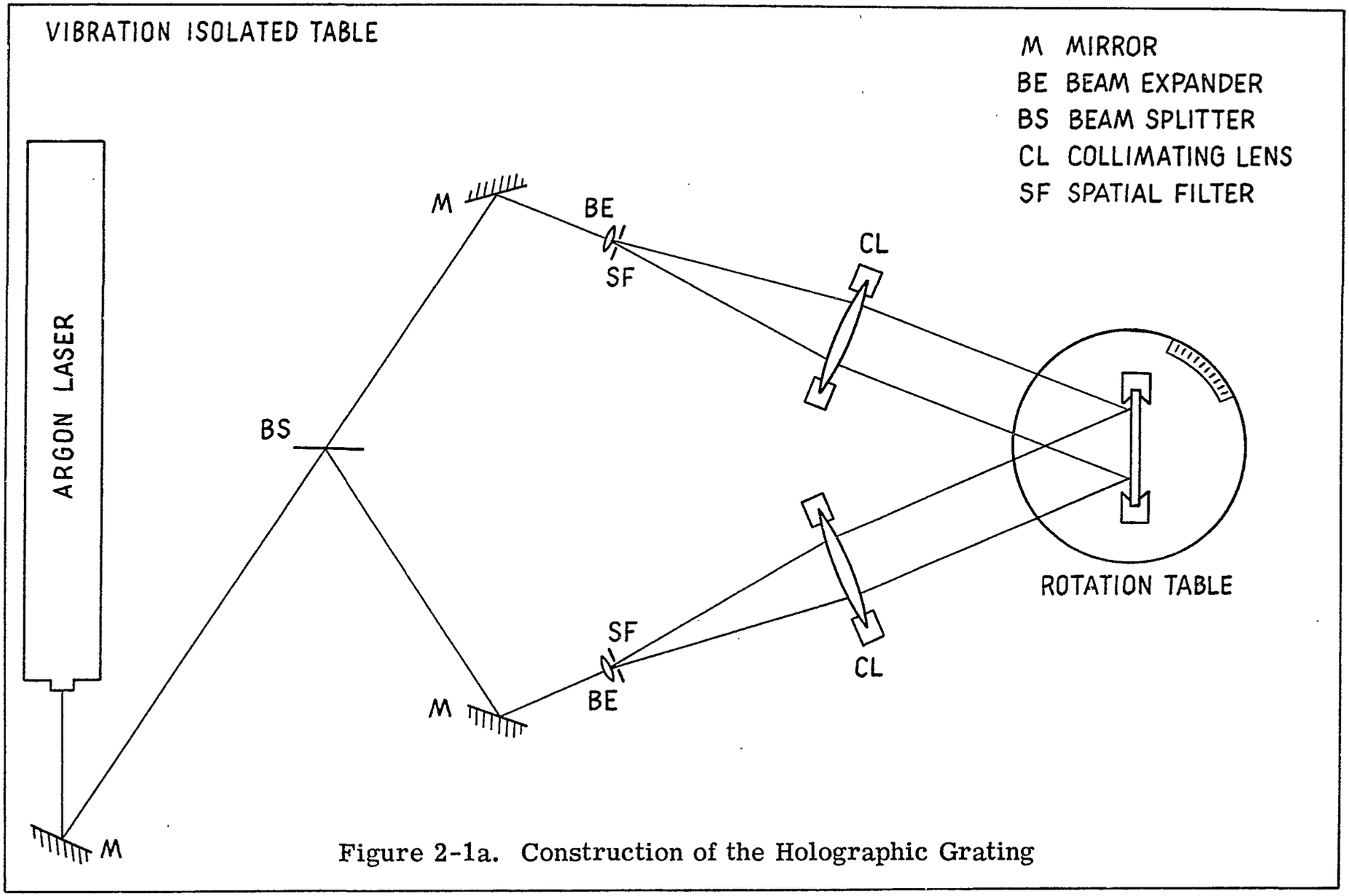


Figure 2-1a. Construction of the Holographic Grating

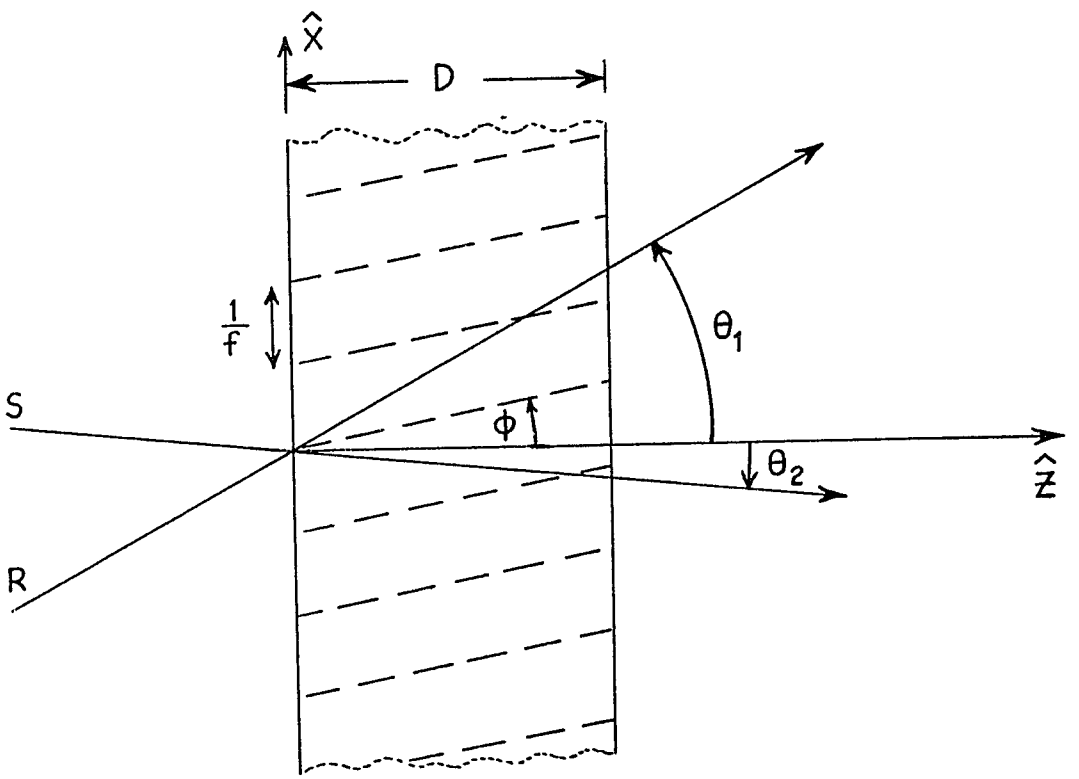


Figure 2-1b. Holographic Grating

where λ_c is the free space wavelength of the construction beams and n_o is the bulk index of the emulsion. (Because we consider monochromatic waves the common time dependence e^{iwt}, $w = 2\pi c/\lambda_c$ is unimportant and is suppressed.) The film responds to the total exposure, $E = I\tau$, where τ is the exposure time. Using a trigonometric identity, the exposure becomes

$$E(x, z) = E_o\left\{1 + r \cos [2\pi f(x - x_o(z))]\right\} \qquad 2.2$$

where $f = n_o/\lambda_c\,|(\sin \theta_1 - \sin \theta_2)|$

$x_o(z) = z \tan \phi$

$\phi = (\theta_1 + \theta_2)/2$ is the slant of the fringe planes

$E_o = \tau\left(a_1^2 + a_2^2\right)$ is the average exposure, and

$r = 2a_1a_2\Big/\left(a_1^2 + a_2^2\right)$ is the modulation.

The fringe planes bisect the angles of the two construction beams. For any plane z = constant, the fringes are sinusoidal with spatial frequency (inverse of spatial period) f. However, because of fringe slant (when the construction beam directions are not symmetric about the z axis), the fringes at z are laterally shifted by $x_o(z)$ relative to those at z = o. The exposed plate is then processed to convert the latent image of the interference pattern to a periodic variation in absorptivity or refractive index.

Here we consider pure-phase recording materials because of their capacity for high diffraction efficiency. We also assume for the moment that the film responds linearly to exposure, $\Delta n = KE$, where Δn is the exposure induced refractive index change. The refractive index can be written as

$$n(x, z) = n_o + n_1 \cos [2\pi f(x - x_o(z))], \qquad 2.3$$

where n_o is the constant average index, n_1 is the index modulation and typically $n_1 << n_o$.

We analyze the propagation of plane waves in the grating by mathematically decomposing the emulsion into a series of thin slabs of thickness Δz, (Fig. 2-2). The magnitude of Δz is assumed to be sufficiently small so that each slab acts simply as a thin grating. We will consider later the restriction on Δz for this to be the case. We also assume that the actual diffraction process takes place discretely at the planes $z = m\Delta z$, $m = 1, 2 \ldots$.

Before proceeding, we digress momentarily to discuss the concept of spatial frequency as used to describe plane waves because it is central to the method of TGD. An infinite plane wave of wavelength λ, propagating at an angle θ_i with respect to the z axis in a medium of average index n_o has a spatial frequency (x component) $f_i = n_o/\lambda \sin \theta_i$ (29). The inverse of f_i is the distance between constant phase planes measured along the x axis. At a z = constant plane the field can be written as $A_i(z)\, e^{i2\pi f_i x}$, where A_i is the total complex amplitude. The concept is useful because the spatial frequencies of an incident plane wave and a spatially modulated thin slab are additive as described by the thin grating equation $f_o = f_i + f$.

The effect of the m^{th} thin slab upon an incident plane wave of arbitrary spatial frequency f_i can be divided into two parts. First, the propagation of the wave over the slab thickness Δz. We assume this to be described by the propagator or transfer function of a material of uniform index n_o which is (30)

$$\exp\left(i\frac{2\pi n_o}{\lambda}\Delta z \cos\theta_i\right) = \exp\left(i\frac{2\pi n_o}{\lambda}\Delta z\left[1 - \left(\frac{\lambda f_i}{n_o}\right)^2\right]^{1/2}\right). \qquad 2.4$$

Second, the separation of the incident wave into various orders which is determined by the amplitude transmittance function at $z = m\Delta z$.

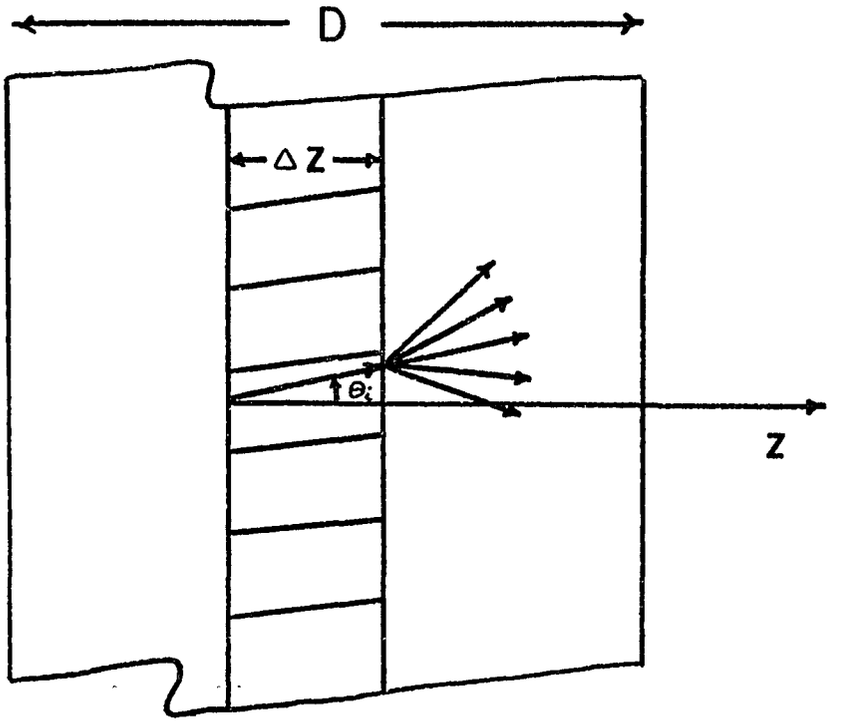


Figure 2-2. Thin-Grating Decomposition

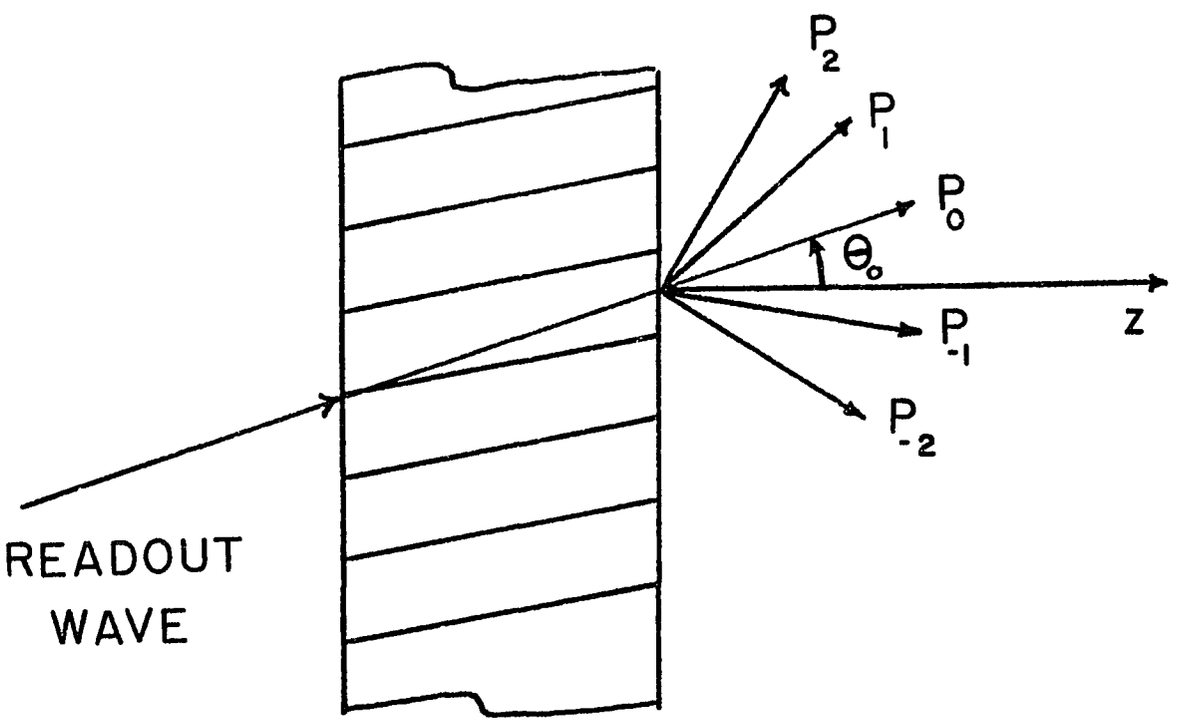


Figure 2-3. Grating Readout

For the single, pure phase sinusoidal grating the amplitude transmittance function can be found as follows. The spatial phase shift introduced by the slab upon an incident plane wave at angle θ_i is

$$\frac{2\pi n(x)\Delta z}{\lambda \cos \theta_i} \qquad 2.5$$

The amplitude transmittance of the m^{th} slab is thus

$$T_A(x, m) = \exp\left\{i\frac{2\pi\Delta z}{\lambda \cos \theta_i}[n_o + n_1 \cos 2\pi f(x - x_o(m))]\right\} \qquad 2.6$$

where z has been replaced by the slab index m, $z = m\Delta z$. Using a familiar expansion, this can be written as

$$T_A(x, m) = \exp(i2\pi n_o \Delta z/\lambda \cos \theta_i)$$

$$\times \sum_{q=-\infty}^{\infty} (i)^q J_q\left(\frac{2\pi n_1 \Delta z}{\lambda \cos \theta_i}\right) \exp\left\{i2\pi qf[x - x_o(m)]\right\}, \qquad 2.7$$

where J_q is the q^{th} order Bessel function. The m^{th} thin grating can therefore be represented by an infinite superposition of amplitude gratings of spatial frequency qf with diffraction amplitudes given by the Bessel function of order q. The exponential outside the summation in Eq. 2.7 represents an unimportant common phase factor and will be dropped. Note that the diffraction amplitudes depend upon the thickness of the thin slab and the wavelength and direction of the incident plane wave as well as upon the index modulation n_1. Also the q^{th} frequency component is shifted in phase by $-2\pi q$ fm $\Delta z \tan \phi$ because of fringe slant.

The effect of the m^{th} slab upon an incident plane wave of spatial frequency f_i and total (complex) amplitude A_i is the product of the input amplitude, the propagator function and the amplitude transmittance. Therefore, the field at $z = m\Delta z$ (out of the m^{th} thin slab) due to a single plane wave incident upon the slab is

$$A(x, m\Delta z) = A_i \exp\left\{ i\frac{2\pi n_o \Delta z}{\lambda}\left[1 - \left(\frac{\lambda f_i}{n_o}\right)^2\right]^{1/2}\right\}$$

$$\times \sum_{q=-\infty}^{\infty} (i)^q J_q\left(\frac{2\pi n_1 \Delta z}{\lambda \cos \theta_i}\right) \exp\left[-i2\pi q f x_o(m)\right]$$

$$\times \exp\left[i2\pi(f_i + qf)x\right]. \qquad 2.8$$

The output field contains plane waves of spatial frequencies $f_{out} = f_i + qf$. These plane waves propagate at angles $\theta_q = \sin^{-1}(\lambda f_q / n_o)$.

Suppose that we illuminate the thick grating at $z = 0$ with a plane wave of spatial frequency f_o and amplitude A_o. We write the total amplitudes of each of the possible plane waves that exit from the m^{th} thin slab by

$$\underset{\sim}{A}(m) = \begin{bmatrix} \cdot \\ \cdot \\ \cdot \\ A_1 \\ A_o \\ A_{-1} \\ \cdot \\ \cdot \\ \cdot \end{bmatrix}, \qquad 2.9$$

where A_q is the total amplitude of the plane wave of spatial frequency f_q. Because Eq. 2.8 is valid for an arbitrary incident plane wave, we can write

$$\underset{\sim}{A}(m) = {}_m\underset{\sim}{H}\underset{\sim}{A}(m - 1) \qquad 2.10$$

where the matrix of coupling coefficients ${}_mH_{kj}$, determined from Eq. 2.8 describe the amplitude and phase shift effected by the m^{th} thin

grating in diffracting the j^{th} wave into the k^{th} one. The matrix element H_{kj} is nonzero only if the thin grating has an amplitude frequency component equal to the difference between f_j and f_k. The functional form of the coupling coefficients can always be found from the thin grating amplitude transmittance which depends upon the type of recording material, number of exposures recorded, linearity of the film response, etc. The subscript m on the coupling matrix emphasizes the longitudinal dependence caused by fringe slant. We shall discuss later how to modify the coupling matrix to avoid this dependence.

The coupling matrix for the pure-phase sinusoidal grating case can be written from Eq. 2.8 as

$$
{}_{m}H_{kj} = (i)^{j-k} J_{(j-k)}\left(\frac{2\pi n_1 \Delta z}{\lambda \cos \theta_j}\right) \times \exp\left\{i \frac{2\pi n_o}{\lambda} \Delta z \cos \theta_j\right\} \exp\left\{-i2\pi f(j-k) m \Delta z \tan \phi\right\}, \quad 2.11
$$

where again, $\cos \theta_q = \left[1 - (\lambda f_q / n_o)^2\right]^{1/2}$. For convenience, we factor the propagation factor for the zero order outside the matrix. If one is only interested in the intensity of the diffracted waves (as is generally the case) this common phase factor can be dropped. Because we make Δz arbitrarily small, we can use the first order approximations of the Bessel functions and keep only terms of first order in Δz, $J_o(y) = 1$, $J_1(y) = y/2$ and $J_q(y) = 0$ for $q \geq 2$. The coupling matrix of Eq. 2.11 can then be written as

$$
{}_{m}H_{kj} = e^{i\alpha_o} \begin{cases} i\dfrac{\delta_1}{\cos\theta_j} \exp\left\{i(\alpha_j - \alpha_o)\right\} \exp\left\{i2\pi(k - j)fm\Delta z \tan\phi\right\} & k \neq j \\ \exp\left\{i(\alpha_j - \alpha_o)\right\} & k = j \end{cases} \qquad 2.12
$$

where $\alpha_j = 2\pi n_o \Delta z/\lambda \cos\theta_j$ and $\delta_1 = \pi n_1 \Delta z/\lambda$.

The output field from the m^{th} thin grating is incident upon the $m + 1$, thus the amplitude vector at $z = m\Delta z$ is

$$
\underset{\sim}{A}(m) = {}_{m}\underset{\sim}{H} \ldots\ldots \underset{1}{\underset{\sim}{H}}\, \underset{\sim}{A}(o), \qquad 2.13
$$

where $\underset{\sim}{A}(o)$ is given by the initial condition at $z = 0$

$$
\underset{\sim}{A}(o) = \begin{bmatrix} \cdot \\ \cdot \\ \cdot \\ 0 \\ 0 \\ 1 \\ 0 \\ 0 \\ \cdot \\ \cdot \\ \cdot \end{bmatrix}, \qquad 2.14
$$

where we assume a unit amplitude incident wave. The amplitudes of each of the plane waves at the exit plane $z = D$ is given by Eq. 2.13 with $m = N = D/\Delta z$. The spatial field dependence at $z = D$ is then given by

$$
A(x, D) = \sum_{q} A_q(D)\, e^{i2\pi f_q x} \qquad 2.15
$$

In practice one is usually interested in the far field some distance removed from the exit plane. In this case, because of the different angles of propagation (Fig. 2-3) and the finite lateral extent of the beams, the various orders are spatially separated and their intensities can be measured individually. The primary quantity of interest is the diffraction efficiency of the q^{th} order which is defined as (13)

$$DE_q = (\cos \theta_q / \cos \theta_o) |A_q|^2. \qquad 2.16$$

The matrix multiplication in Eq. 2.13 can be easily performed by a digital computer. In practice no more than nine orders need be considered because higher orders are of negligible magnitude. In cases where only several orders are significant, the multiplication can, in fact, be performed analytically to give closed-form solutions. Fortunately this is possible in several interesting cases.

For a pure-phase recording material there is no absorption. All the energy incident upon the front surface of the grating (minus reflection losses) must appear in the various propagating orders. This condition is met because the coupling matrix is unitary, or at least approximately so.

Note that it is not necessary that the index modulation of each slab be the same. Therefore, we can treat gratings with nonuniform modulation in depth. A depth dependent index modulation may result naturally due to attenuation of the construction waves (16), or may be intentional to produce a desired angular selectivity response. We will consider the latter in Chapter 5.

2.2.2 Inclusion of Film Nonlinearities

Generally the functional relationship between the index modulation and exposure is not linear (20, 31, 32). In such cases, despite

the fact that the exposure is a cosine function of a single frequency f, the resulting index modulation has harmonic components. We can write

$$n(x, z) = n_o + \sum_{j=1}^{J} n_j \cos 2\pi f[x - x_o(z)], \tag{2.17}$$

where in practice terms beyond J = 3 are insignificant for reasonable exposures. The amplitude transmittance function of Eq. 2.7 becomes

$$T_A(x, m) = \sum_{q_1=-\infty}^{\infty} (i)^{q_1} J_{q_1}(b_1) \exp\left\{i2\pi q_1 f[x - x_o(m)]\right\}$$

$$\times \sum_{q_2=-\infty}^{\infty} (i)^{q_2} J_{q_2}(b_2) \exp\left\{i2\pi q_2 f[x - x_o(m)]\right\}$$

$$\times \ldots . \tag{2.18}$$

where $b_j = 2\pi n_j \Delta z/\lambda \cos \theta$. Because the grating frequency components introduced by the nonlinearity are integer multiples of the fundamental, no new wave components are generated. However, the distribution of energy amongst the orders can be expected to be altered.

Using the first-order approximations to the Bessel functions and dropping terms in Δz of order greater than one, the coupling matrix in the nonlinear single grating case becomes

$$ {}_m H_{kj} = e^{i\alpha_o} \begin{cases} \dfrac{i\pi n_{|k-j|}\,\Delta z}{\lambda \cos \theta_j} \exp\left\{i(\alpha_j - \alpha_o)\right\} \exp\left\{i2\pi f(k-j)m\Delta z \tan\phi\right\}, & k \neq j \\ \exp\left\{i(\alpha_j - \alpha_o)\right\}, \quad k = j. \end{cases} \tag{2.19}$$

Again, the coupling matrix is approximately unitary and the energy flow from one thin slab to the next is conserved. In practice, the matrix must be truncated. To insure energy conservation, the amplitude of the diagonal terms must be adjusted slightly so that the sum of the moduli squared along a column is unity.

2.2.3 Slanted Fringes

For slanted fringes ($\phi \neq 0$) the general coupling matrix of Eq. 2.19 has the longitudinally dependent phase term

$$\exp\left\{i2\pi f(k - j)m\Delta z \tan \phi\right\} \qquad 2.20$$

which is the phase shift that results because of the lateral shift of the m^{th} thin grating relative to the first. Clearly, we could rotate the z axis to measure the phase shift along the direction of the fringe planes. The above phase term will then be zero ($\phi' = 0$) but the propagation factors will become

$$\exp\left\{i\frac{2\pi n_o \Delta z}{\lambda} \cos(\theta_j - \phi)\right\} \qquad 2.21$$

where Δz is still measured normal to the plane of the emulsion. Thus, the propagation factors depend upon the angles with respect to the fringe planes. The general coupling matrix (Eq. 2.19) can be written as

$$H_{kj} = e^{i\alpha'_o} \begin{cases} i\frac{\pi n |k-j| \Delta z}{\lambda \cos \theta_j} \exp\left\{i(\alpha'_j - \alpha'_o)\right\}, & k \neq j \\ \exp\left\{i(\alpha'_j - \alpha'_o)\right\}, & k = j \end{cases} \qquad 2.22$$

where $\alpha'_j = 2\pi n_o \Delta z/\lambda \cos(\theta_j - \phi)$ and $\cos \theta_j$ is determined as usual. The matrix multiplication of Eq. 2.13 becomes

$$\underset{\sim}{A}(m) = \underset{\sim}{H}^{m}\underset{\sim}{A}(o) \qquad 2.23$$

2.2.4 Differential Spatial Dispersion

Fundamental to the problem of propagation in holographic gratings is the concept of spatial dispersion. Simply stated, the optical pathlength of a plane wave depends upon its inclination angle. Because the spatial frequency of a wave is a measure of its inclination angle, we say that propagation is dispersive with respect to spatial frequency. This is expressed by its explicit dependence in the propagation factor (Eq. 2.4).

A great deal of insight about the dependence of the DE upon the grating frequency and readout angle can be gained by analyzing the spatial dispersion curves. Without loss of generality, we consider the case of unslanted fringes, $\phi = 0$. Each element of the j^{th} column of the coupling matrix has the term

$$\exp\left\{i\frac{2\pi n_o \Delta z}{\lambda}[\cos\theta_j - \cos\theta_o]\right\} \qquad 2.24$$

which is the difference in the propagation factors of the zero and j^{th} orders over the thin slab measured relative to the z axis (or, in general, the fringe planes). The total for N slabs ($N = D/\Delta z$) is $2\pi n_o D/\lambda[\cos\theta_j - \cos\theta_o]$. From simple intuitive arguments about constructive interference between wave components diffracted at sequential planes, we expect that the coupling of energy into the q^{th} order will be strong when this differential dispersion term is small. (We will frequently drop the adjective differential.) The q^{th} order dispersion term is zero when the zero and q^{th} orders propagate symmetrically about the fringe planes. The readout angle for which this is true is, of course, the q^{th} order Bragg angle (BA). This can be shown as follows. The q^{th} diffracted order has spatial frequency

$f_o + qf$. For symmetric propagation about the fringe planes (z axis here), we require

$$f_o + qf = -f_o \qquad 2.25$$

$$\Rightarrow\ 2 \sin \theta_{qB} = \frac{-q\lambda f}{n_o} \qquad 2.26$$

where θ_{qB} is the q^{th} order BA. There are other terms used to describe what we call differential spatial dispersion, including dephasing (13), phase mismatch and in non-linear optics, wave-vector mismatch that results from temporal dispersion (33).

In Fig. 2-4, we plot $\cos \theta_q - \cos \theta_o$ (the total q^{th} order differential dispersion/$(2\pi n_o D/\lambda)$) versus the normalized spatial frequency $(2f_o/f)$ of the readout wave for grating frequencies f = 375 and 1000 lines/mm. (We use $n_o = 1.52$ and $\lambda = .488\,\mu$m.) Integer values of the abscissa correspond to Bragg angles. The curves are invariant under change of sign of both f_o and q. In the lower frequency case, the differential dispersion is uniformly small for low values of q. Thus, for a given value of $2\pi n_o D/\lambda$ not too large (we will make the criterion more definite shortly), light will be coupled easily into several orders with only moderate dependence upon the readout angle. Indeed, for sufficiently low f, the dispersion terms are negligibly small for all readout angles. Such a grating is called thin and the amplitude of the q^{th} order is given as in Eq. 2.8 by $J_q(2\pi n_1 D/\lambda \cos \theta_o)$ (12). In this case, there is essentially no dependence upon the grating frequency or readout angle. For acoustic gratings, this is referred to as the Raman-Nath regime (24).

In the case of the higher grating frequency, on the other hand, $\cos \theta_q - \cos \theta_o$ varies dramatically with the readout angle, being rather large except for angles near the q^{th} BA. This large differential dispersion will suppress diffracted orders other than the q^{th}. In particular, near the first BA, significant light will be diffracted into only a single first order. This is the criterion generally used to define a thick grating (13).

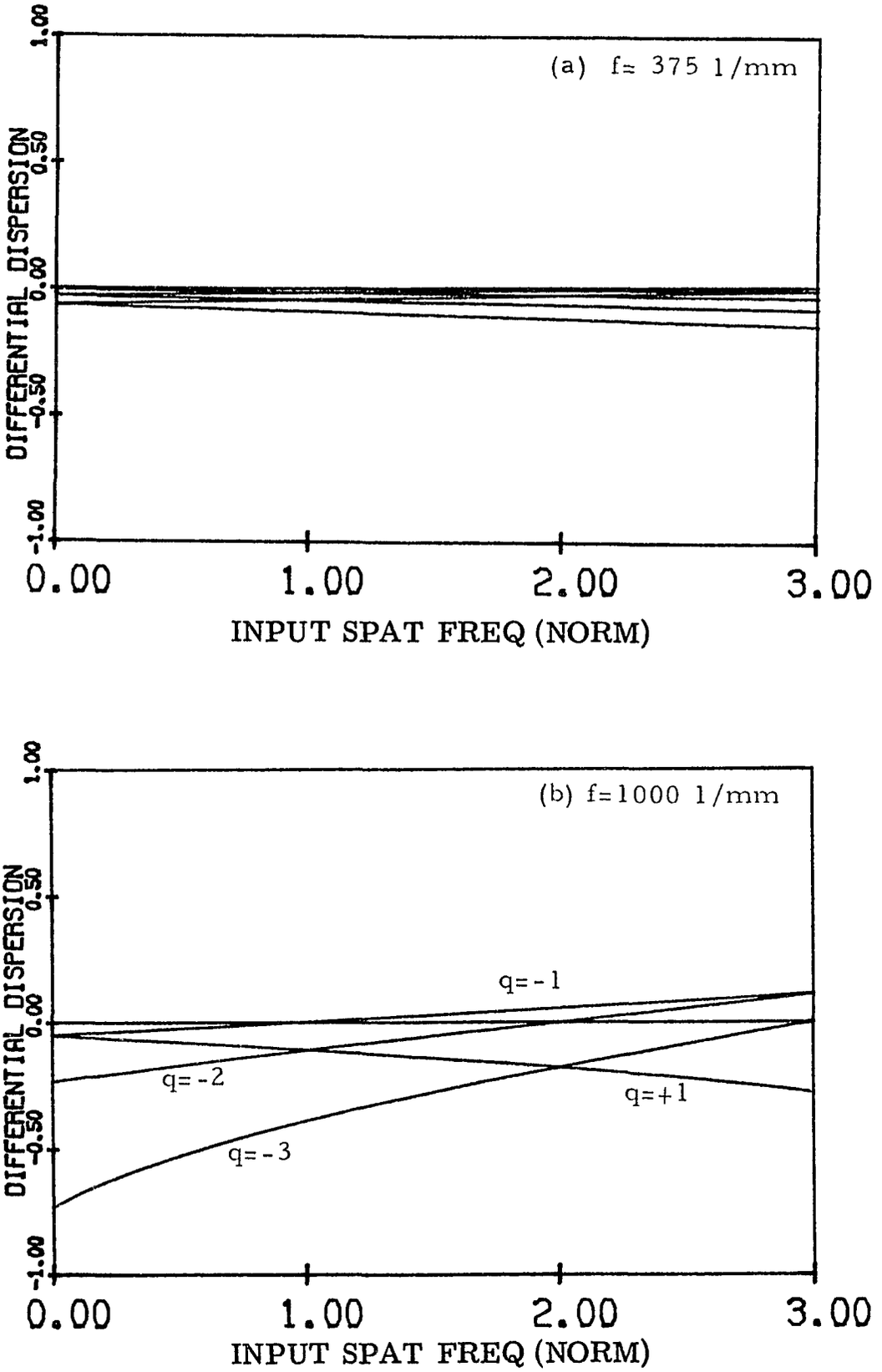


Figure 2-4. Differential Dispersion Versus Readout Spatial Frequency

From a very intuitive point of view, a thin grating is one with large enough grating spacing and small D so that the incident wave intercepts only a single fringe plane. A grating is thick if both the incident and diffracted orders intercept many fringe planes.

Using the method of TGD, we have calculated numerically the diffraction efficiencies of the significant orders for sinusoidal gratings of frequency f = 375 and 1000 1/mm. The other parameters used (typical values): $n_o = 1.52$, $\lambda = .488\ \mu m$, $D = 16\ \mu m$ and $n_1 = .015$. The results are plotted versus the normalized readout spatial frequency in Fig. 2-5. The computed results demonstrate the qualitative comments made above.

2.3 Transition Between the Thin and Thick Regimes

If we restrict ourselves to readout at the first BA, the transition between gratings that can be considered thin to those that are thick can be specified by a single dimensionless parameter. Gratings of intermediate thickness are perhaps the least understood and most difficult to analyze in any way other than numerical. Although we are generally interested in thick gratings because of the higher diffraction into a single order, the associated sharper angular selectivity is sometimes detrimental. In such cases, we might be willing to yield maximum DE to obtain a larger angular readout region.

We consider the pure sinusoidal grating with unslanted fringes. For readout at the first BA, the dispersion between the zero and first orders is, of course, zero. The dispersion terms for the conjugate first and the second orders, which are the lowest nonzero terms, are equal (Fig. 2-4). This total dispersion can be written as

$$\frac{2\pi n_o D}{\lambda}(\cos\theta_1 - \cos\theta_o) = \frac{2\pi n_o D}{\lambda}(\sin\theta_1 - \sin\theta_o)\tan\left(\frac{\theta_o + \theta_1}{2}\right) \qquad 2.27$$

$$\simeq -2\pi\frac{\lambda f^2 D}{n_o \cos\theta_o} \qquad 2.28$$

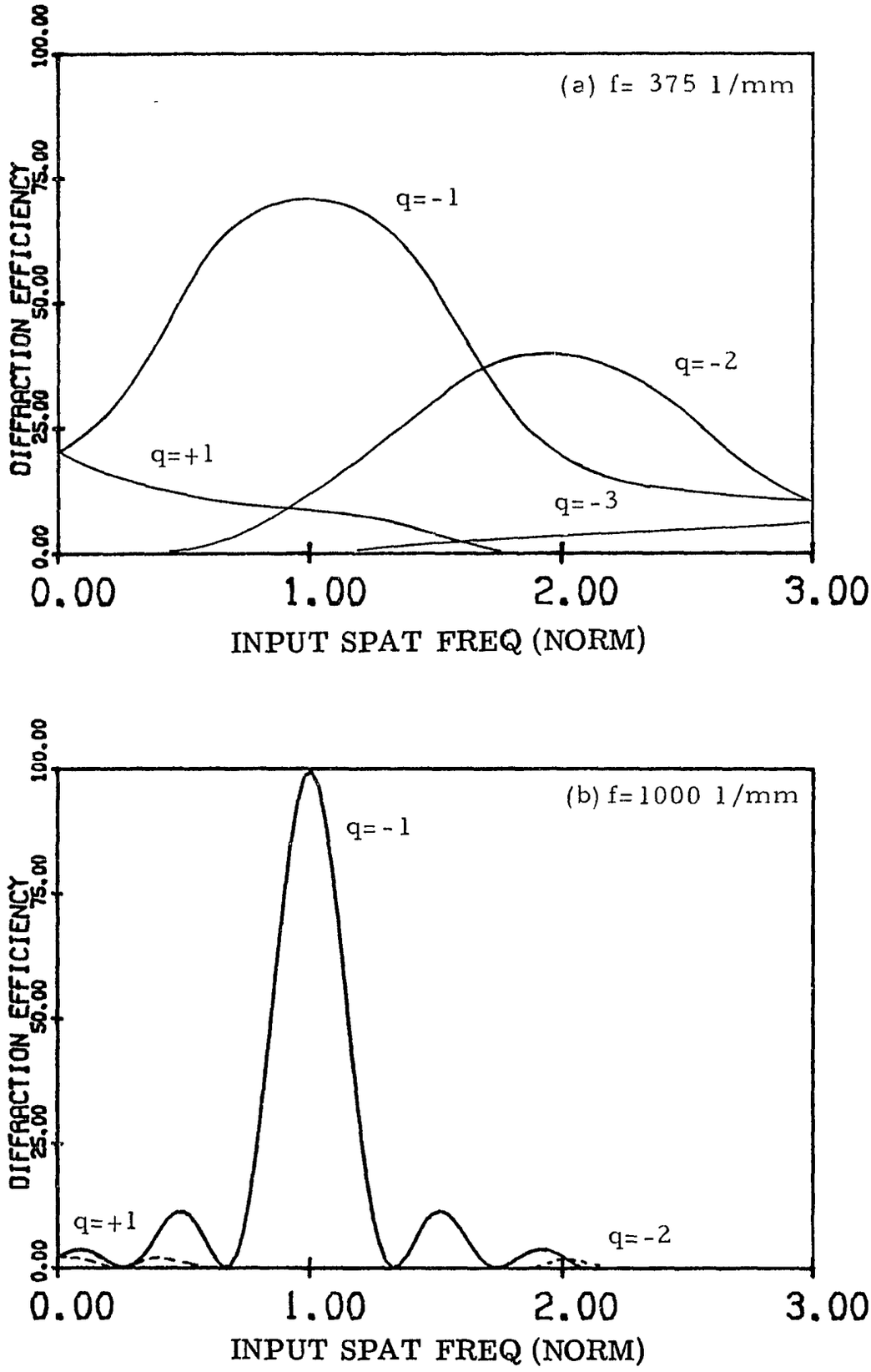


Figure 2-5. Diffraction Efficiency Versus Readout Spatial Frequency

where we have used the grating equation and the first Bragg condition. Except for the geometric factor cos θ_o, this is just the Q factor used by Kogelnik (13). The dispersion associated with higher orders can be shown to be integer multiples of the above value. For a sinusoidal grating there is also only a single grating strength parameter, $\pi n_1 \Delta z/\lambda \cos \theta_o$. For a total thickness D, this becomes $\gamma = \pi n_1 D/\lambda \cos \theta_o$. Therefore, at the first BA, the DE of the propagating waves depends only upon the two dimensionless parameters γ and $Q/\cos \theta_o$ and will be the same for equal values of these parameters regardless of the individual values of n_1, λ, f and D.

Figure 2-6a is a plot of the computed maximum first order DE for readout at the first BA versus $Q/\cos \theta_o$. Included are the corresponding values of the DE of the other orders. For $Q/\cos \theta_o \lesssim 1$ (primary dispersion <1/6 wavelength), a grating can be considered thin; there is no dispersion dependence and the maximum value of $DE_1 \cong 34\%$ agrees very well with the first maximum of J_1^2. For intermediate Q there is a strong Q dependence and a rapid monotonic increase in $DE_{1\ max}$ as the other orders are suppressed. However, a Q of 15 to 20 (primary dispersion of 3 wavelengths) is really necessary before all the other orders are truly suppressed. A plot similar to Fig. 2-6 was calculated by Fillmore and Tynan (31) using the theory of Burckhardt (17). However, they failed to realize the significance of the parameters Q and γ. They calculated the transition as a function of f for a specific D with λ as a parameter. The Q factor is commonly used as the thickness parameter. Although it is clear that the grating frequency is more important than thickness, we will abide by common nomenclature and speak of thin or thick gratings. In Fig. 2-6b, we plot the value γ required to obtain $DE_{1\ max}$ again, versus $Q/\cos \theta_o$. As the other orders are suppressed, the necessary grating strength to achieve maximum first-order diffraction, decreases and becomes constant.

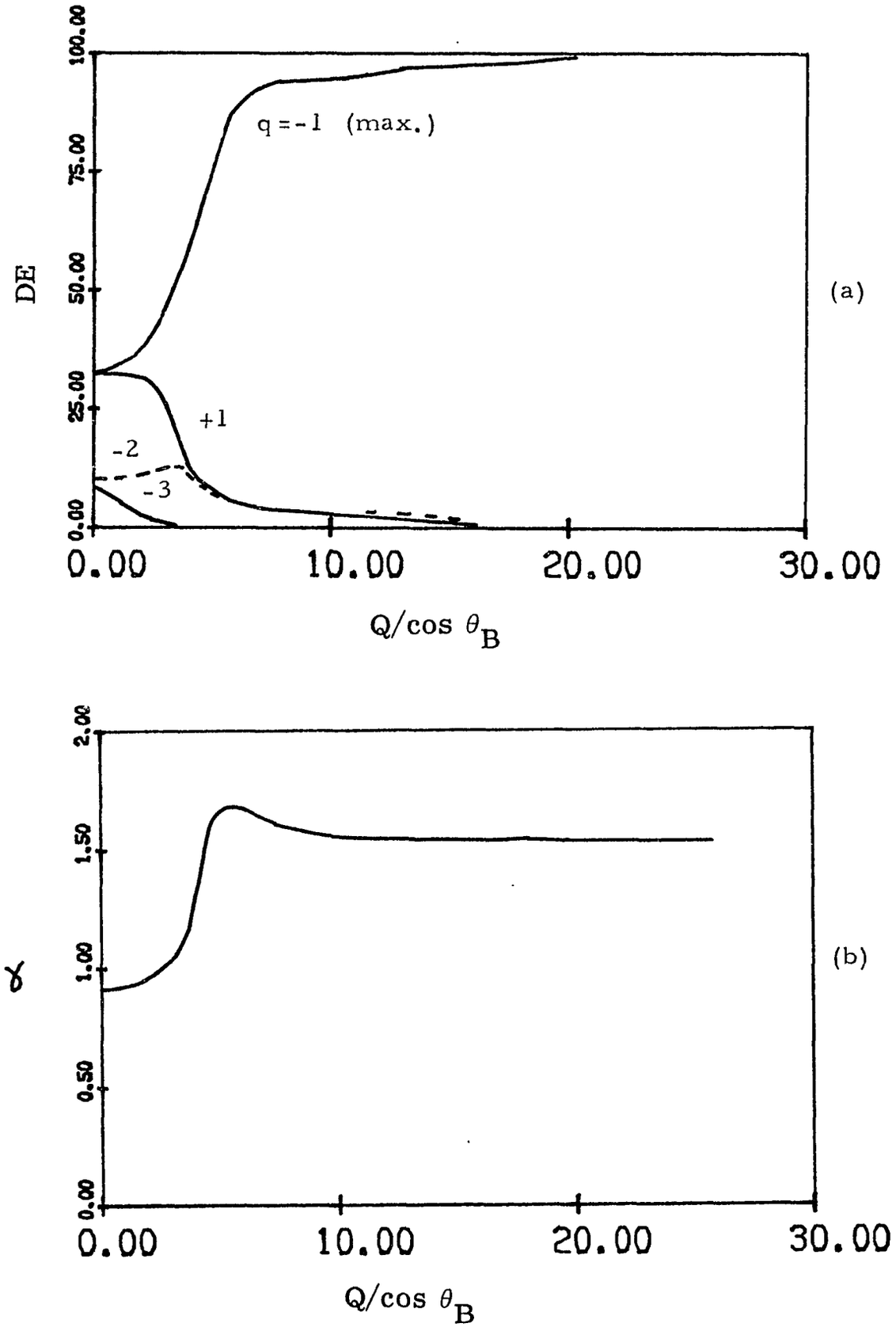


Figure 2-6. Transition Between Thin and Thick Regimes

The value of $DE_{1\ max}$ in Fig. 2-6 is the first maximum. In general, DE_1 is periodic in γ. We shall see that the thickness criterion also depends upon the modulation level. Thus, to suppress all but the first order at its second maximum, requires a larger Q factor. Also, because the dispersion of the +1 or -2 orders decreases as the readout angle moves off the BA (Fig. 2-4), a larger Q is necessary for suppression of these orders for readout angles off the BA. We shall also see in the next chapter that the transition from the thin to the thick regimes is quite different at higher order Bragg angles.

Calculated results indicate that the effect of strong film nonlinearity is important for low and moderate Q gratings. The effect for high Q gratings is, however, quite minimal (for first-order readout). This is expected because in the former case, the low dispersion allows the harmonic grating components to be effective while in the latter, higher-order diffraction is small because of strong Bragg suppression.

2.4 Analytical Results for a Thick, Sinusoidal Grating

We have seen that for a sufficiently large Q factor, only a single diffracted order is significant for readout near the first BA. Using this assumption, Kogelnik has derived analytical results for the first order DE of a sinusoidal grating by an approximate coupled-wave solution of Maxwell's equations. We show here that an equivalent result is obtained using TGD (34).

Assuming that only a single first diffracted order is significant, the general coupling matrix of Eq. 2.22 can be truncated to a 2×2 matrix

$$\underset{\sim}{H} = \begin{bmatrix} 1 & \dfrac{i\delta}{\cos\theta_1} e^{i\Phi} \\ \dfrac{i\delta}{\cos\theta_o} & e^{i\Phi} \end{bmatrix} \qquad 2.29$$

where we have dropped the common phase factor outside the matrix, $\delta = \pi n_1 \Delta z/\lambda$ and $\Phi = 2\pi n_o/\lambda\, \Delta z(\cos\theta_1 - \cos\theta_o)$. (We suppress the minus sign associated with the subscript 1.) We assume a sinusoidal grating with no slope. The corresponding amplitude vector is also truncated to

$$\underset{\sim}{A}(m) = \begin{bmatrix} A_o \\ A_1 \end{bmatrix}_m \qquad 2.30$$

The value of $\underset{\sim}{A}$ after the N^{th} thin slab is

$$\underset{\sim}{A}(N) = \underset{\sim}{H}^N A(0) \qquad 2.31$$

We will analytically perform the above matrix multiplication in the limit $N \to \infty$, $\Delta z \to 0$ such that $N\Delta z = D$.

Before doing that, we wish to simplify and examine the dispersion term Φ. The direction cosines are related through the grating equation $f_1 = f_o - f$. Significant diffraction occurs only for readout near the Bragg angle. Therefore, we write

$$\theta_o = \theta_B + \Delta\theta, \qquad 2.32$$

$$\lambda = \lambda_B + \Delta\lambda, \qquad 2.33$$

where $\Delta\theta \ll 1$ and $\Delta\lambda/\lambda \ll 1$. The angle θ_B is the Bragg angle for readout wavelength λ_B. From the grating equation and trigonometric expansions, we find

$$\cos \theta_o = \cos \theta_B - \Delta\theta \sin \theta_B \tag{2.34}$$

$$\cos \theta_1 = \cos \theta_B + \Delta\theta \sin \theta_B - \tan \theta_B(\Delta\lambda f/n_o) \tag{2.35}$$

We have dropped terms of second order in $\Delta\theta$ and $\Delta\lambda/\lambda$. The situation is depicted in Fig. 2-7. For an incident wave of wavelength λ_B at θ_B, the diffracted wave propagates at an angle $-\theta_B$. The propagation cosines are equal and there is no dispersion between the two waves. However, for angles other than θ_B, the two waves no longer propagate symmetrically about the fringe planes (z axis) and the dispersion term is nonzero. The expression for Φ can be written as

$$\Phi = 2\pi f \Delta z \left(\Delta\theta - \frac{\Delta\lambda f}{2n_o \cos \theta_B} \right) \tag{2.36}$$

Note that near the BA, Φ is proportional to f and $\Delta\theta$. The term in parenthesis in Eq. 2.36 shows the relative effect of readout angle change compared to wavelength change from the construction values in causing the dispersion.

The matrix multiplication of Eq. 2.31 is greatly simplified when $\underset{\sim}{H}$ is represented in a basis such that it is diagonal. The diagonal elements are just the eigenvalues of $\underset{\sim}{H}$ and the basis vectors are the associated eigenvectors. The eigenvalues of $\underset{\sim}{H}$ can easily be shown to be

$$\sigma_{1,2} = e^{i\frac{\Phi}{2}} \exp \left[\pm i \left(\frac{\Phi^2}{4} + \frac{\delta^2}{c_o c_1} \right)^{1/2} \right], \tag{2.37}$$

where we have used the limit $\Delta z \to 0$ to set $\sin^2 \Phi = \Phi^2$. Also, $c_o \equiv \cos \theta_o$ and $c_1 \equiv \cos \theta_1$. The associated eigenvectors $\underset{\sim}{E}_1$, $\underset{\sim}{E}_2$ are then

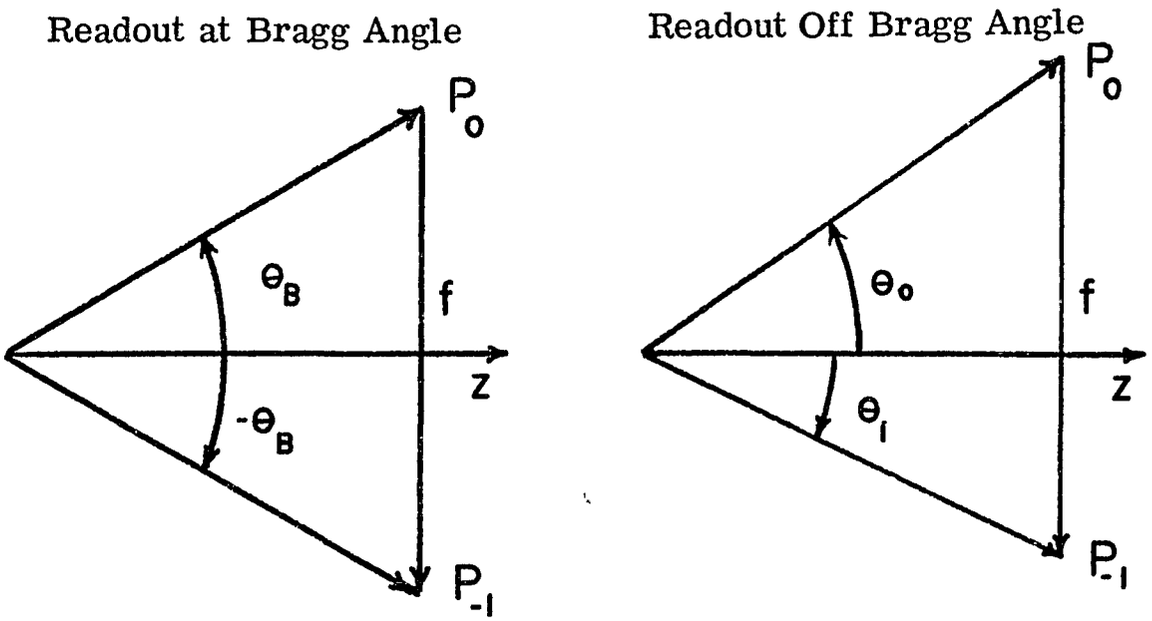


Figure 2-7. Readout of Thick Grating

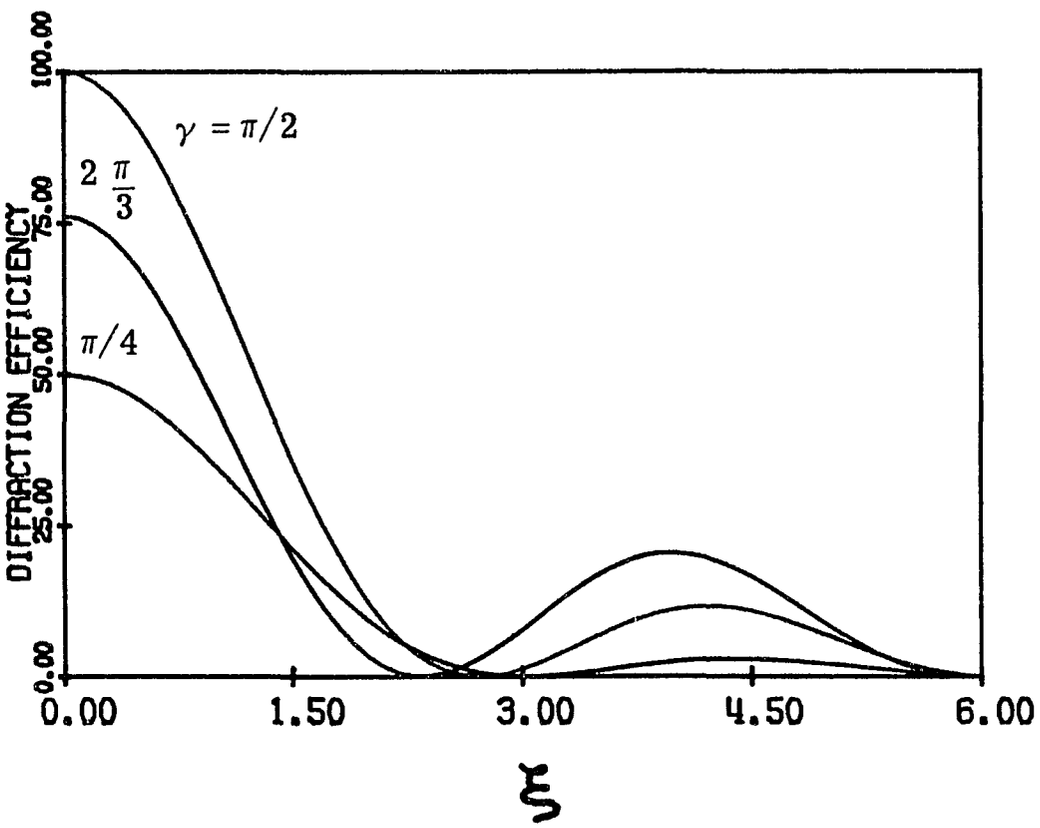


Figure 2-8. First Order DE Versus ξ

$$\begin{bmatrix} E_1 \\ E_2 \end{bmatrix} = \begin{bmatrix} 1 & a_1 \\ 1 & a_2 \end{bmatrix} \begin{bmatrix} A_o \\ A_1 \end{bmatrix}, \tag{2.38}$$

where $a_j = i\frac{c_1}{\delta}(1 - \sigma_j)\, e^{-i\Phi}$. From Eq. 2.38 and the initial condition on $\underset{\sim}{A}$, we find the initial condition in the $\underset{\sim}{E}$ basis, $\underset{\sim}{E}(o) = \begin{bmatrix} 1 \\ 1 \end{bmatrix}$. Therefore, in the diagonal representation,

$$\underset{\sim}{E}(N) = \begin{bmatrix} \sigma_1^N & \\ & \sigma_2^N \end{bmatrix} \begin{bmatrix} 1 \\ 1 \end{bmatrix} = \begin{bmatrix} \sigma_1^N \\ \sigma_2^N \end{bmatrix}. \tag{2.39}$$

We next use the inverse of the transformation of Eq. 2.39 to transform back to the original representation to find the amplitude of the diffracted order,

$$A_1(N) = \frac{1}{a_2 - a_1}\left(\sigma_2^N - \sigma_1^N\right). \tag{2.40}$$

The intensity of the diffracted order is therefore,

$$|A_1(N)|^2 = \left(\frac{\delta}{c_1}\right)^2 \frac{\sin^2\left[N\left(\frac{\Phi^2}{4} + \frac{\delta^2}{c_o c_1}\right)^{1/2}\right]}{\left(\frac{\Phi^2}{4} + \frac{\delta^2}{c_o c_1}\right)}. \tag{2.41}$$

Therefore, we find from the thin grating decomposition approach that the diffraction efficiency is,

$$DE(N) = \frac{1}{\left[1 + \Phi^2 \Big/ \left(\frac{4\delta^2}{c_o c_1}\right)\right]} \sin^2\left[\frac{N^2\Phi^2}{4} + \frac{N^2\delta^2}{c_o c_1}\right]^{1/2}. \tag{2.42}$$

To compare this result with the coupled-wave solution of Maxwell's equations for the thick grating, we make the correspondence

between the parameters above and those of Kogelnik's expression. Because $N\Delta z = D$,

$$\frac{N^2\delta^2}{c_o c_1} = \frac{\pi^2 D^2 n_1^2}{\lambda^2 c_o c_1} \equiv \gamma^2 \qquad 2.43$$

which is ν^2 in Kogelnik's notation. Furthermore because $\cos\theta_1 \simeq \cos\theta_B$ we can write,

$$\frac{N^2\Phi^2}{4} = \left\{\frac{2\pi D n_o \sin\theta_B}{\lambda_B}\left(\Delta\theta - \frac{f\Delta\lambda}{2n_o\cos\theta_B}\right)\right\}^2$$

$$= \left\{\frac{\kappa D\Delta\theta\cos\theta_B}{2\cos\theta_1} - \frac{\kappa^2 D\Delta\lambda}{8\pi n_o\cos\theta_1}\right\}^2 \qquad 2.44$$

where $\kappa = 2\pi f$. Therefore, $N^2\Phi^2/4$ is ξ^2 in Kogelnik's notation. Thus, Eq. 2.43 is

$$DE = \frac{1}{(1 + \xi^2/\gamma^2)}\sin^2(\gamma^2 + \xi^2)^{1/2} \qquad 2.45$$

which is identical to that obtained by Kogelnik (Eq. 43, Ref. 13).

The results of Eq. 2.45 are plotted in Fig. 2-8 for future reference. Note that for $\xi = 0$ (readout at the BA) the results do not depend on the grating frequency, and for values of $\gamma = n\pi/2$, 100% of the incident light is diffracted into the first order. For $\Delta\lambda = 0$, Fig. 2-8 is a plot of the angular selectivity (AS) response of the grating - the DE as a function of the angular difference of the readout wave from the BA. Kaspar has shown that under the restrictions for which the theory is valid (such that there is only a single diffracted order) this result agrees well with the more rigorous theory (20). Experimental results are also in good agreement with Eq. 2.45 (35).

For low DE, so that the zero order is not strongly depleted, the DE relative to its value at the BA is given approximately by $(\sin^2 \xi)/\xi^2$, which is independent of the modulation level (16). However, in general the AS is very dependent upon the modulation level. The width of the mainlobe of the AS curve for a given modulation level is inversely proportional to the grating frequency and thickness. As the grating is overmodulated, $\gamma > \pi/2$, the DE at the BA decreases but significant diffraction occurs at readout angles farther off the BA. The validity of Eq. 2.45 breaks down for angles far off the first BA because other orders may become important.

The analysis ignores losses due to surface reflections and film scattering. Thus, 100% DE means experimentally that all of the light transmitted by the grating is in the first diffracted order. Thick phase gratings that have 100% efficient first orders for readout at the first BA are routinely constructed holographically (28).

2.5 Summary

In this chapter, we have developed the method of thin-grating decomposition for a holographically constructed phase grating of arbitrary thickness. We have shown that useful insight into the properties of gratings can be gained by examining the differential dispersion curves of the diffracted orders. These curves are simply determined by the grating frequency, readout angle and wavelength. We have used TGD to clarify the thickness criterion and to demonstrate the transition from the thin to thick regimes. We have also shown that for a thick, phase grating, we obtain an equivalent expression for the first-order DE as that obtained by a coupled-wave solution of Maxwell's equations.

In subsequent chapters, we will use this method to determine the DE for readout near the second BA of a thick grating; to

investigate the properties of strongly-coupled multiple gratings; and to study the possibility of shaping the AS response of a thick grating.

CHAPTER 3

SECOND-ORDER READOUT OF A SINGLE, THICK HOLOGRAPHIC GRATING

In this chapter we investigate, both theoretically and experimentally, second-order readout of a thick, holographic grating. We begin by using the TGD theory to derive algebraic expressions for the DE of the first and second orders for readout near the second-order Bragg angle. The effect of film nonlinearity is included. The results demonstrate the importance of double diffraction by the fundamental grating as well as diffraction by the harmonic component in producing the second order. Using the numerical approach to allow including many orders, we calculate the transition from the thin to the thick regimes for second-order readout and find the transition to be quite different from that at the first BA. We then describe experiments on second-order readout performed with thick phase gratings constructed in dichromated gelatin. The experimental data are in good agreement with the derived analytical results. Much of the work described in this chapter has been published (36).

The analytical results for second-order readout are derived following the procedure of the last chapter. For a thick grating the coupling matrix can be truncated and the matrix multiplication performed analytically. Before proceeding, it is useful to examine the spatial differential dispersion curves for readout angles near the second BA. For convenience we show again in Fig. 3-1 the curve for a grating with f = 1000 1/mm. Figure 3-1 demonstrates several interesting qualitative features for readout angles near the second BA (normalized input spatial frequency of 2). First, the dispersion for the second order increases in magnitude about twice as rapidly for angles off the second BA as does the

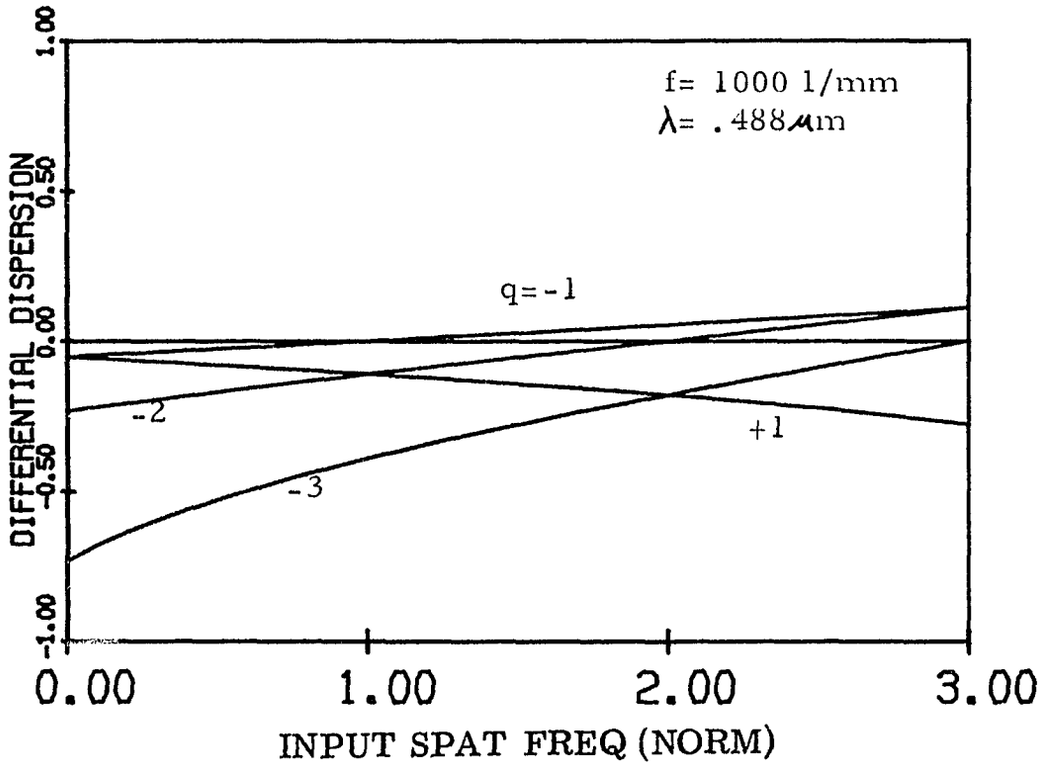


Figure 3-1. Differential Dispersion Versus Readout Spatial Frequency

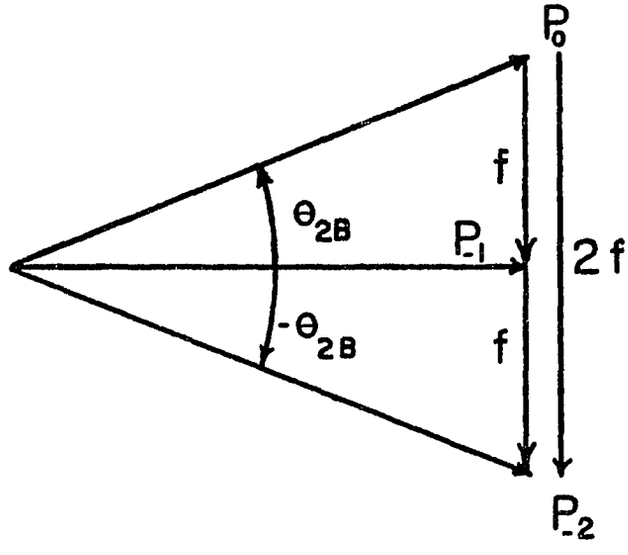


Figure 3-2. Readout at Second Bragg Angle

first order near the first BA. This is expected and results in the second-order angular selectivity being twice as sharp as that of the first order. Second, and more important, the lowest nonzero dispersion term, which is that of the first order, is only half as large as the lowest nonzero term at the first BA. Therefore, for a given λ, f and D, there will be greater suppression of the non-Bragg orders at the first BA than at the second. Also, as we shall see, to obtain significant second-order diffraction requires a rather high index modulation that tends to make the first order strong in spite of Bragg suppression. For these reasons, it is necessary to perform a three-wave analysis including the zero, first and second orders. Our experimental results will verify this assumption.

The film nonlinearity is important for second-order readout because the generated first harmonic provides a grating component that directly couples the readout wave (zero order) into the second order. The index of refraction inside the emulsion can be written as

$$n(x) = n_o + n_1 \cos 2\pi fx + n_2 \cos 4\pi fx, \qquad 3.1$$

where again, n_o is the average index and n_1 and n_2 are the index modulations of the fundamental grating of spatial frequency f and the film generated first harmonic 2f, respectively. In general, higher order nonlinearities may be present, but for readout near the second BA and for the three-wave analysis given here, their effect is negligible. We assume unslanted fringes.

The general coupling matrix derived in the last chapter is truncated to the 3×3 submatrix that describes the coupling between the three significant orders of spatial frequency f_o, $f_o - f$ and $f_o - 2f$.

$$\underset{\sim}{H} = \begin{bmatrix} 1 & i\frac{\delta_1}{c_1} e^{i\Phi_1} & i\frac{\delta_2}{c_2} e^{i\Phi_2} \\ i\frac{\delta_1}{c_o} & e^{i\Phi_1} & i\frac{\delta_1}{c_2} e^{i\Phi_2} \\ i\frac{\delta_2}{c_o} & i\frac{\delta_1}{c_1} e^{i_1} & e^{i\Phi_2} \end{bmatrix}, \tag{3.2}$$

where

$$\delta_j = \frac{\pi n_j \Delta z}{\lambda}, \qquad j = 1, 2 \tag{3.3}$$

$$\Phi_j = \frac{2\pi n_o \Delta z}{\lambda}(\cos \theta_j - \cos \theta_o), \qquad j = 1, 2 \tag{3.4}$$

$$c_j \equiv \cos \theta_j, \quad j = 0, 1, 2. \tag{3.5}$$

We have again supressed the negative signs of the subscripts and have dropped the unimportant common phase factor outside the matrix.

The elements of the coupling matrix in Eq. 3.2 can be interpreted as follows. The 1, 2 and 2, 1 elements couple the zero and first orders due to the fundamental grating while the 1, 3 and 3, 1 elements describe the coupling between the zero and second orders due to the nonlinearity produced harmonic grating. In addition, energy is coupled between the first and second orders by the fundamental grating via elements 2, 3 and 3, 2. We refer to this latter process as double diffraction because energy is transferred from the zero order to the second by two successive interactions with the fundamental grating. We shall see that in interferometrically produced gratings, double diffraction plays a major role in the generation of the second order. A diagram of the propagation directions

for second-order readout is given in Fig. 3-2 for the case of incidence exactly at the second BA.

The procedure is again to analytically compute

$$\underset{\sim}{A}(N) = \underset{\sim}{H}^{N}\begin{bmatrix}1\\0\\0\end{bmatrix} \tag{3.6}$$

in the limit $N \to \infty$, $\Delta z \to 0$ such that $N\Delta z = D$. This is done by transforming to the diagonal representation. While we can and will do that in general, it is illustrative to consider first the special case of incidence exactly at the second BA. The algebra simplifies somewhat in this case, and the physics is less obscured.

3.1 Readout at the Second-Order Bragg Angle

The second-order Bragg condition is $2 \sin \theta_{2B} = 2\lambda f/n_o$. A readout wave at this angle has spatial frequency

$$f_o = n_o \sin \theta_{2B}/\lambda = f \tag{3.7}$$

and the resulting second order, -f. Therefore $\cos \theta_2 = \cos \theta_o$; the two orders propagate symmetrically about the fringe planes; $\Phi_2 = 0$. Furthermore, it can be shown that

$$\cos \theta_1 - \cos \theta_o = (\lambda f/n_o)^2(1 + \cos \theta_{2B})^{-1} \tag{3.8}$$

so that the dispersion between the zero and first orders over a thin slab is (dropping the unnecessary subscript)

$$\Phi = \frac{2\pi n_o \Delta z}{\lambda}(\cos \theta_1 - \cos \theta_o) = \frac{2\pi\lambda f^2 \Delta z}{n_o}(1 + \cos \theta_{2B})^{-1} \tag{3.9}$$

With the above simplification for Bragg-angle incidence we diagonalize the coupling matrix in Eq. 3.2 by finding its eigenvalues. The eigenvalues σ_j of $\underset{\sim}{H}$ satisfy the matrix equation

$$\det (\underset{\sim}{H} - \sigma_j \underset{\sim}{I}) = 0 \qquad 3.10$$

where $\underset{\sim}{I}$ is the identity matrix. It is convenient to make the substitution $\psi_j = i(1 - \sigma_j)$. The solutions of Eq. 3.10 are

$$\psi_o = \delta_2/c_o \qquad 3.11$$

$$\psi_{1,2} = -\frac{1}{2}(\delta_2/c_o + \Phi) \pm \frac{1}{2}\left[\left(\frac{\delta_2}{c_o} + \Phi\right) + 4\left(\frac{2\delta_1^2}{c_o c_1} - \frac{\delta_2 \Phi}{c_o}\right)\right]^{1/2} . \qquad 3.12$$

Because we make Δz arbitrarily small, we have dropped terms of second order in Δz. The eigenvalues are $\sigma_j = 1 - i\psi_j \cong \exp(-i\psi_j)$.

The associated eigenvectors $\underset{\sim}{E}$, that are the basis vectors in the diagonal representation, satisfy the matrix equation

$$(\underset{\sim}{H} - \sigma_j \underset{\sim}{I})\underset{\sim}{E}_j = 0 \qquad 3.13$$

and can be found in terms of the original basis vectors to be

$$\begin{bmatrix} E_o \\ E_1 \\ E_2 \end{bmatrix} = \begin{bmatrix} 1 & 0 & -1 \\ 1 & \frac{-c_1}{\delta_1}[\psi_1 + \delta_2/c_o] & 1 \\ 1 & \frac{-c_1}{\delta_1}[\psi_2 + \delta_2/c_o] & 1 \end{bmatrix} \begin{bmatrix} A_o \\ A_1 \\ A_2 \end{bmatrix} \qquad 3.14$$

From the initial condition on $\underset{\sim}{A}$ and from the transformation of Eq. 3.14, the initial condition in the $\underset{\sim}{E}$ basis is

$$\underset{\sim}{E}(o) = \begin{bmatrix} 1 \\ 1 \\ 1 \end{bmatrix} \qquad 3.15$$

Therefore, in the diagonal representation, the total amplitude after the N^{th} thin grating is

$$\underset{\sim}{E}(N) = \begin{bmatrix} e^{-i\psi_o} & o & o \\ o & e^{-i\psi_1} & o \\ o & o & e^{-i\psi_2} \end{bmatrix}^N \begin{bmatrix} 1 \\ 1 \\ 1 \end{bmatrix} = \begin{bmatrix} e^{-iN\psi_o} \\ e^{-iN\psi_1} \\ e^{-iN\psi_2} \end{bmatrix} \quad 3.16$$

To find the amplitude of the first and second orders after the N^{th} thin grating, we transform back to the original basis via the inverse of the transformation in Eq. 3.14. The result is

$$A_1(N) = \frac{\delta_1}{c_1(\psi_1 - \psi_2)}[\tilde{E}_2(N) - E_1(N)] \quad 3.17$$

$$A_2(N) = \frac{1}{2}\left[-E_o(N) - \frac{(\psi_2 + \delta_2/c_o)}{(\psi_1 - \psi_2)}E_1(N) + \frac{(\psi_1 + \delta_2/c_o)}{(\psi_1 - \psi_2)}E_2(N)\right] \quad 3.18$$

We now note that $N\Delta z = D$ and define

$$\gamma_1 = \frac{\delta_1 N}{(c_1 c_o)^{1/2}} = \frac{\pi n_1 D}{\lambda(c_1 c_o)^{1/2}} \quad 3.19$$

$$\gamma_2 = \frac{\delta_2 N}{c_o} = \frac{\pi n_2 D}{\lambda c_o} \quad 3.20$$

$$\xi = \frac{\Phi N}{2} = \frac{\pi\lambda}{n_o} f^2 D(1 + \cos\theta_{2B})^{-1} \quad 3.21$$

$$\rho = \xi - \gamma_2/2 \quad 3.22$$

$$\chi = \left(\rho^2 + 2\gamma_1^2\right)^{1/2}. \quad 3.23$$

Physically, γ_1 and γ_2 are the total grating strengths of the fundamental and harmonic gratings, respectively; and ξ is 1/2 the total

dispersion (difference in propagation factors) between the zero and first orders. Note, as suggested earlier, that $\xi \simeq Q/4$, and ξ is strongly dependent upon the grating frequency.

The diffraction efficiency, $DE_j = c_j/c_o |A_j|^2$, of the first and second orders after grating thickness D can be found from Eqs. 3.17 and 3.18 using the definitions of Eqs. 3.19-3.23 and the expressions for ψ_j (Eqs. 3.11 and 3.12),

$$DE_1 = \frac{\gamma_1^2}{\chi^2} \sin^2 \chi \qquad 3.24$$

$$DE_2 = \frac{1}{4}\left\{\left[\cos \chi - \cos (3\gamma_2/2 + \xi)\right]^2 + \left[\frac{\rho}{\chi} \sin \chi - \sin (3\gamma_2/2 + \xi)\right]^2\right\}. \qquad 3.25$$

The value of $DE_o = |A_o|^2$ can also be found and it is easy to show that

$$DE_o + DE_1 + DE_2 = 1 \qquad 3.26$$

Energy flow in the z direction is therefore conserved. The fact that $\underset{\sim}{H}$ is unitary also requires that its eigenvalues have unit magnitude.

The results of Eqs. 3.24 and 3.25 are completely general, although perhaps not sufficiently simple to be easily interpreted. We now examine some interesting implications of these results.

3.1.1 Pure Sinusoidal Grating, $n_2 = 0$

It is interesting and informative to examine the general results for the pure sinusoidal case. In this case, all the energy in the second order results from double diffraction by the fundamental

grating, there is no coupling directly from the readout wave to the second order. For $n_2 = 0$, Eqs. 3.24 and 3.25 become

$$DE_1 = \frac{\gamma_1^2}{\chi^2} \sin^2 \chi \tag{3.27}$$

$$DE_2 = \frac{1}{4}\left\{[\cos \chi - \cos \xi]^2 + \left[\frac{\xi}{\chi} \sin \chi - \sin \xi\right]^2\right\} \tag{3.28}$$

where $\chi = \left(\xi^2 + 2\gamma_1^2\right)^{1/2}$. An interesting property of the second order for the pure sinusoidal grating is that its maximum value is periodic with ξ. Suppose $\xi = m\pi$, m a positive integer. Then, the DE of the second order becomes

$$DE_2 = \begin{cases} \frac{1}{4}\frac{m^2\pi^2}{\chi^2} \sin^2 \chi + \sin^4 \frac{\chi}{2}, & m \text{ even} \\ \\ \frac{1}{4}\frac{m^2\pi^2}{\chi^2} \sin^2 \chi + \cos^4 \frac{\chi}{2}, & m \text{ odd} \end{cases} \tag{3.29}$$

where $\chi(m) = \left(m^2\pi^2 + 2\gamma_1^2\right)^{1/2}$. The diffraction efficiency of the second order will be 100% whenever $\chi(m) = (2n + 1)\pi$, for m even or $\chi(m) = 2n\pi$, m odd, where n is also a positive integer and $n > m$. Although it is perhaps not so obvious from Eq. 3.29, the second order can become 100% only for $\xi = m\pi$, regardless of the value of n_1. Therefore, we find that, in addition to the second-order Bragg condition, we have the auxilliary condition

$$\left(\lambda f^2/n_o\right)D(1 + \cos \theta_{2B})^{-1} = m, \quad m \text{ positive integer} \tag{3.30}$$

which must be satisfied if the second order is to be 100% efficient in a pure sinusoidal grating. This is a necessary condition that is completely independent of the index modulation. For a given thickness and readout wavelength, the above condition implies that the second order can be made 100% efficient only for discrete grating frequencies. Physically, the condition of Eq. 3.30 is that the total dispersion between the zero and first order be an integer multiple of 2π.

In a pure sinusoidal grating, diffraction into the second order is totally a second order process through the first order. The dispersion between the zero and first orders is 2ξ and between the first and second is -2ξ. Thus, while the total is zero (at the second BA), that of the intermediate step is not. The zero and first orders do not propagate symmetrically about the fringe planes (z axis, Fig. 3-2), and have much different propagation factors. The condition of Eq. 3.30 is a higher-order phase condition imposed on the intermediate step of the total double diffraction process. It states that double diffraction will be most strong if the dispersion of the intermediate step is an integer number of wavelengths. We shall see in the next chapter that in specially constructed double gratings, it is possible to have a double diffraction process in which the dispersion associated with both the total process and the intermediate step can be zero. In single thick gratings, this is not possible.

In Fig. 3-3, we plot DE_2 vs γ_1 for several values of ξ. The periodicity of the maximum value of DE_2 with ξ is clearly evident. For $\xi = m\pi$, DE_2 is 100% for $\gamma_1 = \sqrt{\frac{2m+1}{2}}\pi$. Thus, for m = 2, a fundamental grating strength about three times that necessary to make the first order 100% efficient for readout at the first BA ($\gamma_1 = \pi/2$), is needed to make the second order 100% at its BA.

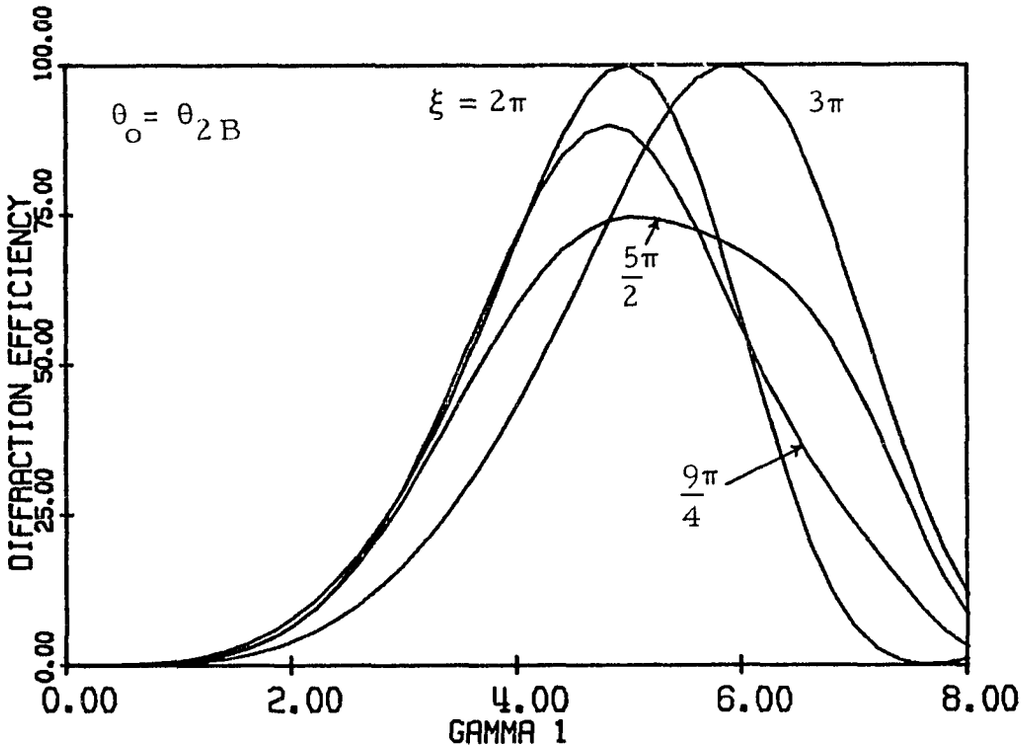


Figure 3-3. Second-Order DE Versus Fundamental Grating Strength, ($n_2 = 0$)

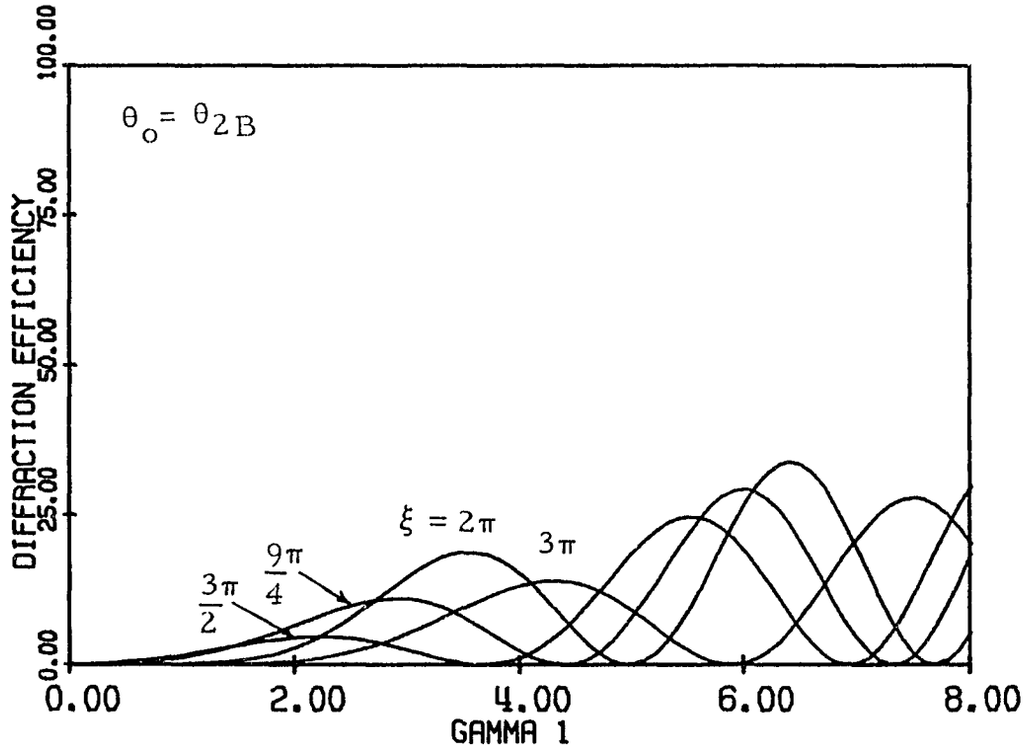


Figure 3-4. First-Order DE Versus Fundamental Grating Strength, ($n_2 = 0$)

For very large values of m, we can show that this effect becomes much less pronounced in that even for half-integer values of m, the maximum value of DE_2 can be made nearly 100% for proper γ_1. We shall see that for the same limit (ξ very large) only the zero and second orders are important. The condition imposed by Eq. 3-30 is a result of the presence of 3 significant waves. In Fig. 3-4, we plot the diffraction efficiency of the first order, DE_1, for readout at the second BA. In general, DE_1 increases more slowly with γ_1 for larger ξ.

3.1.2 The General Case, $n_2 \neq 0$

In most cases of interferometrically constructed gratings in a material such as dichromated gelatin, the film response is non-linear and we must include the effects of both n_1 and n_2. This is especially true for the high exposures required to obtain a significantly strong second order (32). Several general conclusions can be made concerning the general results of Eqs. 3.24 and 3.25. Because of the amplitude term, γ_1^2, the DE of the first order depends primarily upon n_1. The diffraction efficiency of the second order depends quite strongly on both n_1 and n_2; however, the relative effect of double diffraction (n_1 dependence) decreases as ξ increases. We shall see, though, that just as in the pure sinusoidal case, this dependence is not monotonic in ξ.

A condition similar to Eq. 3.30 applies also in the general case if DE_2 is to be made 100%. The condition is now between γ_2 and ξ and is that $3\gamma_2/2 + \xi = m\pi$, m an integer. In this case, the expression for DE_2 becomes

$$DE_2 = \begin{cases} \frac{1}{4}\frac{\rho^2}{\chi^2}\sin^2\chi + \sin^4\frac{\chi}{2}, & m \text{ even} \\ \\ \frac{1}{4}\frac{\rho^2}{\chi^2}\sin^2\chi + \cos^4\frac{\chi}{2}, & m \text{ odd,} \end{cases} \qquad 3.31$$

where $\chi(m) = \left(\rho^2 + 2\gamma_1^2\right)^{1/2}$ and $\rho(m) = m\pi - 2\gamma_2$. The necessary and sufficient conditions for the second order to be 100% efficient are therefore by inspection of Eq. 3.31

$$\frac{3\gamma_2}{2} + \xi = m\pi, \quad m \text{ integer} \qquad 3.32$$

and

$$\chi(m) = \begin{cases} (2n+1)\pi, & m \text{ even} \\ \\ 2n\pi, & m \text{ odd.} \end{cases} \qquad 3.33$$

Note that for a small nonlinearity, $3/2\,\gamma_2 << \xi$, the condition of Eq. 3.32 indicates a small shift in the grating frequencies for which maximum second order occurs. Because the condition on ξ (Eq. 3.32) includes γ_2, DE_2 can be made 100% for a given thickness and wavelength for arbitrary grating spatial frequencies by proper choice of n_1 and n_2. However, for interferometrically constructed gratings, we generally do not have rigid control over the relative strength of n_1 and n_2. Thus, by merely varying the exposure level, we can not be assured of obtaining the correct combination of n_1 and n_2 to obtain a 100% efficient second order. Because the requirements between n_1, n_2 and ξ for a highly efficient second order result from the competing effects of double diffraction and diffraction by the harmonic grating, as ξ increases and double diffraction

becomes less important, DE_2 is determined primarily by n_2 (we shall show this more clearly in the next section). In this case, if n_2 is a reasonably monotonically increasing function of exposure, an exposure can be found such that DE_2 is 100% (provided the film has a sufficiently nonlinear response).

An interesting feature of the expression for DE_2 (Eq. 3.24) is that the effect of double diffraction (n_1 dependence) opposes that of diffraction by the harmonic grating (n_2 dependence) if n_2 is positive. This effect is shown in Fig. 3-5 where we plot DE_2 versus γ_2 for several values of ξ and for a fixed value of $\gamma_1 = 2.5$. The value of DE_2 for $\gamma_2 = o$ is due entirely to double diffraction by the fundamental grating. As γ_2 is increased positively, DE_2 decreases. Then, as γ_2 is increased even more, and the opposing effect of double diffraction is completely overcome, DE_2 increases to a relatively large value. This opposition between double diffraction and harmonic diffraction will be more readily apparent in the approximate expression for DE_2 which will be derived in the next section.

In a real material, we vary the exposure and the values of n_1 and n_2 for any exposure are determined by the nonlinear response of the film. In a material like dichromated gelatin, n_1 increases initially much more rapidly with exposure than does n_2 (32). (This is probably true of most phase materials.) If n_2 were positive relative to n_1, then as a function of exposure, DE_2 would initially increase due to the dominant effect of the n_1 dependence. As the exposure was increased so that n_2 became comparable to n_1, DE_2 would begin to decrease after having reached a relative maximum value which might be rather small depending on the relative generation of n_1 and n_2 with exposure. As the exposure was increased further, DE_2 would decrease to some low value

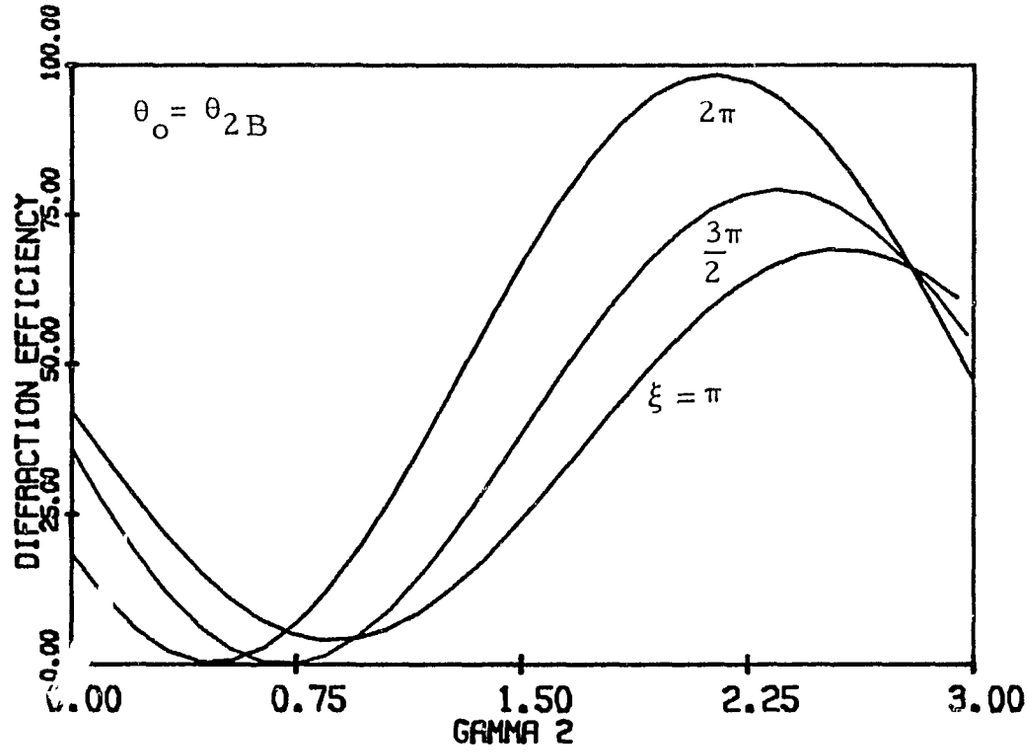


Figure 3-5. Second-Order DE Versus Harmonic Grating Strength, (γ_1 = 2.5)

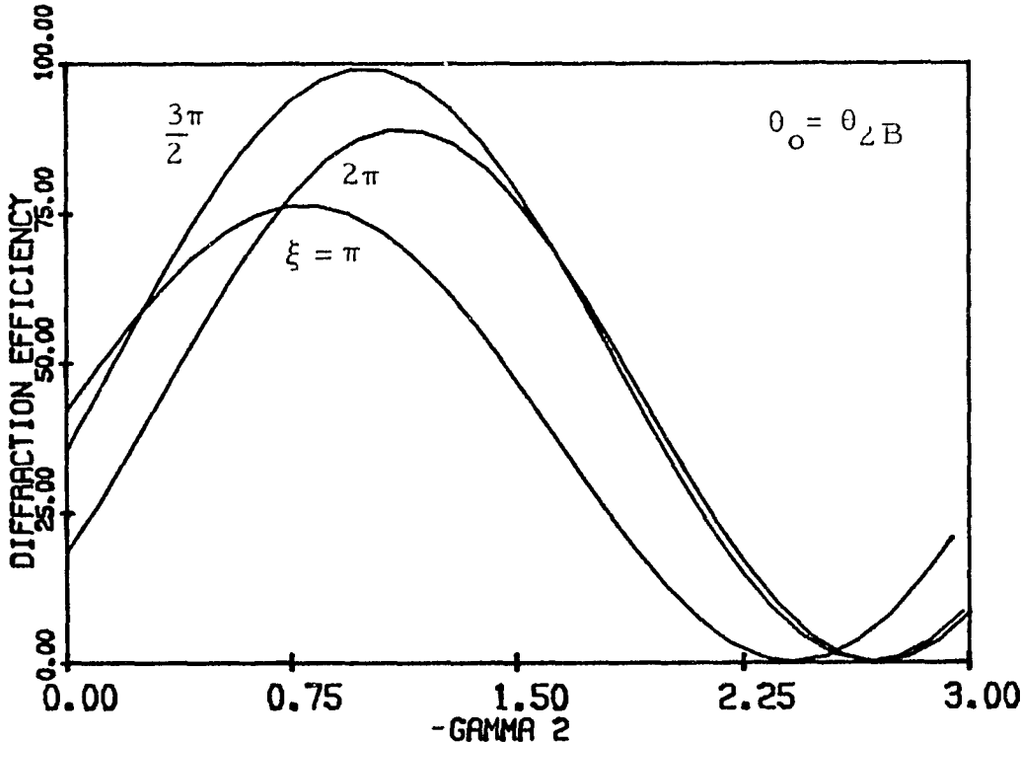


Figure 3-6. Second-Order DE Versus Negative Harmonic Grating Strength, (γ_1 = 2.5)

and then increase again just as in Fig. 3-5. In fact, this behavior is not observed experimentally. Instead, DE_2 increases monotonically with exposure to a rather large value (although not necessarily 100% for reasons mentioned earlier) before peaking and then decreasing. (We will show experimental results later.) Indeed, the fact that the above situation is not observed, is one of several reasons for concluding that n_2 is negative with respect to n_1, i.e., the harmonic component is shifted by π radians relative to the fundamental for typical nonlinear generation in dichromated gelatin (32), and probably for other phase materials. (This fact has been shown previously by Fillmore and Tynan (31), who used a numerical approach to invert diffraction efficiency data. A similar π phase shift between the first and second order absorptivity modulations occurs in silver-based photographic emulsions (37).) Therefore, the nonlinear generation of n_2 and the propagation properties of the second order nicely complement each other to give a strong second order that increases with exposure to a relatively large value. These two properties are, of course, completely independent of each other. In Fig. 3-6, we plot DE_2 versus $-\gamma_2$ for several values of ξ and for a fixed value of $\gamma_1 = 2.5$. These curves clearly demonstrate that for n_2 negative, the two mechanisms producing the second order act together to produce a large DE_2.

3.1.3 Simplified Results for γ_1/ξ, $\gamma_2/\xi \ll 1$

The general results of Eqs. 3.24 and 3.25 can be greatly simplified under the assumption of low index modulation relative to the square of λf, γ_1/ξ $\gamma_2/\xi \ll 1$. Physically, this assumption requires the total grating strength to be much smaller than the total dispersion between the zero and first orders. While the simplified results are informative and illustrate more readily some of the implications of the general results, we stress again, as mentioned

earlier, that for typical gratings with a moderate Q factor, the above assumptions are not met under exposure conditions required to produce a strong second order and the general results must be used. Nevertheless, the simplified results are instructive and are valid for gratings of very high spatial frequency or for materials in which the nonlinearity is very strong such that $n_2 \simeq n_1$ or the thickness is large so that the modulation can be kept very low and still have a significant second order produced.

We define

$$t_1 = \gamma_{1/\xi} \simeq \frac{2n_o n_1}{(\lambda f)^2} \tag{3.34}$$

$$t_2 = \gamma_{2/\xi} \simeq \frac{2n_o n_2}{(\lambda f)^2} \tag{3.35}$$

After some tedious manipulations and using the assumptions t_1, $t_2 << 1$, DE_2 from Eq. 3.25 is

$$DE_2 \simeq \sin^2\left[\frac{\xi}{2}\left(t_1^2 - 2t_2\right)\right] + \frac{t_1^2}{2}\sin\left[\xi\left(1 - t_1^2 - \frac{t_2}{2}\right)\right]\left\{\sin\left[\xi\left(1 + \frac{3t_2}{2}\right)\right] - \sin\left[\xi\left(1 + t_1^2 - \frac{t_2}{2}\right)\right]\right\}. \tag{3.36}$$

Then dropping the second term in Eq. 3.36, because of the factor $t_1^2 << 1$, we have simply

$$DE_2 \cong \sin^2\left[\gamma_1^2/2\xi - \gamma_2\right] \tag{3.37}$$

In this same approximation, $DE_1 \simeq t_1^2 \simeq 0$, so that only the zero and second orders are significant. For $n_2 = 0$ ($\gamma_2 = 0$) and with the

same restriction on γ_1/ξ so that only the zero and second orders are assumed important, Bergstein and Kermisch (18) and Baugh (38) have found similar results. Also, this result should agree with that of Su and Gaylord, who have recently performed a general m^{th} Bragg angle analysis, again in the approximation that only two orders are important (39). As suggested earlier, in this limit, the periodic dependence upon ξ of the maximum value of DE_2 for $n_2 = 0$ is gone and DE_2 can be 100% for arbitrary grating frequencies. For $\gamma_1^2/2\xi << \gamma_2$, the result reduces to the form of that for the first order for readout at its BA except, of course, that the grating strength is determined by n_2.

Equation 3.37 shows quite clearly the opposing effect of the n_1 and n_2 dependence of DE_2 if n_2 is positive. Also readily apparent is that the relative importance of double diffraction decreases as ξ increases. Again, the degree of the film nonlinearity is important because, if for a given exposure level, the harmonic generation is low (n_2 small relative to n_1), the effect of the fundamental grating will be important even for large ξ. This is typically the case for dichromated gelatin. As mentioned in the previous section, both of the above properties are also true for the general expression for DE_2.

3.2 Readout Angles Near the Second Bragg Angle

When the readout wave is not incident exactly at the second-order BA, the general coupling matrix in Eq. 3.2 must be used where Φ_2 is no longer zero. The mathematical procedure is the same, but the algebra of diagonalizing the matrix and doing the multiplication, is more complicated. We shall find, in the next chapter on double gratings, the need to diagonalize the most general form of the 3×3 coupling matrix. To eliminate mathematical

duplication, we therefore diagonalize and do the necessary matrix multiplication for the most general 3 × 3 coupling matrix in the Appendix. The matrix of Eq. 3.2, for second-order readout of single gratings, is a special case of that considered in the Appendix (A. 2) with $\delta_1' = \delta_1$, $\delta_2' = \delta_2$ and $\delta_3' = \delta_1$. The results for the first and second order diffraction efficiencies for readout near the second BA are thus given by Eq. A.25 and A.26 respectively with

$$\gamma_1 = \pi n_1 D/\lambda(c_o c_1)^{1/2}; \; \gamma_3 = \pi n_1 D/\lambda(c_1 c_2)^{1/2} \qquad 3.38$$

$$\gamma_2 = \pi n_2 D/\lambda(c_o c_2)^{1/2} \qquad 3.39$$

$$\xi_j = (\pi n_o D/\lambda)(\cos\theta_j - \cos\theta_o), \qquad j = 1, 2 \qquad 3.40$$

$$\cos\theta_j = \left\{1 - \left[\frac{\lambda}{n_o}(f_o - jf)\right]^2\right\}^{1/2}, \; j = 0, 1, 2 \qquad 3.41$$

Because we do not require second Bragg angle incidence, there are two dispersion terms.

The general angular selectivity results above depend on four parameters. The two dispersion terms are not independent, but are related through the readout angle. For purposes of illustration, representative results have been evaluated and are plotted in Fig. 3-7 (f = 850 1/mm, n_1 = .027) and Fig. 3-8 (f = 1000 1/mm, n_1 = .0285). In both cases, D = 16 μm, λ = .488 μm and n_o = 1.52. Although the film nonlinearity, in fact, depends upon the level of modulation (32), we assume a ratio n_2/n_1 = -.33 in both cases. The value of $\Delta\theta$ is $\theta_o - \theta_{2B}$, the angular difference of the readout angle from the second BA. The presence of the first order in the lower frequency case (Fig. 3-7) is very prominent, especially for

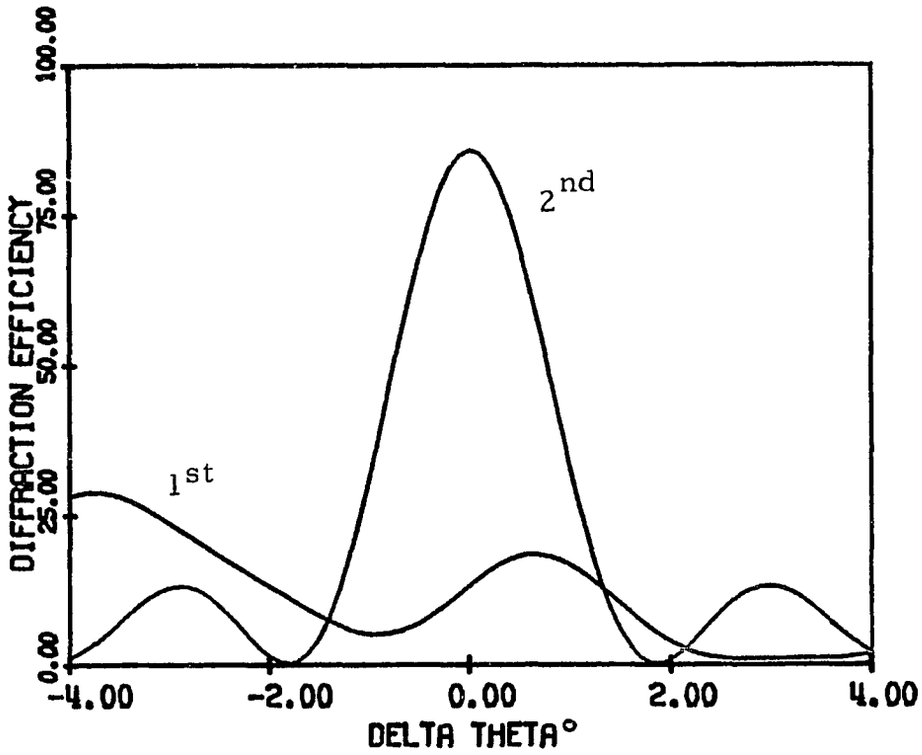


Figure 3-7. Angular Selectivity for Second-Order Readout, f = 850 ℓ/mm

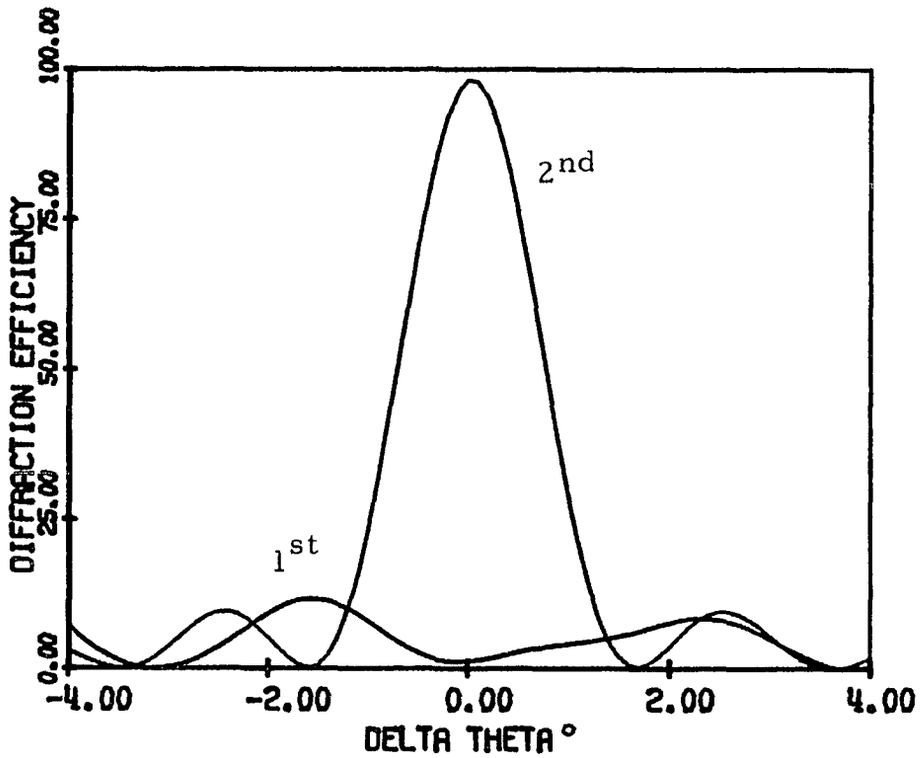


Figure 3-8. Angular Selectivity for Second-Order Readout, f = 1000 ℓ/mm

readout angles toward the first BA. This results, because, with respect to first-order readout, the grating is strongly overmodulated which tends to overcome Bragg suppression, even far off the first BA. Also, the second-order sidelobes are very evident. An interesting conclusion that can be made from examining the angular selectivity results for various levels of nonlinearity is that the shape of the second order AS is not very dependent upon the generation mechanism. That is, whether the second order is produced entirely by double diffraction ($n_2 = 0$) or primarily by the harmonic grating ($n_2 \simeq n_1$), the value of DE_2 versus $\theta_o - \theta_{2B}$ is essentially the same, given the same value at θ_{2B} in the two cases. This is in spite of the fact that, in the former case, there is a significant first order in this angular region, while in the latter, there is none. The AS is just slightly broader for total generation by double diffraction, but the sidelobes are equally strong in either case.

3.3 Transition Between the Thin and Thick Regimes at the Second Bragg Angle

An argument, like that used in the last chapter, can be given to show that for a pure sinusoidal grating and for readout at the second BA, the diffraction efficiency of the propagating orders depends only upon the dimensionless differential dispersion parameters $\xi \cong Q/4 \cos \theta_{2B}$ and the fundamental grating strength. This is true even for gratings that are thin or of intermediate thickness. Doing the necessary matrix multiplication numerically and including nine orders, we have calculated the first maximum of DE_2 versus $Q/\cos \theta_{2B}$. The results, computed for the pure sinusoidal case, are shown in Fig. 3-9. These results are in striking contrast to the transition at the first BA. In particular, the peaks in $DE_{2\,max}$ for $\xi = m\pi$ and minima for half integer values, indicated in the derived analytical results for thick gratings, extend into the

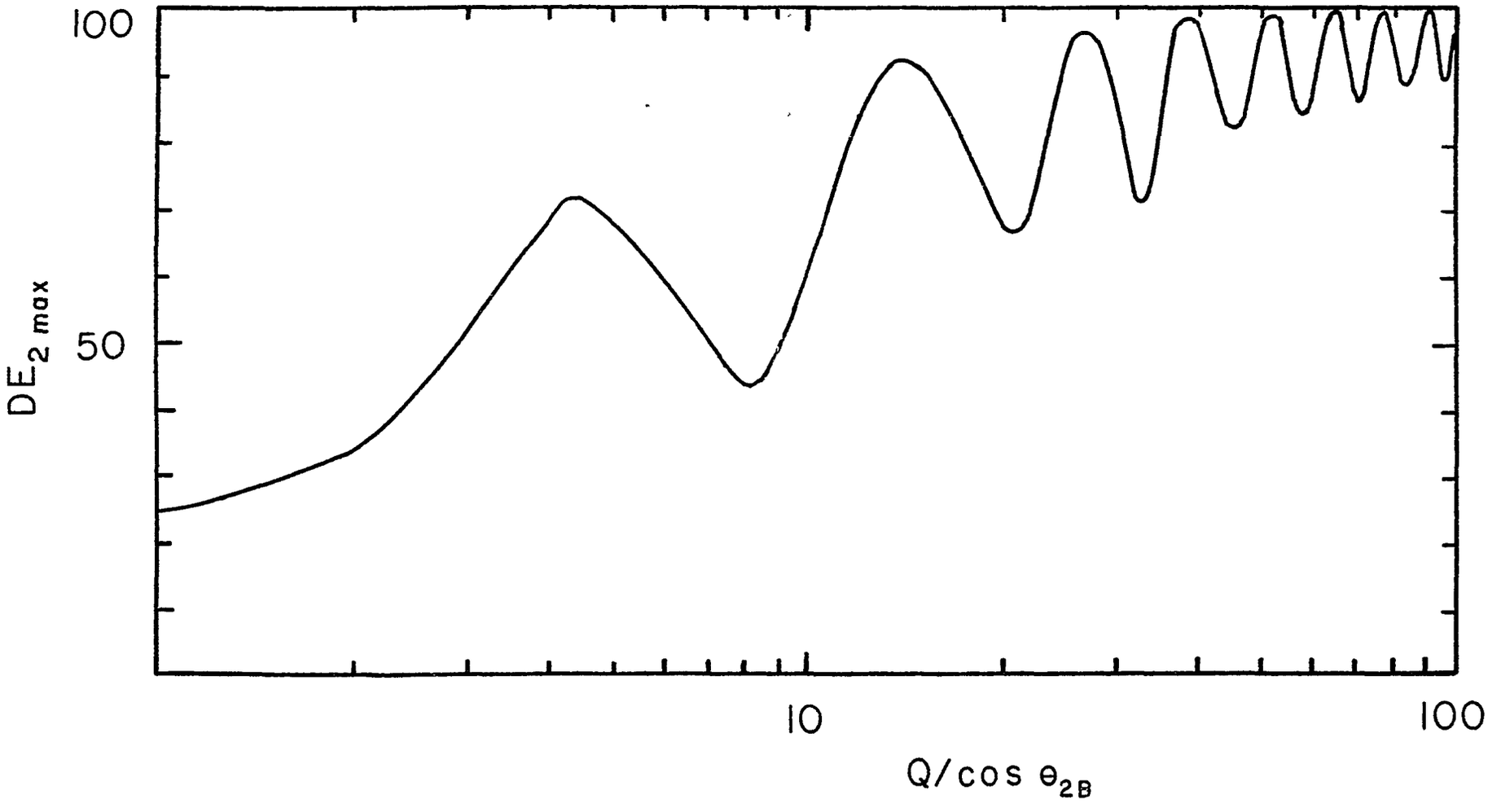


Figure 3-9. Transition Between Thin and Thick Regimes for Second-Order Readout

intermediate regime. Thus, the transition is very oscillatory. This is a result of the phase condition on the intermediate step of the double diffraction process. For low Q, the peaks do not occur exactly for $\xi = m\pi$, probably because higher order processes are also important. For $Q > 20$, only the zero, first, and second orders are significant, while $Q > 200$ is necessary to also suppress the first order. Thus, by doing a three-wave analysis, we considerably increase the range of validity of our analytical results. This is especially true for readout angles between the first and second Bragg angles.

The effect of the film generated n_2 on the results of Fig. 3-9, is to shift the curve (to the left for $n_2 < 0$) as suggested by Eq. 3.32. Also, the oscillations are smoothed out as $|n_2|$ is increased because the relative importance of double diffraction is decreased. As $|n_2|$ becomes comparable to n_1, the effect of double diffraction will become negligible except for very low Q and the transition will become more like that at the first BA.

3.4 Experimental Verification

Several experiments were performed with gratings holographically constructed in dichromated gelatin film to verify the results derived above. Dichromated gelatin film is a pure-phase material that can be exposed to yield a very high index modulation (4-6, 31, 32, 40). It is less sensitive than standard silver-based holographic films and is not sensitive to radiation in longer wavelength region of the visible spectrum. The preparation and development of this material is discussed in the literature. The dichromated gelatin plates were prepared from standard Kodak 649-F plates using the procedure described by Chang (41). The silver is first removed by a fixing process. The remaining gelatin is sensitized by being

soaked in a solution of ammonium dichromate. Except where noted, a 1 1/2% solution of ammonium dichromate was used. The mechanism responsible for the generation of index modulation in dichromated gelatin is adversely affected by excessive humidity. The dichromated gelatin plates were exposed, processed, readout and stored in an environment of a relative humidity less than 40% (40).

There is some controversy (5, 6) about the actual mechanism of hologram formation in dichromated gelatin. However, recent experimental data (31, 32) agrees with the assumption that the index modulation is a true volume effect rather than a large scale gelatin-air surface relief effect (5). Thus, the theory that we have used is applicable to this material.

A schematic of the experimental arrangement is the same as in Fig. 2-1. A continuous wave argon laser operating at λ = .488 μm was used to construct and readout the gratings. Beam expanders (microscope objective), spatial filters (small pinhole) and collimating lenses were used to produce beams of plane wavefronts and approximately uniform amplitude. The lowest mode output from the laser has a transverse Gaussian amplitude profile (33). By expanding the beam and then using only a small center section of the expanded beam, we obtain a beam of nearly uniform amplitude. Because of the short coherence length (the laser does not have a cavity etalon), the pathlengths were adjusted to within 1 cm of each other. The plate holder was rotated so that the perpendicular to the plate bisected the angle between the two beams. The recorded fringe planes were thus perpendicular to the plate. The intensity of the diffracted orders was measured with a standard photometer that uses a photo-voltaic cell. Because only relative values are required, absolute calibration is not necessary.

Because the analysis ignores surface reflections, the experimental diffraction efficiencies are corrected for surface reflections by normalizing the measured intensity of each order by the total transmitted intensity. The grating frequency was changed by varying the angle between the two construction beams. The recording beams were made approximately equal in amplitude to give maximum fringe contrast. The emulsion thickness, D, was approximately 16 μm as determined by measuring the angular deviation from the first BA at which DE_1 goes to zero (Eq. 2.45). Variations of as much as 10% for the same plate were noted and there was some dependence upon the exposure level. The axis of polarization of the readout beam was along the direction of the fringes (perpendicular to the plane of incidence).

3.4.1 Readout at the Second Bragg Angle

Experiments were performed to make both qualitative and quantitative comparison with the theory. To make quantitative comparison, single gratings were made with spatial frequencies of 850 and 1200 1/mm. Various exposures were used, but the same exposures were used for gratings of each frequency. Different grating frequencies result in different dispersion terms, ξ, in the two cases. By using the same exposure, we hope to obtain the same values of n_1 and n_2 for each of the two gratings. Because of the dependence of DE_2 upon grating frequency, the same values of index modulation in the two cases should not produce the same values of DE_2. We therefore verify the theoretical results by using the theory to invert the diffraction efficiency data for one grating frequency to find n_1 and n_2 for that exposure level. Those values were then used in Eq. 3.24 to predict the value of DE_2 for the other grating for the same exposure level. After development, the gratings were returned to the plate holder mounted on the

rotation table (Fig. 2-1). They were readout at their first-order Bragg angles and the measured first order diffraction efficiencies were inverted to find n_1 (Eq. 2.45) (42). At the first BA, the first order DE does not depend upon the grating frequency. We found that the same exposure gave essentially the same n_1 for each spatial frequency so that the film displayed a uniform spatial frequency response. (Fillmore and Tynan (31) have found that dichromated gelatin has a flat spatial frequency response over the range from 100 1/mm to 2500 1/mm.) The diffraction efficiencies of the first and second orders for readout at the second Bragg angles were then measured. Using the value of n_1 determined above, and the expression for DE_2 (Eq. 3.24), the measured DE_2 for the higher frequency grating (f = 1200 1/mm) was inverted to find n_2. The values of n_2 were found to be negative. These values of n_1 and n_2 were then used in Eq. 3.24 to predict DE_2 for the lower frequency grating for the same exposure. In Fig. 3-10, we plot the experimentally measured DE_2 for each of the two grating frequencies versus the determined value of n_1. The theoretically predicted values for the lower frequency grating are also shown. The difference in DE_2 for the same values of n_1 and n_2 for the two different grating frequencies is quite evident. The agreement between experiment and theory, as shown in Fig. 3-10 is quite good. The largest difference is 7%.

Experiments also clearly demonstrate that the first order is not negligible for readout at the second-order Bragg angle for the high exposures needed to produce significant second order. To demonstrate this fact, we plot in Fig. 3-11 the experimentally measured DE_1 for readout at the second-order Bragg angle versus the determined value of n_1 for gratings with f = 850 1/mm and

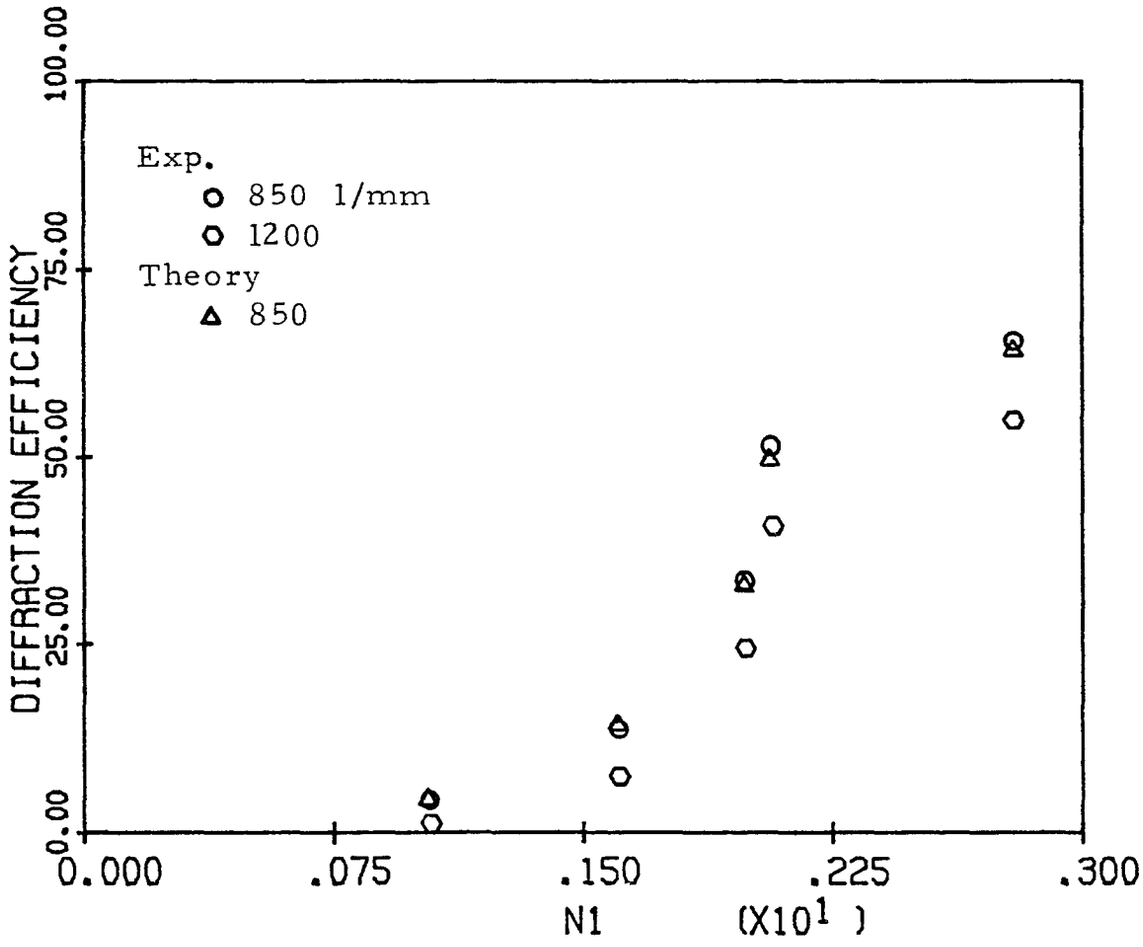


Figure 3-10. Second-Order DE: Comparison of Experiment and Theory

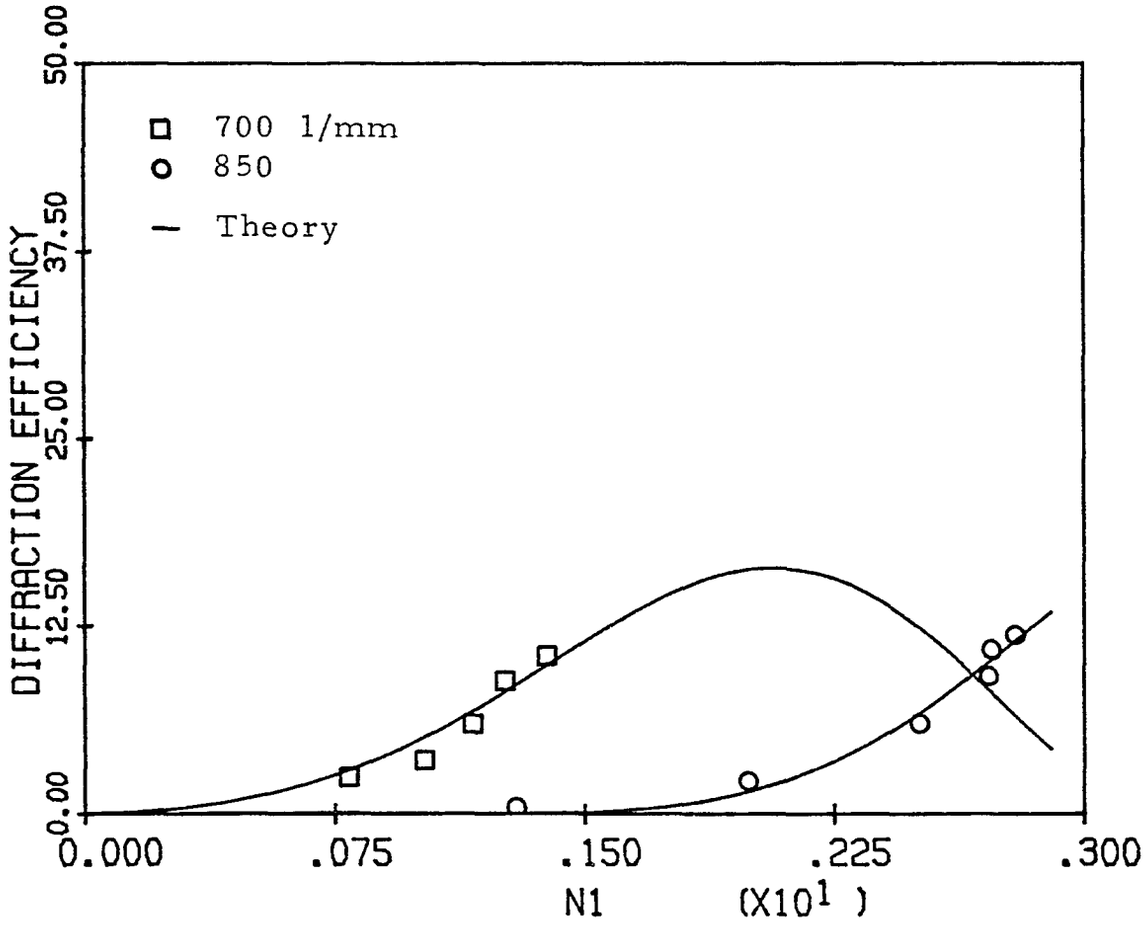


Figure 3-11. First-Order DE: Comparison of Experiment and Theory

f = 700 1/mm. Included in Fig. 3-11 are the theoretical curves for $n_2 = 0$ (as suggested earlier, n_2 is relatively unimportant in determining DE_1). Again, the agreement with theory is good. The experimentally measured 14% in the first order is clearly not ignorable.

Finally, in Fig. 3-12, we show experimentally measured values of DE_2 for three grating frequencies (f = 700, 925 and 1200 1/mm) versus the determined value of n_1. (Note that n_2 is non-zero.) This data clearly demonstrates that both the rate of increase with index modulation, as well as the maximum of DE_2 depends upon the grating frequency. Generally, for lower frequencies the rate of increase with index modulation is greater, but the maximum value is lower because a larger fraction of the total energy is in the first order. As suggested in the analytical results, this effect is not monotonic with the grating frequency. The maximum value of DE_2 is about the same for f = 700 1/mm and f = 925 1/mm. The data of Fig. 3-12 was taken from a plate sensitized at a higher level (5% solution of ammonium dichromate; this is generally the standard solution used) so that the nonlinear generation is lower than for the 1 1/2% case (32). As a result, the importance of double diffraction is even greater than in the data of Fig. 3-10 as is indicated by the stronger dependence upon grating frequency. That is, for given values of n_1 and n_2, there is a larger difference in DE_2 for the different frequencies. We also note that the experiments demonstrated that for the grating frequencies considered ($Q \gtrsim 15$) and for the index modulation achievable in dichromated gelatin (which is quite large), only the zero, first and second orders are significant for readout at the second Bragg angle. By way of reference, the first-order DE for readout at the first BA, reaches its first maximum for $n_1 \simeq .015$, independent of the grating frequency.

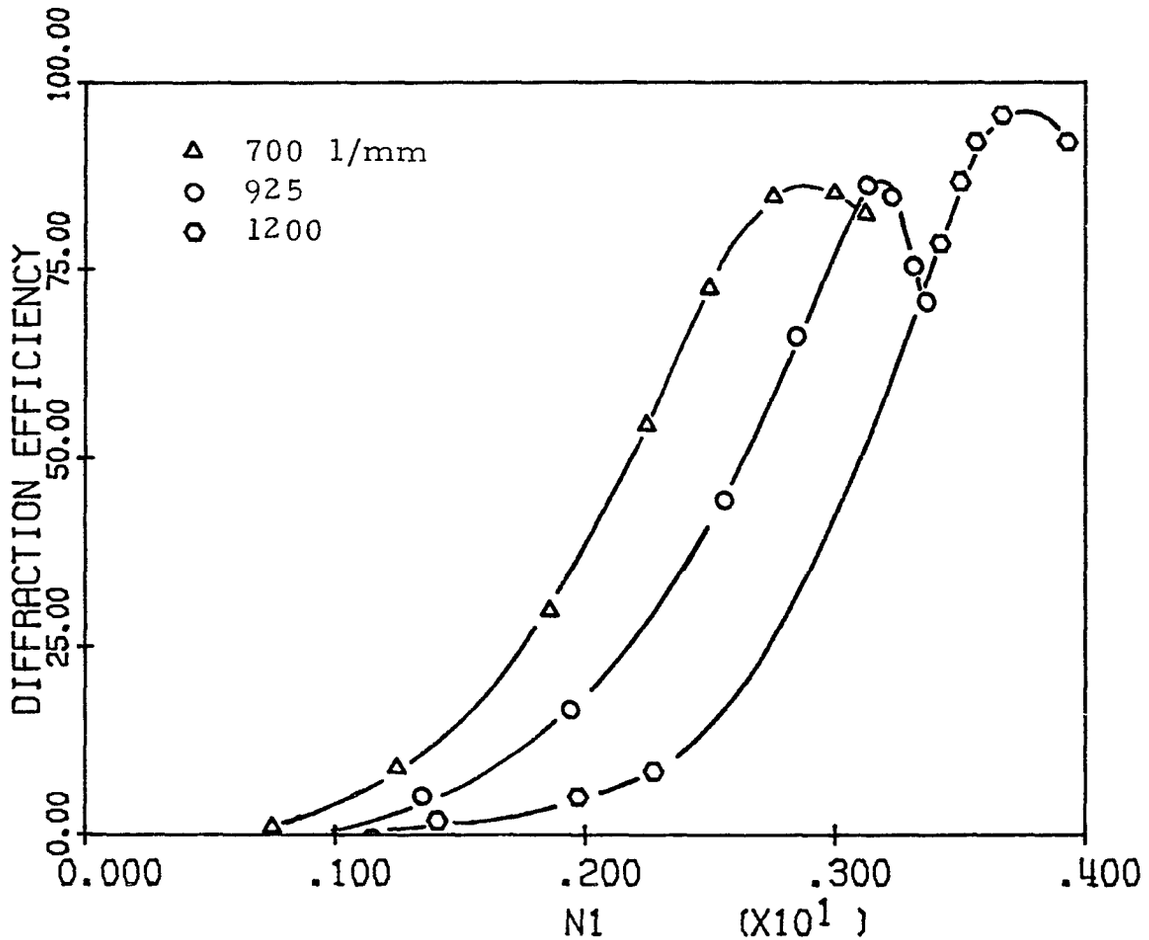


Figure 3-12. Experimental Second-Order DE Versus Determined n_1

3.4.2 Determination of the Film Nonlinearity

The derived second-order results have been used to invert diffraction data to determine the nonlinear response of dichromated gelatin. The procedure is to make gratings at incremental exposure levels; measure the first-order DE at the first BA; then measure the second-order DE at the second BA. This data can be inverted using Eqs. 2.45 and 3.24 to find n_1 and n_2, and an experimentally determined plot of the first and second-order index modulations versus exposure can be made. An example of such results for a plate sensitized with a 1 1/2% solution of ammonium dichromate is shown in Fig. 3-13 (32). Note that the values of n_2 are negative. The first-order index modulation achievable is quite large. The nonlinearity is actually rather small except for high exposures. This fact makes the effects of double diffraction very important in dichromated gelatin.

3.4.3 Angular Selectivity

A representative plot of the experimentally measured angular selectivity for second-order readout is shown in Fig. 3-14. The readout angle is varied by simply rotating the plate. The grating has a fundamental grating frequency of approximately 925 1/mm. The readout angles are internal. The theoretical results are also given, where n_1 and n_2 were determined by inverting the DE at the BA. The value of D was varied to fit to the second-order AS. As Fig. 3-14 shows, the same parameters predict a first-order DE that agrees with experiment.

3.5 Extension of Analytical Results for First-Order Readout

We can increase the accuracy of the analytical results for readout near the first BA by including more orders. This is especially true for gratings of moderate Q factor or very high index

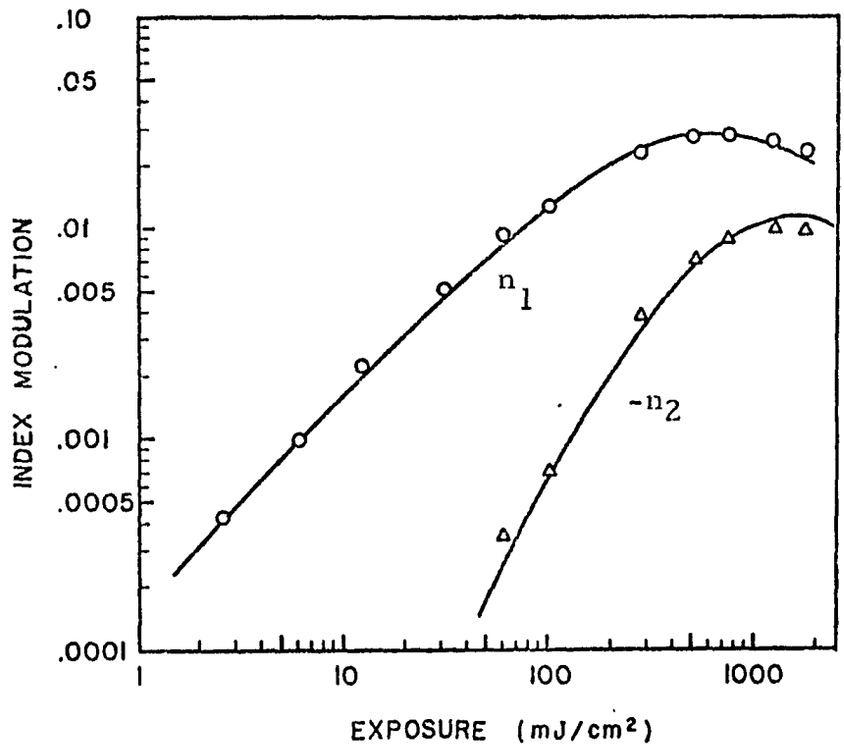


Figure 3-13. Nonlinear Film Response of Dichromated Gelatin

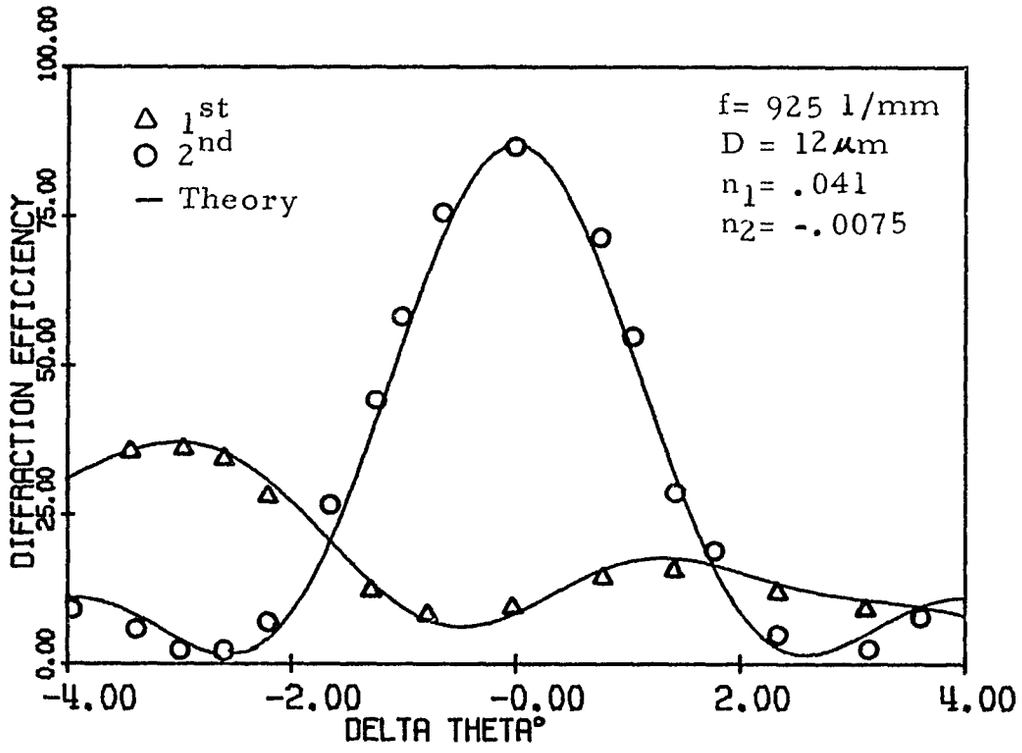


Figure 3-14. Angular Selectivity for Second Order Readout: Comparison of Experiment and Theory

modulation. Unfortunately, at the first BA, the dispersion associated with the conjugate first (Fig. 3-1) is the same as that for the second order, and in general, these orders can be of comparable importance. However, from the dispersion curves, we expect that in the angular region between $\theta_o = 0$ and the first Bragg angle, the conjugate first order (+1) is more important, while between the first and second Bragg angles, the second is more important. Numerical results verify these conclusions. Thus, we can perform a three-wave analysis near the first BA including the appropriate extra order. The coupling matrix will be a 3 × 3 matrix and we can use directly the general results derived in the Appendix.

For example, suppose we include the zero, first and conjugate first orders of spatial frequencies f_o, $f_o - f$ and $f_o + f$, respectively. Then, from the general coupling matrix derived in Chapter 2 (Eq. 2.22) we have the truncated form

$$\underset{\sim}{H} = \begin{bmatrix} 1 & i\frac{\delta_1}{c_1} e^{i\Phi_{-1}} & i\frac{\delta_1}{c_2} e^{i\Phi_1} \\ i\frac{\delta_1}{c_o} & e^{i\Phi_{-1}} & i\frac{\delta_2}{c_2} e^{i\Phi_1} \\ i\frac{\delta_1}{c_o} & i\frac{\delta_2}{c_1} e^{i\Phi_{-1}} & e^{i\Phi_1} \end{bmatrix} \qquad 3.42$$

where

$$\Phi_{-1} = (2\pi n_o \Delta z/\lambda)(\cos\theta_{-1} - \cos\theta_o) \qquad 3.43$$

$$\Phi_1 = (2\pi n_o \Delta z/\lambda)(\cos\theta_1 - \cos\theta_o) \qquad 3.44$$

and the amplitude vector is $\begin{bmatrix} A_0 \\ A_{-1} \\ A_1 \end{bmatrix}$. As a special case, consider readout at $\theta_0 = 0$ (equal angular distance from each of the first BA) with $n_2 = 0$. Then, $\cos \theta_1 = \cos \theta_{-1}$, so $\Phi_{-1} = \Phi_1$ (see Fig. 3-1) and we have the special case (from the Appendix, A. 36)

$$DE_{-1} = DE_1 = \frac{\gamma^2}{\xi^2 + 2\gamma^2} \sin^2 [\xi^2 + 2\gamma^2]^{1/2} \qquad 3.45$$

where $\gamma = \pi n_1 D/\lambda(\cos \theta_1)^{1/2}$ and $\xi = 2\pi n_0 D/\lambda(\cos \theta_1 - \cos \theta_0) \simeq -\pi\lambda Df^2/2n_0$.

We can use the above result to show that the thickness criterion is, in fact, dependent upon the level of modulation, as well as upon the Q factor. For the two first orders to have no angular region of overlap (i.e., to have a thick grating), it is necessary that the DE of each order be zero at $\theta_0 = 0$ by virtue of $\xi^2 + 2\gamma^2$ being large. Suppose $[\xi^2 + 2\gamma^2]^{1/2} \geq 3\pi$ (no overlap before the third sidelobe minima). Note that $|\xi| = Q/2$. Therefore, we require

$$Q^2/4 + 2\gamma^2 \geq 9\pi^2 \qquad 3.46$$

If we restrict γ to values required to reach the first maximum at the first BA, $\gamma = \pi/2$, then

$$Q^2/4 + \frac{\pi^2}{2} \geq 9\pi^2$$

$$Q \geq 6\pi$$

which is comparable to the criterion found in Chapter 2 by including many orders. Note, however, that the thickness criterion in

general depends upon the level of modulation (Eq. 3.46) as shown by others (18). This is because high modulation tends to overcome dispersive effects and diffraction occurs even for large angles off the BA.

3.6 Summary and Conclusions

Using the method of TGD, we have derived analytical expressions for the DE of the first and second orders for readout angles near the second BA of a thick, holographic grating. The results demonstrate the importance of double diffraction by the fundamental grating in addition to diffraction by the harmonic component in producing the second order. For a pure-sinusoidal grating, we find that an auxilliary phase condition between the zero and first orders must be satisfied if the second order is to be made 100% efficient. This condition is independent of index modulation. For a given thickness and readout wavelength, it places a restriction on the grating frequencies for which the second order can be made 100% efficient. Because of the π phase shift between the first and second-order index modulations in a material like dichromated gelatin, the effects of double diffraction and diffraction by the harmonic grating combine to give a strong second order. If n_2 is positive with respect to n_1, the two mechanisms oppose each other.

The AS of the second order is about twice as narrow as that of the first order near the first BA and is broadened somewhat in the case where the second order is produced primarily by double diffraction. The transition between the thin and thick regimes for readout at the second BA of a sinusoidal grating is very oscillatory because of the periodic dependence of double diffraction upon the Q factor. While a Q factor of >20 is sufficient to suppress all but the zero, first and second orders, a value more than 10 times that is

necessary to also suppress the first order. We might use the criterion that a grating can be considered thick with respect to readout near its m^{th} BA if only the zero and m^{th} orders are important (39). But this criterion is overly restrictive for typical gratings with moderate Q factors. That is, for sinusoidal gratings with given λ and D, the fundamental grating frequency must be $\sqrt{10}$ times larger for the grating to be considered thick for second order readout than that necessary for first order readout, on the basis of the above criterion. As the nonlinearity increases, this difference decreases somewhat, but for typical nonlinearities, it is still rather large. The significance of including three waves is that it allows the analytical results to treat, at modulations levels required to make the second order strong, the same gratings (i.e., same f and D) that are considered thick with respect to first order readout. It is generally true that highly modulated, nearly sinusoidal gratings act less "thick," in terms of Bragg suppression, at higher-order BAs. For example, when the constructed gratings were readout at the third BA, there was small but measurable diffraction into the first, second and third orders.

The experimental results from gratings constructed in dichromated gelatin film are in good agreement with the analytical results. In particular, the strong grating frequency dependence of the second order DE for readout at its BA has been demonstrated. We have also shown that for moderate Q factors and exposures sufficient to produce a strong second order, DE_1 is not negligibly small for readout near the second BA. The derived results have been used to invert diffraction efficiency data to measure the nonlinear film response of dichromated gelatin film.

CHAPTER 4

PROPAGATION IN STRONGLY-COUPLED MULTIPLE THICK GRATINGS

A problem of considerable interest for various applications of holography, including optical data storage and optical elements, is that of the properties of strongly-coupled multiple gratings recorded in the same thick emulsion. Such gratings are strongly coupled because they share a common or almost common construction angle. In this chapter we use the method of thin-grating decomposition to analyze propagation in such structures. The basic coupling mechanisms of multiple thick gratings are investigated. Analytic results are derived for the efficiency of the diffracted orders of two superimposed gratings with arbitrary relative slope and for arbitrary readout angles. We examine the necessary difference in the almost common construction angles to effectively decouple the two gratings. An interesting property of double gratings which we predicted is the possibility of 100% cross coupling of energy between the two gratings (14). We show that this phenomenon can be understood as second-order readout of the two-grating combination and is thus similar to second-order readout of single gratings (36). We also examine the properties of the three grating structure made by simultaneously interferring three plane waves. The derived results are verified by extensive experimental results from double gratings constructed in dichromated gelatin. In particular, the predicted 100% cross-coupled order has been measured. Some of the theoretical and experimental work discussed here has been published (14, 15), although we previously calculated the diffraction efficiencies numerically.

4.1 Background

The angular selectivity of a thick grating is frequently used to Bragg-angle multiplex several holograms in the same thick emulsion (16). Each hologram is stored as a modulated grating structure whose Bragg angle is sufficiently different from the others so that a particular hologram can be readout with high DE with little or no effect from the other holographic structures. This technique is of particular importance for optical data storage (43, 28). It has also been used to make multicolor holograms (44) and multiply-exposed optical elements (45, 11, 46).

Despite the frequent use of multiply-exposed thick gratings, there has been no general analysis of their properties. Baugh has used a perturbation approach to analyze diffraction by a thick hologram made by interferring a plane reference wave with multiple signal waves (38). He used this approach to model thick holograms of general objects and assumed that the gratings constructed by any two signal waves were ignorable. He analyzed only the case of readout exactly at the same angle as the reference beam. This angle is the common Bragg angle for each of the gratings.

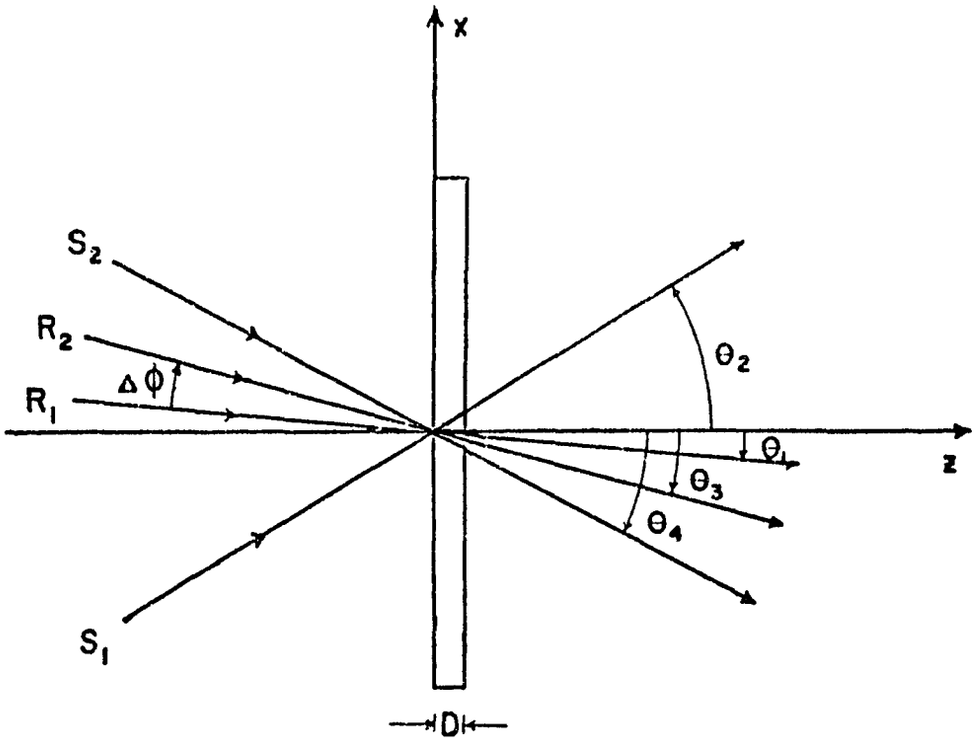
A thick grating constructed with two fringe structures of arbitrary spatial frequency and orientation (slant) is more complicated than the single grating. If two gratings recorded in the same emulsion have a common or nearly common Bragg angle, then for a readout wave in that angular region, light will be diffracted by both gratings. Because of the thickness of the emulsion, depletion of the incident wave by one grating leaves less energy in the zero order to be diffracted by the other grating. Furthermore, for certain readout angles, there is the possibility that light diffracted by one structure will subsequently be diffracted by the other. In both cases, it is necessary to consider the combined effects of both

gratings, including the coupling between them to determine the total field that exits from the emulsion. In the case of Bragg-angle multiplexing, the intention is to make the Bragg angles sufficiently different so that the structures are decoupled; i.e., there is no overlap in the angular regions for which significant diffraction occurs for each of the holograms. While we analyze for simplicity, the case of plane gratings, the results derived are applicable qualitatively to holograms of arbitrary objects as is typically the case in Bragg-angle multiplexing.

4.2 Incoherent Superposition Construction I

We consider the double grating that is constructed holographically as shown in Fig. 4-1. Plane waves R_1 and S_1 and subsequently R_2 and S_2 interfere to create two sets of fringes (referred to as grating 1 (G_1) and grating 2 (G_2), respectively) throughout the volume of the emulsion. There is no interference between S_1 and S_2 or R_1 and R_2; thus, the result is an incoherent superposition of two gratings (Fig. 4-1b). Because we assume a readout wavelength equal to the construction wavelength, the Bragg angles for each of the gratings correspond to the angles of either of the construction beams for that grating. The construction waves are assumed to be infinite plane waves, with propagation vectors in the xz plane. Therefore, there is no variation along the y direction of the emulsion. R_1 and R_2 are separated in angle by $\Delta\phi$ ($\Delta\phi$ is positive for the case depicted in Fig. 4-1), which is the difference in the nearly equal Bragg angles for the two gratings. For $\Delta\phi$ small, we expect effective diffraction directly from the readout beam by each grating for an incident wave in the angular region of the nearly equal Bragg angles. We refer to this coupling between the two gratings through the zero-order wave as direct coupling. In addition, for readout angles approximately equal to θ_2, for

(a)



(b)

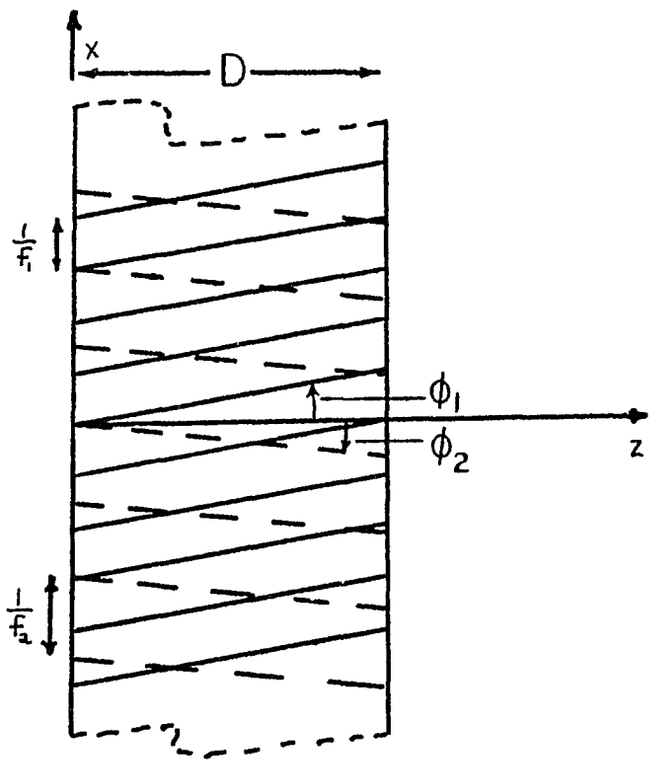


Figure 4-1. Geometry for Incoherent Superposition I

example, the diffracted wave from G_1 is near the Bragg angle of G_2 and may be subsequently diffracted by it before emerging from the emulsion. The result is a diffracted wave that emerges at about θ_4. This coupling between the two gratings via a diffracted wave is referred to as cross coupling. We shall see that this double-diffraction process is very similar to that for second-order readout of a pure-sinusoidal single grating. However, it is much stronger because the differential dispersion of the intermediate step can be made zero for $\Delta\phi = 0$. In both the direct and cross-coupling readout modes, there are two diffracted orders because we assume that the Q factors for the individual gratings are large enough that the conjugate and higher orders of the individual gratings, as well as other multiply-diffracted orders, are negligible. Also, in both cases, the effect of G_2 is generally to decrease the diffraction due to G_1 by either depleting the zero-order wave directly (direct coupling) or the first-order diffracted wave (cross coupling). Although most of the discussion deals with the case where the readout and construction wavelengths are the same, the general results derived are valid for arbitrary readout wavelengths.

For the two-grating incoherent superposition, the total exposure can be written as

$$E(x, z) = E_1\left\{1 + r_1 \cos\left[2\pi f_1(x - x_1(z))\right]\right\} + E_2\left\{(1 + r_2 \cos 2\pi f_2(x - x_2(z))\right\} \qquad 4.1$$

where E_j and r_j are the average exposure and modulation, respectively; f_j is the spatial frequency in any z = constant plane, and $x_j(z) = z \tan \phi_j$ is the lateral shift of the fringes at z relative to z = 0 due to fringe slope, all for the j^{th} thick grating (j = 1, 2). The fringe slopes are $\phi_1 = (\theta_1 + \theta_2)/2$ and $\phi_2 = (\theta_3 + \theta_4)/2$. For the recording material, we consider a pure-phase material and assume

a linear relationship between exposure and Δn, $\Delta n = KE$. For only two superpositions and low exposures, this has been shown to be a good assumption for dichromated gelatin (32). Because we are only interested in first-order readout and consider thick gratings, nonlinearities will be unimportant anyway. (We must be careful to avoid a construction geometry, in which one of the construction angles corresponds to a second BA of another grating.)

The spatially modulated refractive index can therefore be written as

$$n(x, z) = n_o + n_1 \cos 2\pi f_1(x - x_1(z)) + n_2 \cos 2\pi f_2(x - x_2(z)) \quad 4.2$$

where n_j is the first-order index modulation of grating G_j. We stress that throughout this chapter, n_2 is the first order index modulation of G_2 and not a film generated second-order modulation as in Chapter 3. The amplitude transmittance of the m^{th} thin slab is

$$T_A(x, m) = \exp\left[i\frac{2\pi n(x, m)}{\lambda \cos \theta_i}\right]$$

$$= \sum_{q_1=-\infty}^{\infty} (i)^{q_1} J_{q_1}\left(\frac{2\pi n_1 \Delta z}{\lambda \cos \theta_i}\right) \exp\left\{i\, 2\pi q_1 f_1[x - x_1(m)]\right\}$$

$$\times \sum_{q_2=-\infty}^{\infty} (i)^{q_2} J_{q_2}\left(\frac{2\pi n_2 \Delta z}{\lambda \cos \theta_i}\right) \exp\left\{i 2\pi q_2 f_2[x - x_1(m)]\right\}$$

$$T_A(x, m) \simeq 1 + i\frac{\pi n_1 \Delta z}{\lambda \cos \theta_i}\Big\{\exp\left(i\, 2\pi f_1[x - x_1(m)]\right)$$

$$+ \exp\left(-i\, 2\pi f_1[x - x_1(m)]\right)\Big\}$$

(Eq. 4.3 concluded on following page)

$$+ i\frac{\pi n_2 \Delta z}{\lambda \cos \theta_i}\left\{\exp\left(i\,2\pi f_2[x - x_2(m)]\right)\right.$$

$$\left. + \exp\left(-i\,2\pi f_2[x - x_2(m)]\right)\right\} \qquad 4.3$$

where we have retained only first-order terms in Δz.

Following the method of TGD developed in Chapter 2, we now derive the coupling matrix for the significant propagating waves in the two grating structure described above. For readout in either the direct or cross-coupling modes, there are three significant orders. The coupling matrix is 3×3 and we can use the general results derived in the Appendix for diagonalizing the matrix and doing the necessary matrix multiplication. The angular regions of readout for the two modes are different, so we can examine the effects of direct coupling and cross coupling separately.

4.2.1 Direct Coupling

A diagram of the propagation directions for readout in the direct-coupling mode is shown in Fig. 4-2. An incident wave, P_o, in the angular region of the nearly common Bragg angles is strongly diffracted by each of the two gratings generating the diffracted waves P_1 and P_2. For an incident plane wave of spatial frequency (x component) f_o, the diffracted waves have spatial frequencies $F_1 = f_o + f_1$ and $F_2 = f_o - f_2$. Other orders can be included, but for the case where each grating has a large Q factor, their effect was found to be negligible. This fact is verified in the experimental results. The matrix elements H_{jk} that describe the coupling between these three orders can be found from the amplitude transmittance function in Eq. 4.3 by simply invoking the thin grating equation $F_j = F_k \mp f_{1,2}$ and including the propagation factor over the thin slab thickness, Δz. That is, the matrix element ${}_mH_{jk}$ is the product of the propagation factor of the plane wave of spatial

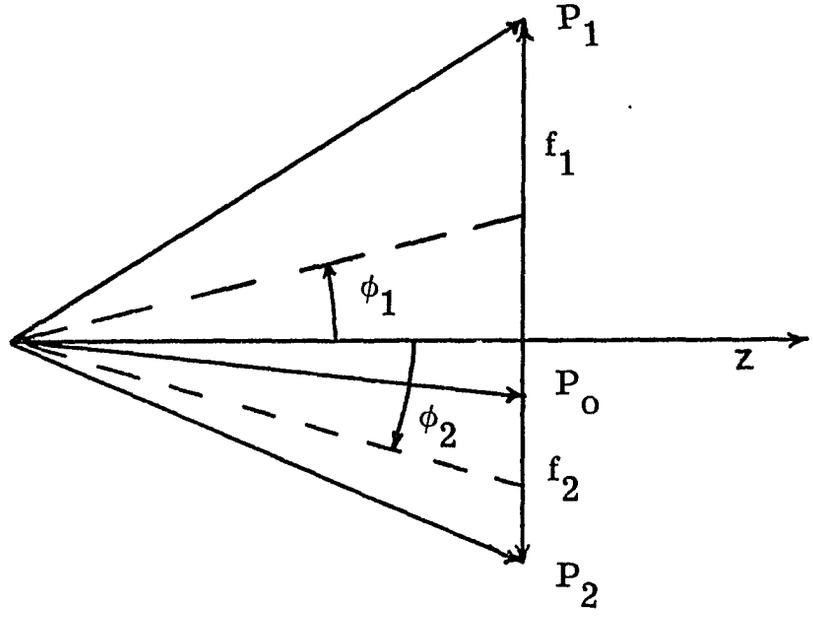


Figure 4-2. Direct-Coupling Readout

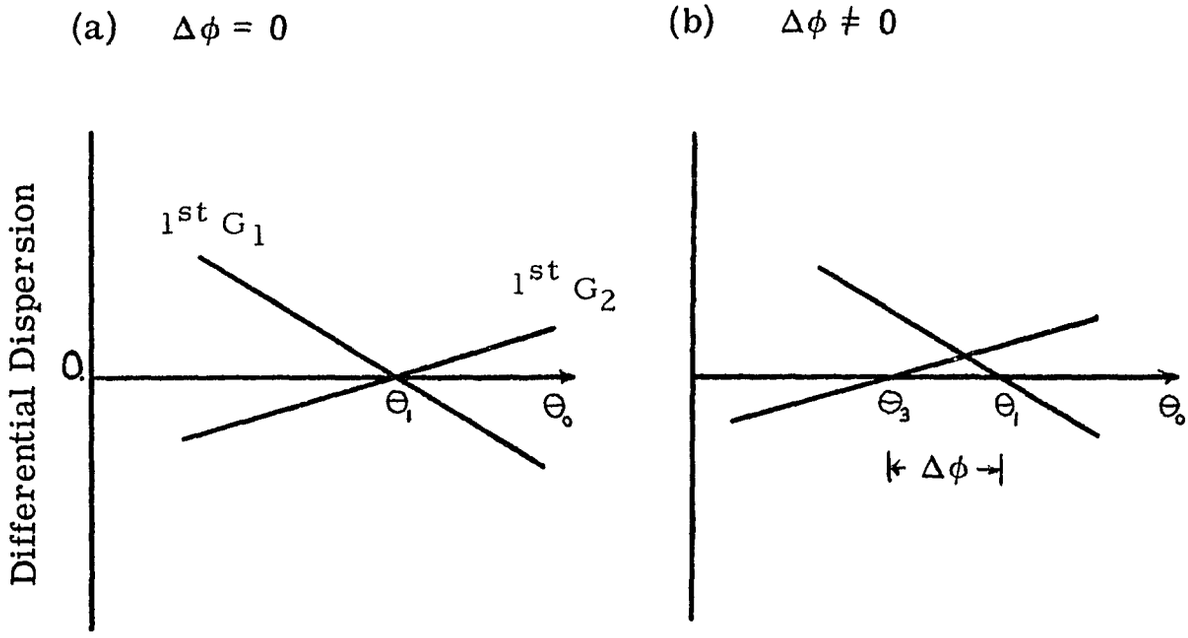


Figure 4-3. Differential Dispersion for Direct-Coupling Readout

frequency F_k and the coefficient of the amplitude transmittance term of spatial frequency f_i, where $f_i = F_j - F_k$. The coupling matrix is

$$\underset{\sim}{m}H = \begin{bmatrix} e^{i\alpha_o} & i\frac{\delta_1}{c_1} e^{i\alpha_1} e^{i\beta_1(m)} & i\frac{\delta_2}{c_2} e^{i\alpha_2} e^{-i\beta_2(m)} \\ i\frac{\delta_1}{c_o} e^{i\alpha_o} e^{-i\beta_1(m)} & e^{i\alpha_1} & 0 \\ i\frac{\delta_2}{c_o} e^{i\alpha_o} e^{i\beta_2(m)} & 0 & e^{i\alpha_2} \end{bmatrix} \quad 4.4$$

where

$$\beta_j(m) = 2\pi f_j m \Delta z \tan \phi_j \qquad j = 1, 2$$

$$\delta_j = \frac{\pi n_j \Delta z}{\lambda} \qquad j = 1, 2 \quad 4.5$$

$$\alpha_q = \frac{2\pi n_o}{\lambda} \cos \theta_q \quad 4.6$$

$$F_o = f_o,\ F_1 = f_o + f_1,\ F_2 = f_o - f_2 \quad 4.7$$

$$c_q = \cos \theta_q = \left[1 - \left(\frac{\lambda F_q}{n_o}\right)^2\right]^{1/2} \quad 4.8$$

The corresponding amplitude vector is $\underset{\sim}{A} = \begin{bmatrix} A_o \\ A_1 \\ A_2 \end{bmatrix}$, where A_q is the total amplitude of the plane wave of spatial frequency F_q. In general, the coupling matrix depends upon the slab index m because of fringe slope. However, just as in the single grating case, this dependence can be removed by calculating the difference in the propagation factors between the zero order and the diffracted order of G_j relative to the direction of the corresponding fringe planes rather than relative to the z direction. Thus, the coupling matrix for each slab can be written as

$$\underset{\sim}{H} = \begin{bmatrix} 1 & i\frac{\delta_1}{c_1} e^{i\Phi_1} & i\frac{\delta_2}{c_2} e^{i\Phi_2} \\ i\frac{\delta_1}{c_o} & e^{i\Phi_1} & 0 \\ i\frac{\delta_2}{c_o} & 0 & e^{i\Phi_2} \end{bmatrix} \qquad 4.9$$

where

$$\Phi_1 = \frac{2\pi n_o \Delta z}{\lambda}[\cos(\theta_1 - \phi_1) - \cos(\theta_o - \phi_1)], \qquad 4.10$$

$$\Phi_2 = \frac{2\pi n_o \Delta z}{\lambda}[\cos(\theta_2 - \phi_2) - \cos(\theta_o - \phi_2)], \qquad 4.11$$

and the values of θ_q are given by $\sin\theta_q = \lambda F_q / n_o$. The Φ_j are the differences in the propagation factors of the zero and j^{th} diffracted orders measured relative to the direction of the j^{th} set of fringe planes. There is no grating component that connects P_1 and P_2; therefore, $H_{23} = H_{32} = 0$.

The difference in cosine factors included in the brackets in Φ_1 and Φ_2 is sketched in Fig. 4-3a ($\Delta\phi = 0$) and Fig. 4-3b ($\Delta\phi \neq 0$) for two gratings with different spatial frequencies. The abscissa is the readout angle θ_o. For $\Delta\phi = 0$, the differential spatial dispersion associated with each first order is zero for readout at the common construction angle, $\theta_1 = \theta_3$, because the zero order and each of the diffracted orders propagate symmetrically about its respective fringe planes (Fig. 4-2). The coupling between the two gratings is therefore very strong. As $\Delta\phi$ is made nonzero, the differential dispersion terms are no longer simultaneously small for any readout angle and the coupling between the two gratings decreases because the angular regions over which effective diffraction occurs for each grating no longer overlap. Thus, the coupling between the two gratings results from the dependence of Φ_1 and Φ_2 upon the readout angle θ_o. We shall see that the angular selectivity and decoupling of double gratings depends very strongly upon the relationship between Φ_1 and Φ_2 as a function of θ_o. The dispersion terms for higher or multiply-diffracted orders are very large for the readout angles shown in Fig. 4-3. That is the reason these other orders are not important.

The coupling matrix of Eq. 4.9 is a special case of the general 3×3 matrix in the Appendix with $\delta_1' = \delta_1$, $\delta_2' = \delta_2$, $\delta_3' = 0$ and Φ_1 and Φ_2 as given in Eqs. 4.10 and 4.11. The expressions for the DE of the first orders of G_1 and G_2 are therefore given by Eqs. A.25 and A.26, respectively with

$$\xi_1 = \frac{N\Phi_1}{2} = \frac{\pi n_o D}{\lambda}[\cos(\theta_1 - \phi_1) - \cos(\theta_o - \phi_1)] \qquad 4.12$$

$$\xi_2 = \frac{N\Phi_2}{2} = \frac{\pi n_o D}{\lambda}[\cos(\theta_2 - \phi_2) - \cos(\theta_o - \phi_2)] \qquad 4.13$$

$$\gamma_1 = \frac{N\delta_1}{(c_o c_1)^{1/2}} = \frac{\pi n_1 D}{\lambda (c_o c_1)^{1/2}}; \gamma_2 = \frac{N\delta_2}{(c_o c_2)^{1/2}} = \frac{\pi n_2 D}{\lambda (c_o c_2)^{1/2}} \qquad 4.14$$

For the special case of $\Delta\phi = 0$ and readout at the common BA, θ_1, $\Phi_1 = \Phi_2 = 0$, and the results reduce to (Eq. A.37)

$$DE_1 = \frac{\gamma_1^2}{\gamma_1^2 + \gamma_2^2} \sin^2 \left(\gamma_1^2 + \gamma_2^2\right)^{1/2} \qquad 4.15$$

$$DE_2 = \frac{\gamma_2^2}{\gamma_1^2 + \gamma_2^2} \sin^2 \left(\gamma_1^2 + \gamma_2^2\right)^{1/2} \qquad 4.16$$

in agreement with those obtained by Baugh (38) and others (28, 47) (for this special case only). For $\gamma_1 = \gamma_2 = \frac{\sqrt{2}}{2}\pi$; $DE_1 = DE_2 = 50\%$.

To examine the more general case of arbitrary readout angles and $\Delta\phi \neq 0$, we evaluate and plot the results of the general expressions for the DE using a computer. As a typical example for illustration, we use the following parameters (Fig. 4-1): $\theta_1 = \theta_3 = 0^o$, $\theta_2 = 20^o$, $\theta_4 = -16^o$, $\lambda = .488\ \mu m$, $n_o = 1.52$ and $D = 16\ \mu m$. As $\Delta\phi$ is varied, both θ_3 and θ_4 are changed to keep the angle between them constant. The grating spatial frequencies are $f_1 = 1065$ 1/mm and $f_2 = 860$ 1/mm. To allow comparison with the single grating case, we use as the grating strength unit γ_1^o, which is that necessary to obtain 100% DE by G_1 for readout at its BA in the absence of G_2. For the angular selectivity results, we normalize the angular distance from the BA by the angular half-width at cutoff of G_1 for the single grating case, at a modulation of γ_1^o (found from Eq. 2.45, ≈2.7). The offset angle is also normalized by this value.

In Fig. 4-4, we plot the computed AS of the diffracted order of G_1 for several levels of modulation with the two grating strengths

$$\gamma_1 = \frac{N\delta_1}{(c_o c_1)^{1/2}} = \frac{\pi n_1 D}{\lambda (c_o c_1)^{1/2}}; \quad \gamma_2 = \frac{N\delta_2}{(c_o c_2)^{1/2}} = \frac{\pi n_2 D}{\lambda (c_o c_2)^{1/2}} \qquad 4.14$$

For the special case of $\Delta\phi = 0$ and readout at the common BA, θ_1, $\Phi_1 = \Phi_2 = 0$, and the results reduce to (Eq. A.37)

$$DE_1 = \frac{\gamma_1^2}{\gamma_1^2 + \gamma_2^2} \sin^2 \left(\gamma_1^2 + \gamma_2^2\right)^{1/2} \qquad 4.15$$

$$DE_2 = \frac{\gamma_2^2}{\gamma_1^2 + \gamma_2^2} \sin^2 \left(\gamma_1^2 + \gamma_2^2\right)^{1/2} \qquad 4.16$$

in agreement with those obtained by Baugh (38) and others (28, 47) (for this special case only). For $\gamma_1 = \gamma_2 = \frac{\sqrt{2}}{2}\pi$; $DE_1 = DE_2 = 50\%$.

To examine the more general case of arbitrary readout angles and $\Delta\phi \neq 0$, we evaluate and plot the results of the general expressions for the DE using a computer. As a typical example for illustration, we use the following parameters (Fig. 4-1): $\theta_1 = \theta_3 = 0^o$, $\theta_2 = 20^o$, $\theta_4 = -16^o$, $\lambda = .488\ \mu m$, $n_o = 1.52$ and $D = 16\ \mu m$. As $\Delta\phi$ is varied, both θ_3 and θ_4 are changed to keep the angle between them constant. The grating spatial frequencies are $f_1 = 1065$ 1/mm and $f_2 = 860$ 1/mm. To allow comparison with the single grating case, we use as the grating strength unit γ_1^o, which is that necessary to obtain 100% DE by G_1 for readout at its BA in the absence of G_2. For the angular selectivity results, we normalize the angular distance from the BA by the angular half-width at cutoff of G_1 for the single grating case, at a modulation of γ_1^o (found from Eq. 2.45, ≈2.7). The offset angle is also normalized by this value.

In Fig. 4-4, we plot the computed AS of the diffracted order of G_1 for several levels of modulation with the two grating strengths

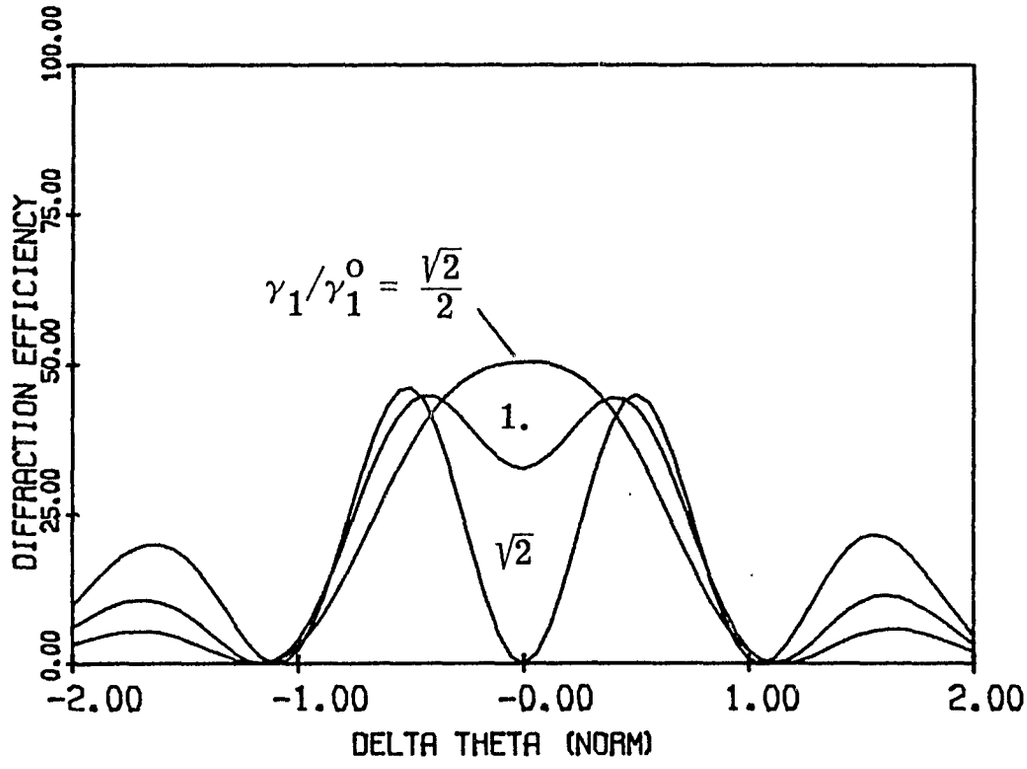


Figure 4-4. Angular Selectivity for Direct-Coupling Readout, $n_1 = n_2$

equal ($\gamma_1 = \gamma_2$), and $\Delta\phi = 0$. The results for the diffracted order of G_2 are of similar form, but of different width because of the lower frequency of G_2. Perhaps the most striking feature of the AS is that the double gratings tend to overmodulate easily; the angles of maximum DE move symmetrically off the BA. This can be shown to be due to the fact that the sum of the dispersion terms for G_1 and G_2 remain small as the readout angle moves off the common construction angle because of the different signs of the dispersion terms (Fig. 4-3a). The width of the AS curve is slightly greater than for the single grating case, due to the perturbation of G_2. The sidelobe level increases with the modulation level as in the single grating case. The AS that results as γ_2 is decreased, are given in Ref. 15. A ratio of $\gamma_2/\gamma_1 = .1$, is sufficient to extinguish the effect of G_2.

Of particular interest is the angular decoupling of the two gratings that results from making $\Delta\phi$ nonzero. This is the question when determining the necessary angle of separation for Bragg-angle multiplexing. In Fig. 4-5, we plot the computed AS for each of the diffracted orders for $\gamma_1 = \gamma_2 = \gamma_1^o$ and for a normalized offset, $\Delta\phi = 0$(a), .5(b) and 1.5(c). For $\Delta\phi = 0$ (this is the same case shown in Fig. 4-4, except here we show the DE of each of the two orders); note that the increase in DE off the common BA is greater for the lower frequency grating (G_2). This difference becomes even more pronounced as the difference in the grating frequencies is increased. For a normalized offset of .5, there is substantial decoupling. Note that the diffracted order of the lower frequency grating (G_2) tends to return to a higher maximum DE more rapidly with offset than that of the higher grating frequency (G_1). A very interesting aspect of the decoupling process is that the maximum DE of each grating is not achieved for readout exactly

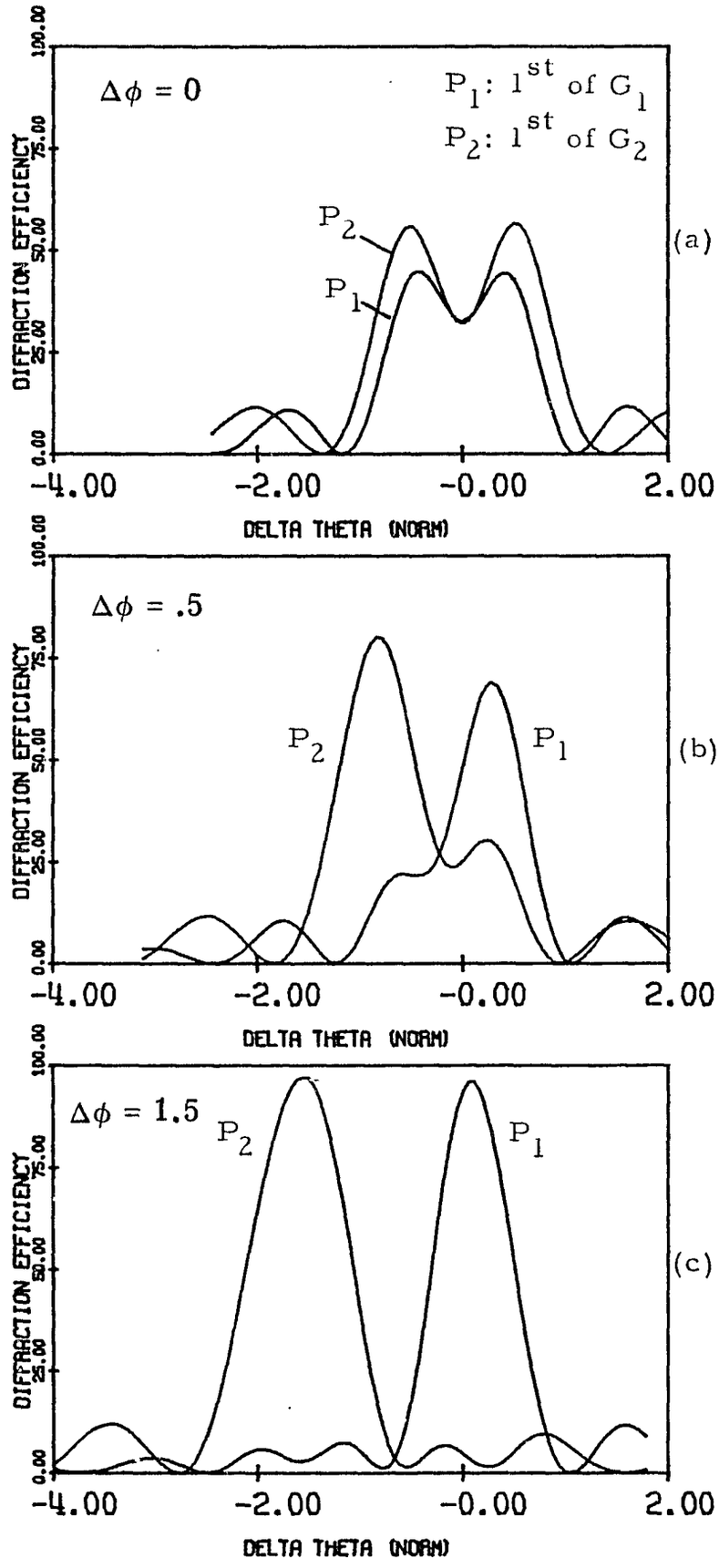


Figure 4-5. Decoupling with Offset: Direct-Coupling Mode, $\gamma_1 = \gamma_1^o$

at its respective BA ($\Delta\theta = 0$ for G_1 and $\Delta\theta = -\Delta\phi$ for G_2), because of the perturbation of the other grating. The angular difference between the diffraction maxima is greater than the BA difference. However, as the offset is increased and the coupling is reduced, the readout angles of maximum DE approach the respective BAs as expected. For $\Delta\phi = 1.5$, there is no overlap in the mainlobes of the two AS curves. Each grating is nearly 100% efficient for a readout angle very near its BA. The difference in width results from the different grating frequencies. For two gratings with the same grating frequency, an offset of $\Delta\phi \simeq 1$ is sufficient to make each grating nearly 100% efficient. The offset here (normalized by the half-width of G_1) is larger because the half-width of G_2 is greater. Thus, we find that one can have sufficient decoupling for an angular separation somewhat smaller than what one might expect from single grating theory. This is because the mainlobes in the interaction region are somewhat narrower than in the single-grating case. Based on intuitive arguments, one might expect a necessary normalized offset of 2 or greater. Computed results indicate that for this level of modulation $\left(\gamma_1 \simeq \gamma_1^o\right)$, and a given offset $\Delta\phi$, we can not significantly increase the DE by increasing the modulation.

The necessary offset to decouple the two gratings depends upon the level of modulation, as well as upon the grating frequencies and thickness. Intuitively, this is expected. For very low modulation, there is very little depletion of the incident wave and therefore effectively no coupling between the two gratings. For readout at the BA of G_1, $\xi_1 = 0$. ξ_2, which depends upon the offset $\Delta\phi$ and the frequency of G_2 (for $\Delta\phi \ll 1$, $\xi_2 = \pi\Delta\phi f_2 \cos\phi_2 D$, where ϕ_2 is the slope of G_2 for no offset), is the only dispersion parameter. Thus, at the BA of G_1, the DE of G_1 is independent of its grating frequency. However, it does depend upon the frequency

of G_2 and the offset between the BAs. The extent to which the maximum DE of G_1 occurs off its BA does depend on f_1 as well as f_2 and $\Delta\phi$. In Fig. 4-6, we plot the calculated DE of G_1 for readout at its BA as a function of $2\xi_2$. The results are computed for several levels of modulation $\left(\gamma_1/\gamma_1^o\right)$ with $\gamma_1 = \gamma_2$. For lower modulations, a smaller total differential dispersion (i.e., smaller offset and/or lower f_2) is needed to suppress the effect of G_2 and return the DE of G_1 to its single grating value. The DE of G_1 in Fig. 4-6 does not correspond to its maximum except for large $2\xi_2$, because as mentioned, until the gratings are completely decoupled, the DE are not maximized at the BAs. The decoupling for $\gamma_1 = \gamma_1^o$ is initially quite rapid, then proceeds more slowly.

For $\gamma_1 = \gamma_1^o$, the curve in Fig. 4-6 is very similar to that of Fig. 2-6 which shows the maximum first-order DE in the transition from the thin to thick regimes of a single grating. This is interesting but really not too surprising. In the double grating case, the first order of G_2 is the only other important diffracted order and its dispersion term is increased (and its importance at the BA of G_1 reduced) by making the offset between the two gratings nonzero. In the single grating case, the conjugate first and higher orders are important. The spatial dispersion of these orders, which is proportional to $Q/\cos\theta_B$, is increased by increasing the grating frequency (for fixed λ and D). This, of course, has the effect of increasing the angular separation between the Bragg angles, just as increasing $\Delta\phi$ does for double gratings. The decoupling is somewhat more rapid in Fig. 4-6 than in Fig. 2-6 because in the former case, only one order must be suppressed. Again, the Q factor of G_1 is sufficiently large that its higher orders are suppressed.

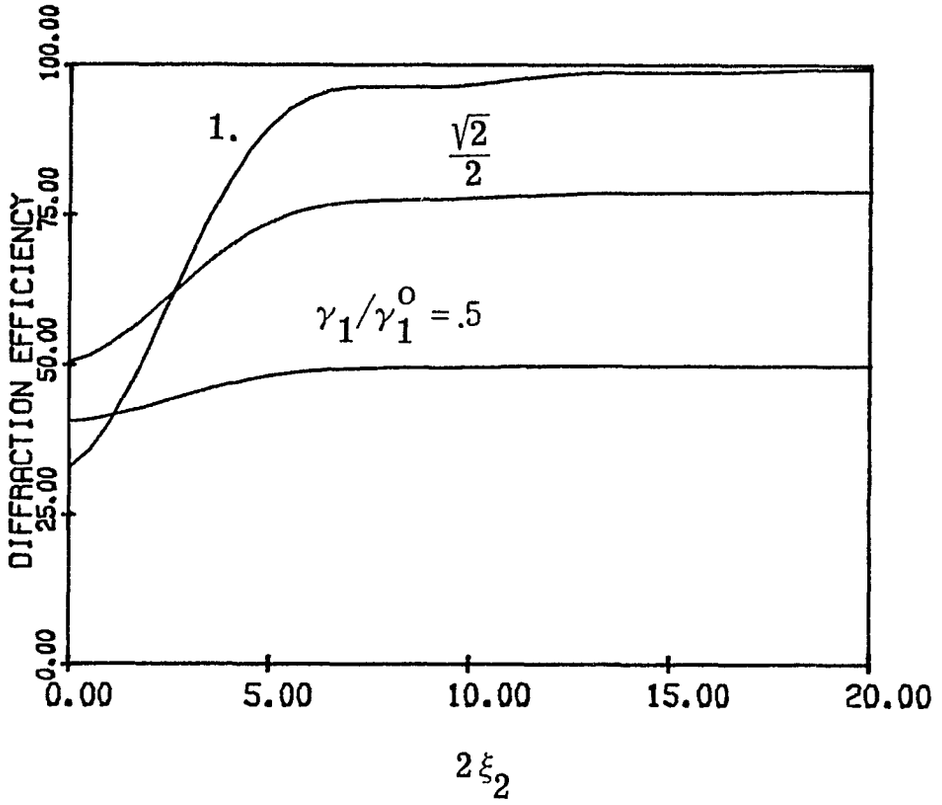


Figure 4-6. Modulation Dependence of Decoupling: DE of G_1 for Readout at Its Bragg Angle Versus the Total Dispersion of the Diffracted Order of G_2

We can also examine the modulation dependence of decoupling by considering readout at an angle between the two BAs. For a readout angle such that $\xi_1 = \xi_2$ (see Fig. 4-3b; this corresponds to the readout angle where the two dispersion curves intersect), the expressions for the DEs simplify considerably (A.36).
Note that the results of Eqs. 4-15 and 4-16 are a special case of these expressions where $\xi_1 = \xi_2 = 0$. For gratings of equal index modulation, the two gratings are equally efficient at this readout angle. If the gratings are to be completely decoupled, the DEs must be zero. One can then use the same procedure used in Chapter 3.5 to determine the necessary value of ξ_1 (and therefore offset $\Delta\phi$) to achieve decoupling for a desired modulation level.

4.2.2 Cross Coupling

Cross coupling of energy from one grating to the other is important for readout about one of the noncommon construction angles (θ_2 or θ_4 in Fig. 4-1), because the diffracted wave of one grating is at, or near the BA of the other grating. A diagram of the propagation directions is shown in Fig. 4-7, where the readout wave is at or near the BA of G_1. The first order of G_1 (P_1) and the cross-coupled order (P_2) have spatial frequencies, $F_1 = f_o - f_1$ and $F_2 = f_o - f_1 - f_2$, respectively, where f_o is the spatial frequency of the readout wave. Note that for the incoherent addition, there is no grating component that directly couples P_o to P_2. Energy reaches the cross-coupled order only by double diffraction, once by G_1 and then by G_2.

From the amplitude transmittance function of Eq. 4.3, the diagram in Fig. 4-7 and the general method of TGD as used in the direct-coupling case, we can simply write down the coupling matrix for the three significant waves

$$\underset{\sim}{H} = \begin{bmatrix} 1 & i\frac{\delta_1}{c_1} e^{i\Phi_1} & 0 \\ i\frac{\delta_1}{c_o} & e^{i\Phi_1} & i\frac{\delta_2}{c_2} e^{i\Phi_2} \\ 0 & i\frac{\delta_2}{c_1} e^{i\Phi_1} & e^{i\Phi_2} \end{bmatrix} \tag{4.17}$$

where

$$\delta_j = \frac{\pi n_j \Delta z}{\lambda} \qquad j = 1, 2 \tag{4.18}$$

$$\Phi_1 = \frac{2\pi n_o \Delta z}{\lambda}[\cos(\theta_1 - \phi_1) - \cos(\theta_o - \phi_1)] \tag{4.19}$$

$$\Phi_2 = \frac{2\pi n_o \Delta z}{\lambda}[\cos(\theta_1 - \phi_1) - \cos(\theta_o - \phi_1)] + \cos(\theta_2 - \phi_2) - \cos(\theta_1 - \phi_2)] \tag{4.20}$$

$$F_o = f_o,\ F_1 = f_o - f_1 \text{ and } F_2 = f_o - f_1 - f_2 \tag{4.21}$$

$$\cos\theta_q = \left[1 - \left(\frac{\lambda F_q}{n_o}\right)^2\right]^{1/2} \tag{4.22}$$

The spatial dispersion term associated with the cross-coupled order, Φ_2, is the sum of that between P_o and P_1 with respect to the fringe planes of G_1 and that between P_1 and P_2 with respect to the fringe planes of G_2. This is also true for the case of the doubly diffracted order for single gratings, except that in the latter case, G_1 and G_2 are identical and there is only a single slope angle.

The geometric part of the differential dispersion terms Φ_1 and Φ_2 are sketched in Fig. 4-8a ($\Delta\phi = 0$) and Fig. 4-8b ($\Delta\phi \neq 0$) versus

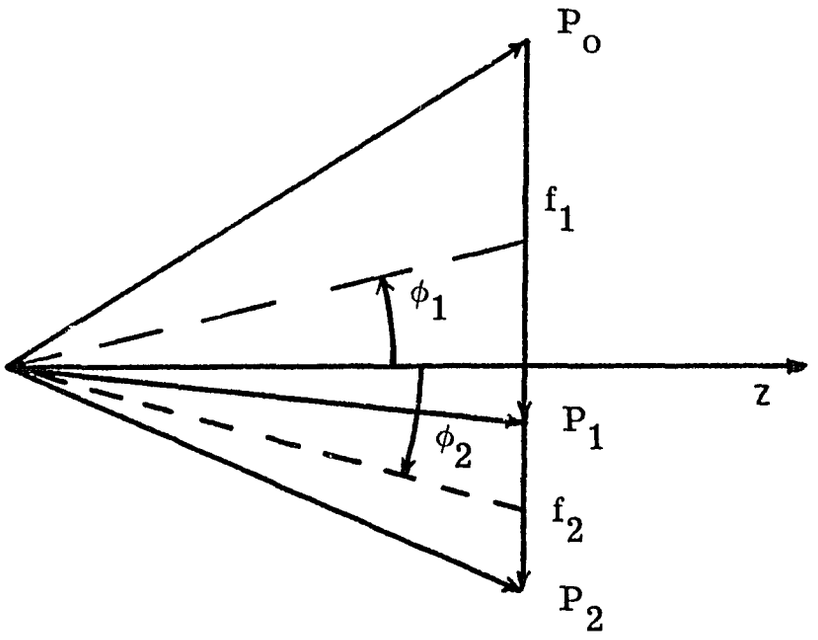


Figure 4-7. Cross-Coupling Readout

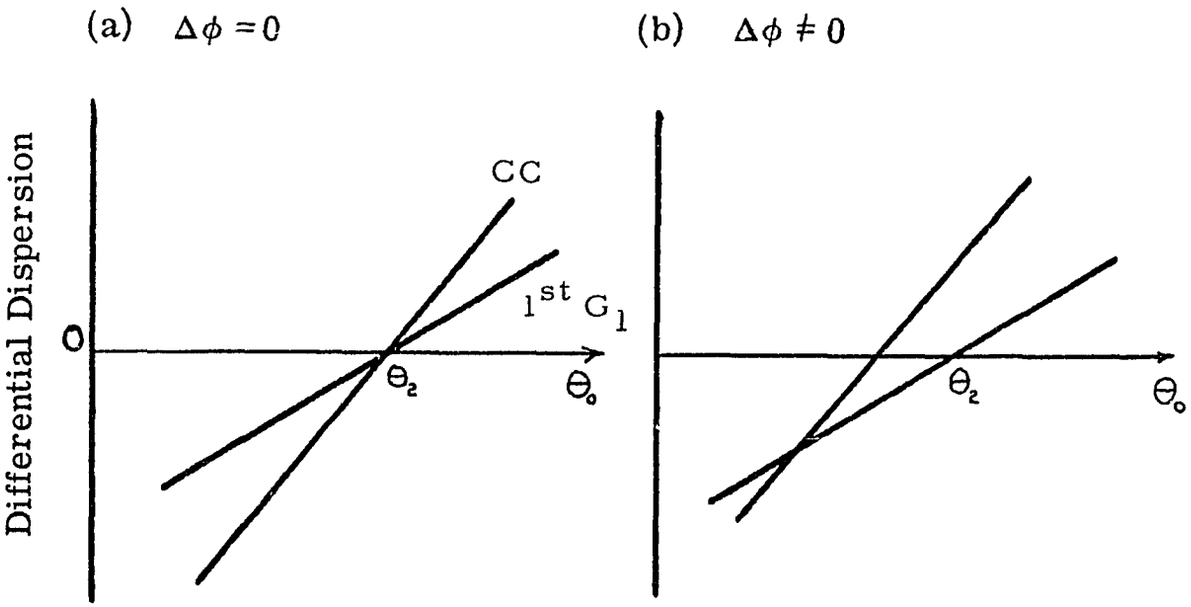


Figure 4-8. Differential Dispersion for Cross-Coupling Readout

the readout angle, θ_o. For $\Delta\phi = 0$, both Φ_1 and Φ_2 are zero for readout at θ_2. For $\Delta\phi \neq 0$, Φ_1 is still zero at the BA of G_1 (θ_2), but Φ_2 is nonzero at that angle. There is, however, still a readout angle for which Φ_2 is zero. Note that the slope of the dispersion curve for the cross-coupled order is greater than that of the first order. This results because the difference in spatial frequency of this order relative to the readout wave is the sum of the frequencies of each of the gratings. The dispersion curve of Fig. 4-8b is very similar to that for second-order readout of a single grating (Fig. 3-1). The coupling matrices are also of the same form (for the pure-sinusoidal single grating, Eq. 3.2 with $n_2 = 0$), except in the double grating case, there are two different gratings with possibly different first-order index modulations.

The angle at which Φ_2 is zero is essentially the second BA of the two grating combination. For $\Delta\phi \neq 0$, the spatial dispersion associated with the intermediate first order is not zero at that angle. This is the same situation as in second-order readout of single gratings. However, for $\Delta\phi = 0$, both the differential dispersion of the double diffraction process (Φ_2) and that of the intermediate step (Φ_1) are zero. The result is that double diffraction in double gratings can be very strong.

The coupling matrix of Eq. 4.17 is a special case of that in the Appendix with $\delta_1' = \delta_1$, $\delta_2' = 0$ and $\delta_3' = \delta_2$. Therefore, the general expressions for the DE of the first and cross-coupled orders are given by A.25 and A.26, respectively, with

$$\gamma_1 = \frac{N\,\delta_1}{(c_o c_1)^{1/2}} = \frac{\pi n_1 D}{\lambda (c_o c_1)^{1/2}};\ \gamma_3 = \frac{N\,\delta_2}{(c_o c_1)^{1/2}} = \frac{\pi n_2 D}{\lambda (c_o c_2)^{1/2}} \qquad 4.23$$

$$\xi_1 = \frac{N\Phi_1}{2} = (\pi n_o D/\lambda)[\cos(\theta_1 - \phi_1) - \cos(\theta_o - \phi_1)] \quad 4.24$$

$$\xi_2 = \frac{N\Phi_2}{2} = (\pi n_o D/\lambda)[\cos(\theta_2 - \phi_1) - \cos(\theta_1 - \phi_1)$$

$$+ \cos(\theta_1 - \phi_2) - \cos(\theta_o - \phi_2)] \quad 4.25$$

Note that γ_3 is the total grating strength of G_2. This somewhat awkward notation is necessary to allow using a single general analysis for both readout modes.

For the special case of readout at the effective second-order BA, $n_1 = n_2$ (so the double diffraction is by gratings of equal strength) and for arbitrary offset, the general results reduce to those found in Chapter 3 for second-order readout at the second BA of a single sinusoidal grating (no nonlinearity), Eq. 3.20, with ξ given by ξ_1 (Eq. 4.24). (Actually the cosine factors in the grating strength terms are slightly different depending upon the construction geometry; the results are exactly equivalent if $\cos\theta_o = \cos\theta_2$ and $\cos\theta_1 = 1$.) For the more special case of $\Delta\phi = 0$, so that $\xi_1 = \xi_2 = 0$ and for arbitrary n_1 and n_2, the general results reduce to (A.40 and A.41)

$$DE_1 = \frac{\gamma_1^2}{\left(\gamma_1^2 + \gamma_3^2\right)} \sin^2\left(\gamma_1^2 + \gamma_3^2\right)^{1/2} \quad 4.26$$

$$DE_2 = \frac{4\gamma_1^2\gamma_3^2}{\left(\gamma_1^2 + \gamma_3^2\right)^2} \sin^4 \frac{1}{2}\left(\gamma_1^2 + \gamma_3^2\right)^{1/2} \quad 4.27$$

For this special case, similar results have been derived by a coupled-wave approach (47). Because $\xi_1 = 0$, the general condition,

$\xi_1 = m\pi$ (m = 0), is satisfied and as Eq. 4.27 shows, all the incident energy can be coupled through the diffracted order of G_1 into the diffracted order of G_2. Indeed, the 100% conversion can be accomplished with a relatively low modulation because the intermediate dispersion term is zero. A plot of the DE of the first and cross-coupled orders versus the normalized grating strength is given in Fig. 4-9 for $n_1 = n_2$. A grating strength, $\sqrt{2}\gamma_1^o$, is needed to place 100% of the incident energy into the doubly-diffracted order. For a sequential arrangement of single gratings, of course, $2\gamma_1^o$ would be required.

Because of the similarity with second-order readout, the general comments made in Chapter 3 are valid here also. In particular, the periodic dependence of the maximum value of DE_2 with ξ_1 is very important. Here, ξ_1 increases with the offset, $\Delta\phi$. But as we have seen, the doubly-diffracted order can be very large at the second BA, even for a large first-order dispersion term. Thus, the cross-coupled order can still be significant for large offset, although generally higher modulations are necessary. In fact, the maximum value of DE_2 will be periodic in $\Delta\phi$. However, for large $\Delta\phi$ the second BA of the two grating combination is well separated from the first BA of G_1 (Fig. 4-8b). The two orders will be angularly decoupled. Nevertheless, even for large offset between the two gratings, one must be aware of the possibility of this extraneous diffracted order.

The AS results for the cross-coupling case are found by evaluating the general expressions, A.25 and A.26, with the grating strength and dispersion terms given by Eqs. 4.23-4.25. As a representative example, we use the same parameters used in the last section. Again, we normalize $\theta_o - \theta_2$ (θ_2 is the BA of G_1) and $\Delta\phi$ by the single grating angular half-width of G_1. In Fig. 4-10 is a

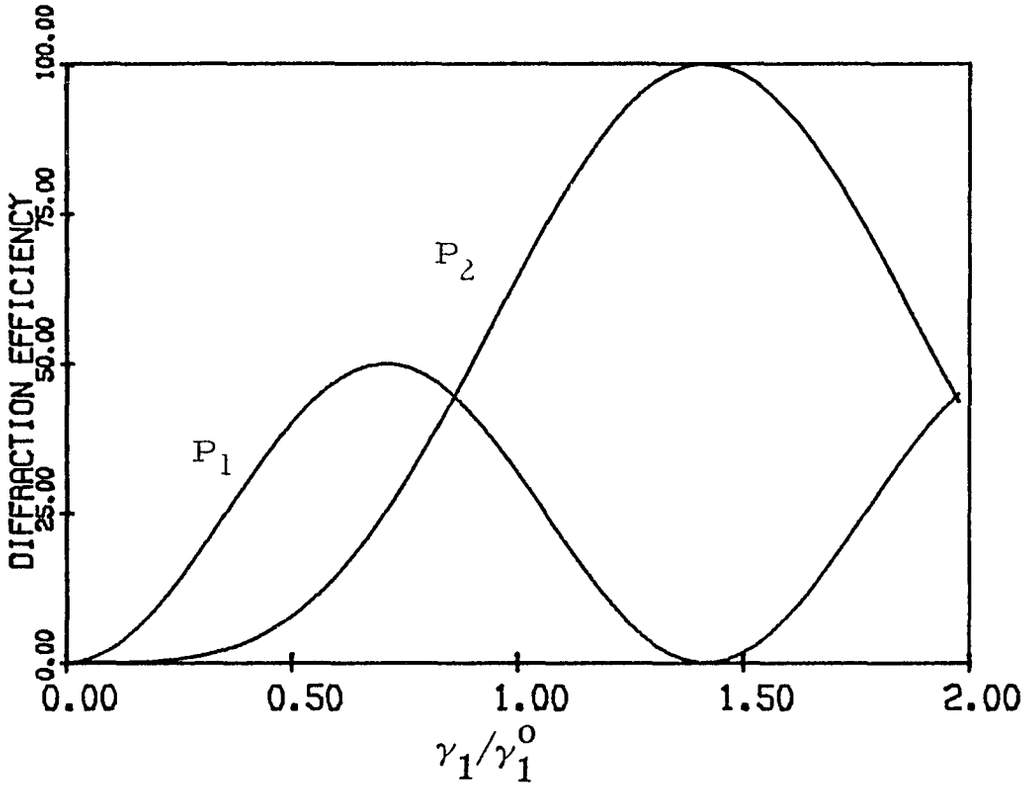


Figure 4-9. DE of the First (P_1) and Cross-Coupled Orders (P_2) for Readout at the Noncommon Bragg Angle

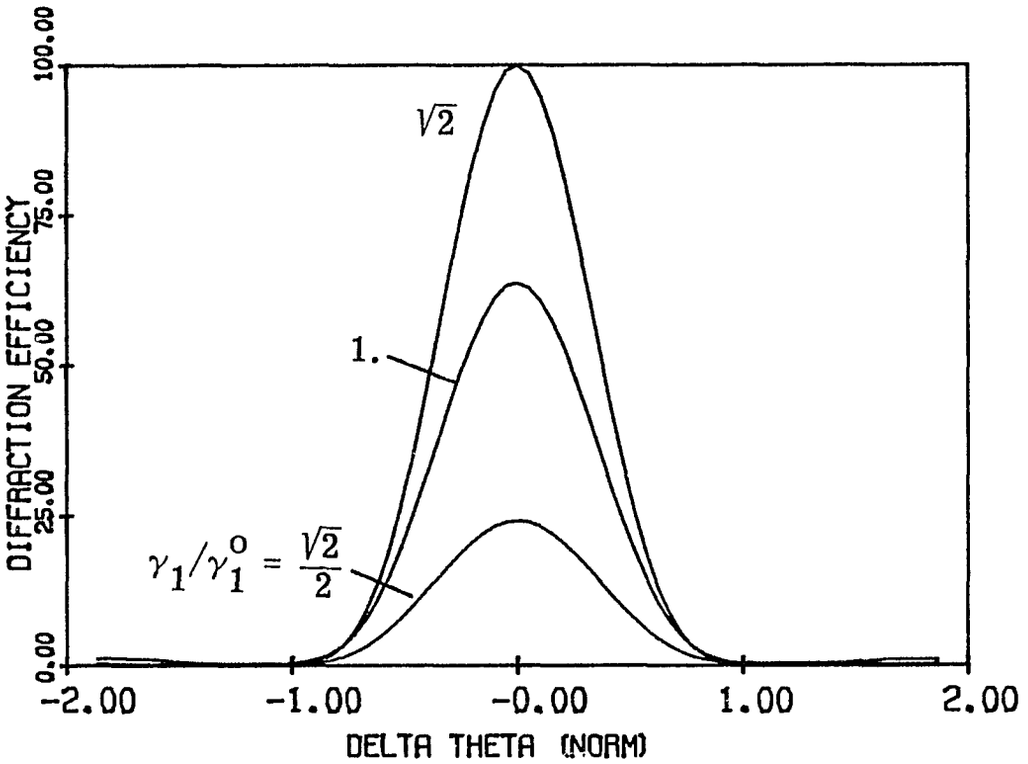


Figure 4-10. Angular Selectivity of Cross-Coupled Order, $n_1 = n_2$

plot of the AS of the cross-coupled order for several levels of modulation $\left(\gamma_1/\gamma_1^o\right)$ with $n_1 = n_2$. The curves for the first order are very similar to those in the direct-coupling case and are excluded for clarity. A very striking feature of the angular selectivity of the cross-coupled order is the lack of any significant sidelobes. The maximum sidelobe level is $\simeq 1\%$, compared to 12% for a single grating modulated to give 100% DE at its BA. Thus, the phenomenon of cross coupling in double gratings may find useful application in filtering devices (angular or wavelength), where suppression of sidelobes is important.

The effect that offset, $\Delta\phi$, plays in decoupling the two gratings is shown in Fig. 4-11. The calculated DE of the first order of G_1 (P_1) and the cross-coupled order (P_2) is shown for normalized offset $\Delta\phi = 0$ (a), .5 (b), and 1.5 (c). The two gratings have equal index modulation and $\gamma_1 = \gamma_1^o$. Because the dispersion of the cross-coupled order for readout angles off θ_2 is greater than that of the first order (see Fig. 4-8a), it has a sharper angular selectivity. As the offset is increased, the AS of the cross-coupled order remains symmetrical about an angle that can be shown to be the second BA of the double-grating combination. The first order, on the other hand, maximizes at an angle other than its BA ($\Delta\theta = 0$), just as in the direct-coupling case, until the offset is rather large. For an offset of 1.5, the first order of G_1 has essentially returned to the single grating result except in the sidelobe region overlapped by the cross-coupled order. Note, however, that the latter is still quite strong. The curve showing the modulation dependence of decoupling that corresponds to Fig. 4-6 for direct coupling is essentially identical to that result and is not shown.

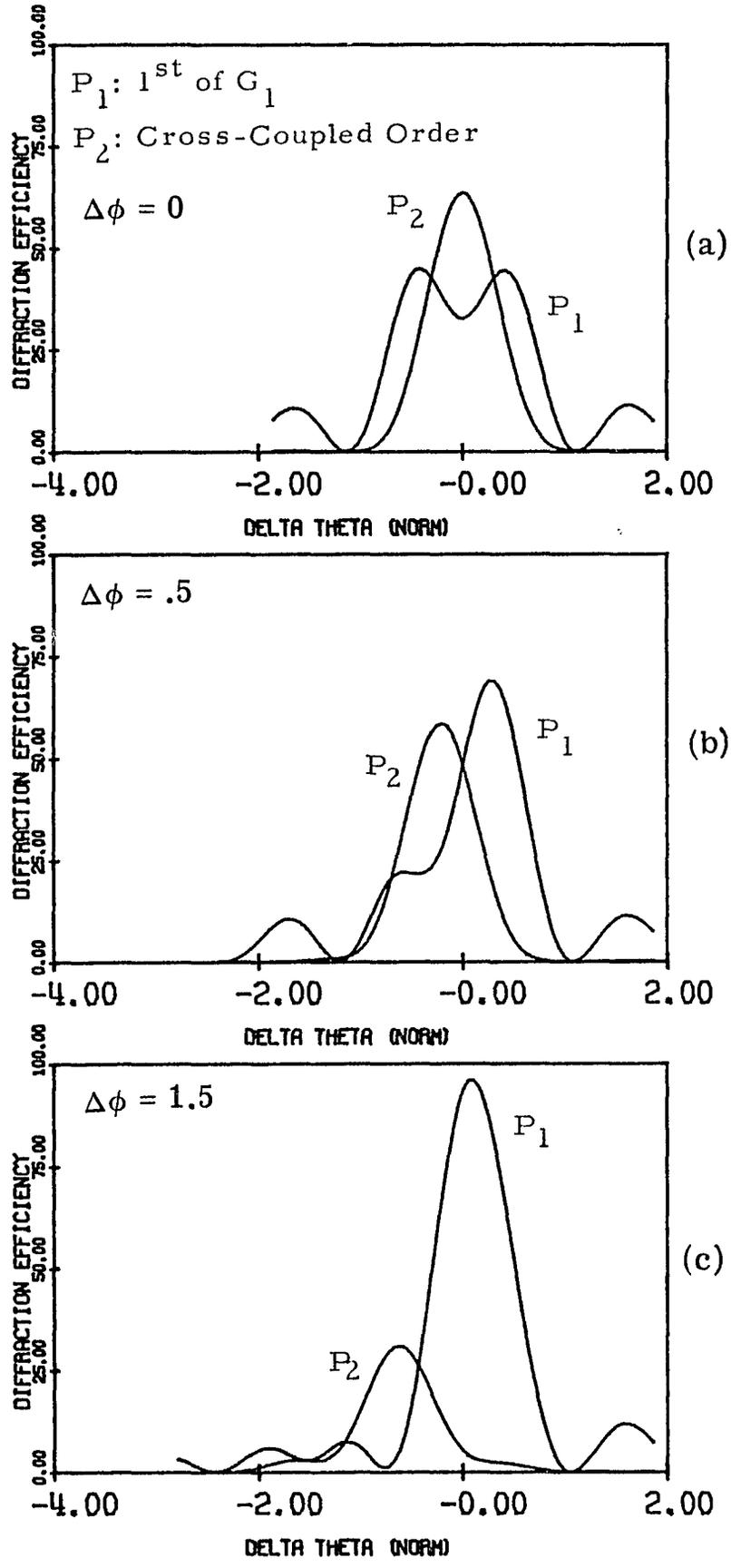


Figure 4-11. Decoupling with Offset: Cross-Coupling Mode, $n_1 = n_2$, $\gamma_1 = \gamma_1^o$

It is interesting to compare the results for the direct and cross coupling readout modes. Here, because of our choice of the angular readout region, the first order in the cross-coupling case is that diffracted by G_1. Therefore, we consider this first order in the two cases. We might expect that because the cross-coupled order is a doubly diffracted wave, its effect in taking energy from the first order may be less than that of the other first order in the case of direct coupling. However, this is obviously not true. If we compare Fig. 4-5 and 4-11, we see that as $\Delta\phi$ is increased, the increase of the DE of G_1 is no more rapid for direct coupling than for cross coupling. Indeed, the angular selectivity of G_1 is essentially the same in the two cases. Cross coupling is, therefore, a very strong effect in multiple thick gratings, and must be considered whenever such structures are made. This is an interesting and rather unexpected result.

4.2.3 The Two Extremes of Double Diffraction

The difference between double diffraction in single gratings and in double gratings made with a common construction angle, for readout at the effective second-order BA in either case, is that in the latter case, the intermediate differential dispersion term is zero. The expressions for the DE of the doubly diffracted order for the two limiting cases are

$$DE_2 = \sin^2\left(\gamma_1^2/2\xi\right)$$

for the intermediate dispersion, ξ, very large (Eq. 3.37 with no nonlinearity); and

$$DE_2 = \sin^4\left(\frac{\sqrt{2}}{2}\gamma_1\right)$$

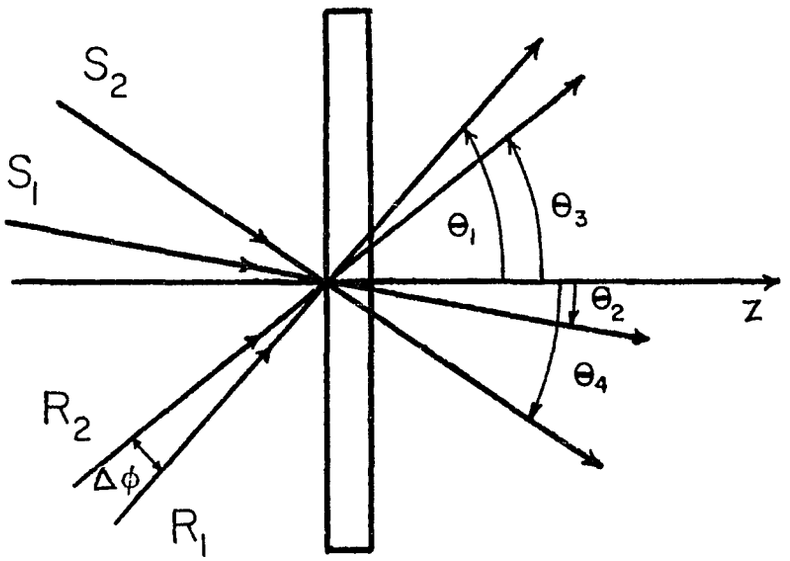
for $\xi = 0$ for two gratings with the same index modulation (Eq. 4.27). The latter case is, of course, much stronger.

4.3 Incoherent Superposition Construction II

Another possible geometry for a double (or, in general, multiple) grating incoherent addition is shown in Fig. 4-12. Plane waves R_1 and S_1 and subsequently, R_2 and S_2 are interferred to construct G_1 and G_2, respectively. Again, there are two gratings superimposed throughout the volume of the emulsion. This is a typical configuration for optical data storage systems (28), with a single reference beam (R) and multiple signal beams (S_j). The difference from the geometry of Fig. 4-1 is that the common or almost common construction beams (R_1 and R_2) are no longer the center beams. We again assume that the Q factors of G_1 and G_2 are sufficiently large for the modulation level required so that each grating produces only a single diffracted order for readout near its BA. In addition, we assume that the angle between S_1 and S_2 is large enough so that during readout, a wave propagating near the angle θ_2, for example, has a large enough dispersion with respect to G_2 that it is effectively diffracted only by G_1. If this is not the case, multiple diffracted orders will appear as in the case of a thin grating. We could include these orders and do the matrix multiplication numerically. By making the above assumption, we limit the number of diffracted orders to two. The general analytical results derived in the Appendix can, therefore, be applied. In general, the above assumption will be satisfied if the angle between S_1 and S_2 is such that the effective Q factor corresponding to that angle is larger than 15. There is, however, no grating recorded between S_1 and S_2.

While one might initially assume that the results for this geometry would be identical to those found for the previous incoherent geometry, there are, in fact, some very interesting differences. The diagrams of the propagation directions for the two readout modes are shown in Fig. 4-13. For a readout wave, P_o, in the

(a)



(b)

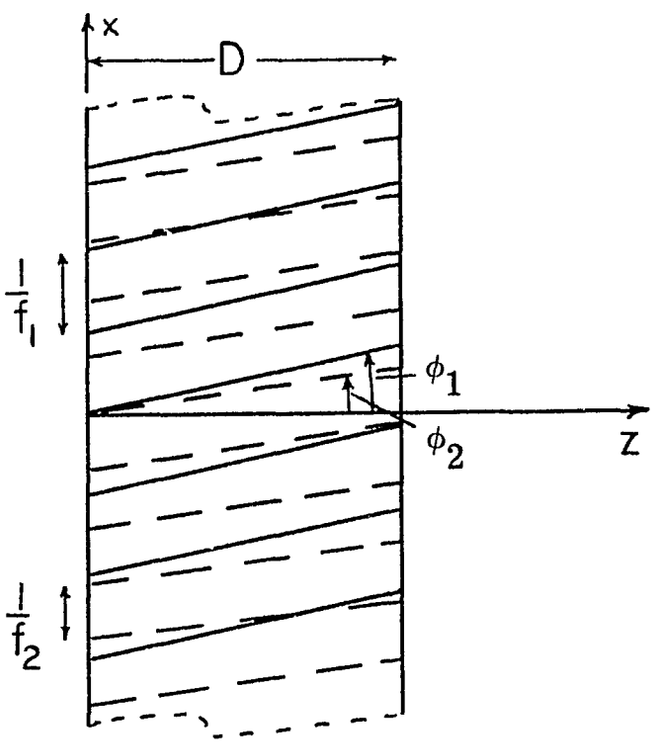


Figure 4-12. Geometry for Incoherent Superposition II

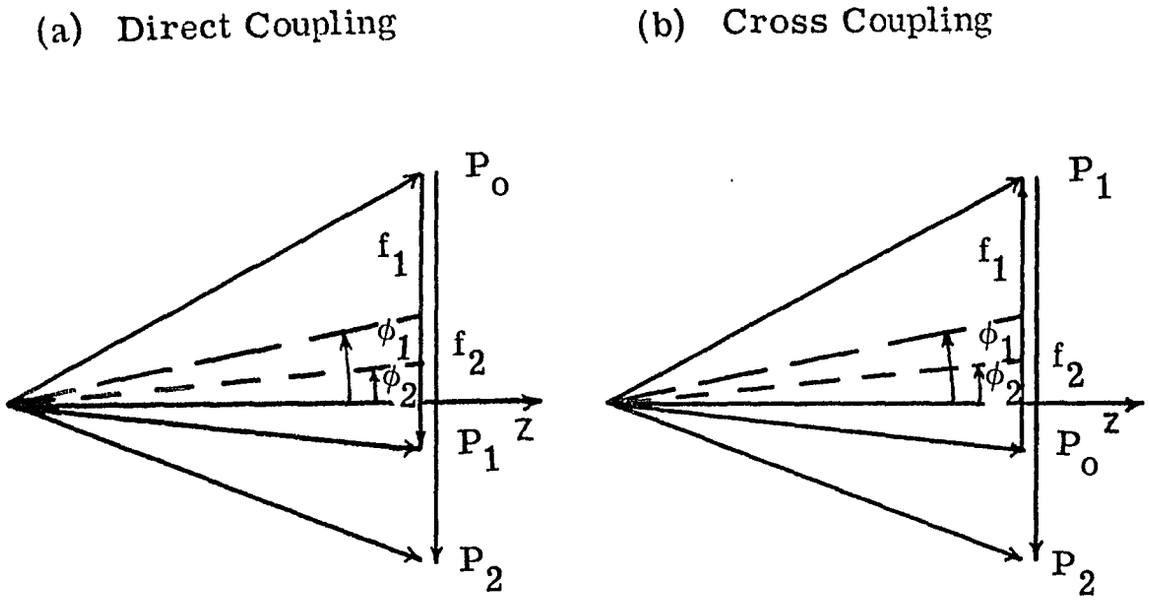


Figure 4-13. Readout Modes

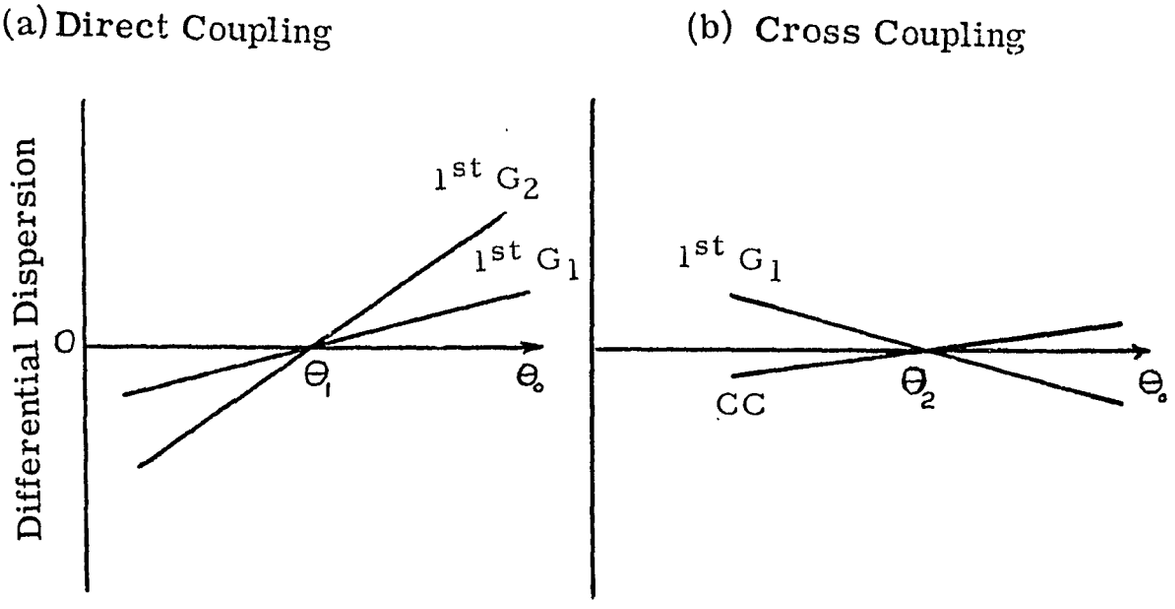


Figure 4-14. Differential Dispersion for Type II Geometry

angular region of the nearly common construction waves (R_1 and R_2), there is direct coupling into the first orders of G_1 and G_2. The diffracted orders P_1 and P_2 have spatial frequencies $F_1 = f_o - f_1$ and $F_2 = f_o - f_2$, respectively. Cross coupling is important for readout near one of the noncommon BA's, θ_2, for example. The first diffracted order (of G_1) has a spatial frequency $F_1 = f_o + f_1$ and the doubly diffracted order, $F_2 = f_o + f_1 - f_2$.

The important difference between this geometry and the one considered previously can be seen in the angular dependence of the differential dispersion terms that are sketched in Fig. 4-14 for the case, $\Delta\phi = 0$. In the case of direct coupling (Fig. 4-14a), the dispersion terms for each first order have the same sign, although different slopes because of the different grating frequencies. This results because of the common negative sign in determining their spatial frequencies with respect to the incident frequency. This, in turn, is a result of the fringe slopes for the two gratings being of the same sign (see Fig. 4-13). The result is that the sum of the two dispersion terms, which is important in the analytical expressions for the DE's (see the Appendix, A.5), does not remain small for readout angles off the common BA as it does in the case of the previous geometry (see Fig. 4-3a). This fact has important consequences upon the shape of the AS curves. The doubly diffracted order ($F_2 = f_o + f_1 - f_2$) has a spatial frequency relative to the readout wave that is increased by G_1 but decreased by G_2. Its dispersion term is the sum of that due to each of the individual diffractions. Because of the difference in sign of the two terms, the spatial dispersion for the cross-coupled order is less than that of either first order (Fig. 4-14b). This is to be contrasted to the case for the previous geometry, where the cross-coupled order has a differential dispersion term that is a positive sum (see Fig. 4-8a).

We shall see that this fact results in a much broader angular selectivity.

The form of the coupling matrices for the two cases of readout are exactly the same as previously, Eq. 4.9 for direct coupling and Eq. 4.17 for cross coupling. The only difference is that the spatial frequencies of the diffracted orders are as given above with the resulting different angular dependence of the dispersion terms which are calculated as before. For no offset between the two gratings ($\Delta\phi = 0$) and readout at any of the construction angles, both the dispersion terms are zero. Thus, for this case, we must obtain the same expressions for the diffraction efficiencies as before, Eqs. 4.15 and 4.16 and Eqs. 4.26 and 4.27 for readout at the common BA or one of the noncommon BAs, respectively. The angular dependence of the DE will not be the same, however. The general expressions derived in the Appendix can again be applied.

To illustrate the general properties of double gratings constructed in this geometry, we calculate and plot representative results for the following example: $\theta_1 = \theta_3 = 25^o$, $\theta_2 = 0^o$, $\theta_4 = -7^o$, $\lambda = .488\ \mu m$, $n_o = 1.52$ and $D = 48\ \mu m$. The larger thickness is required because of the small angle between θ_2 and θ_4. The resulting grating frequencies are $f_1 = 1300$ 1/mm and $f_2 = 1700$ 1/mm. Note that G_1 is the lower frequency grating. The two frequencies can not be made equal in this geometry. We again use γ_1^o as the grating strength unit. The difference in readout angle from the BA of G_1 and the offset angle, $\Delta\phi$, are normalized by G_1's single grating half-width ($\sim.8^o$). We consider separately the two modes of readout.

4.3.1 Direct Coupling

In Fig. 4-15, we plot the computed AS (about the angle θ_1) of the diffracted order of G_1 for several levels of modulation. The two grating strengths are equal. Again, the results for the first order of G_2 are of similar form and are deleted for clarity. We find the interesting result, that for this geometry the maximum DE tends to remain at the BA even for the higher modulation levels. This is to be contrasted with the results of Fig. 4-4 where the maximum occurs at angles symmetrically off the common BA (compare at the modulation level, $\gamma_1/\gamma_1^o = 1$). As discussed above, this difference results from the different angular dependence of the dispersion terms in the two cases. For very high modulation, such that the DE has become zero at the BA, the maxima occur off the BA.

The ramifications of the altered dispersion curves for this geometry show up most significantly as the two gratings are offset relative to each other. In Fig. 4-16, we plot the computed AS of the first orders of each of the gratings for $\gamma_1 = \gamma_2 = \gamma_1^o$, and the normalized offset angle, $\Delta\phi = 0$ (a), .5 (b) and 1.5 (c). The BA of G_1 corresponds to $\Delta\theta = 0$ and that of G_2 to $\Delta\theta = -\Delta\phi$. We see from Fig. 4-16 that as the gratings are separated, the maximum DE for each grating occurs for readout at its BA. This is in striking contrast to the results for the other geometry. As a result, the gratings seem to decouple more slowly with offset than previously. However, if one looks at the DE for readout at either of the BAs, the decoupling is the same as for the previous geometry. That is, for readout at the BA of G_1 so that $\xi_1 = 0$, the curves of the DE of G_1 versus the differential dispersion of the diffracted order of G_2, which is proportional to the offset, are the same as that found previously (Fig. 4-6). It is just that in the other

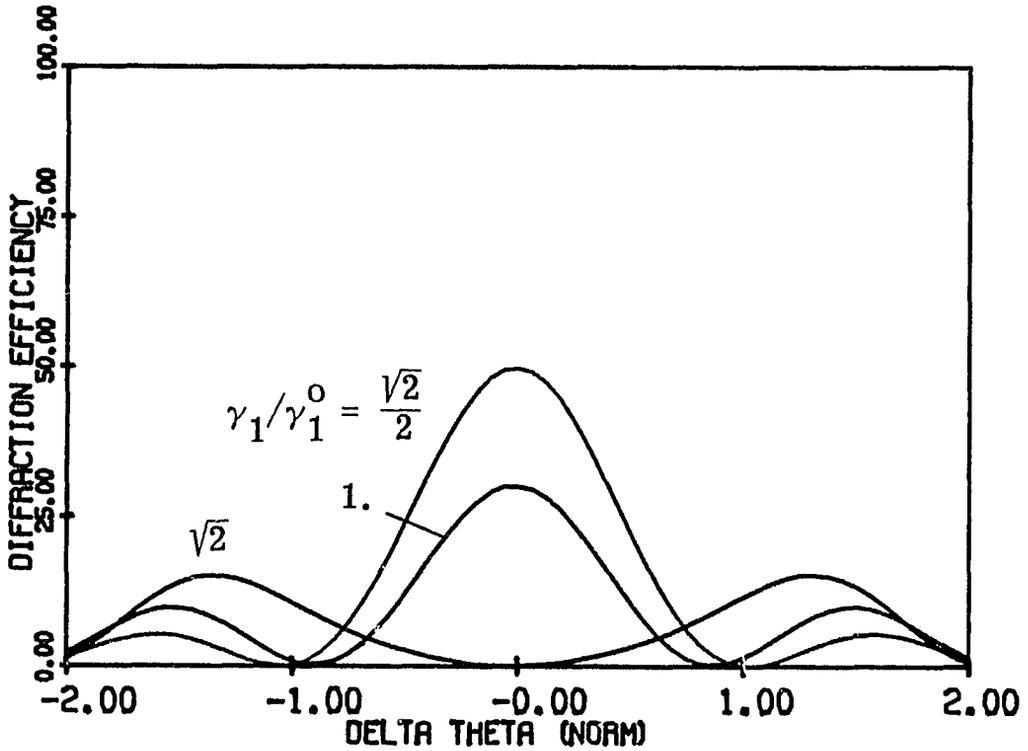


Figure 4-15. Angular Selectivity for Direct-Coupling Readout, $n_1 = n_2$

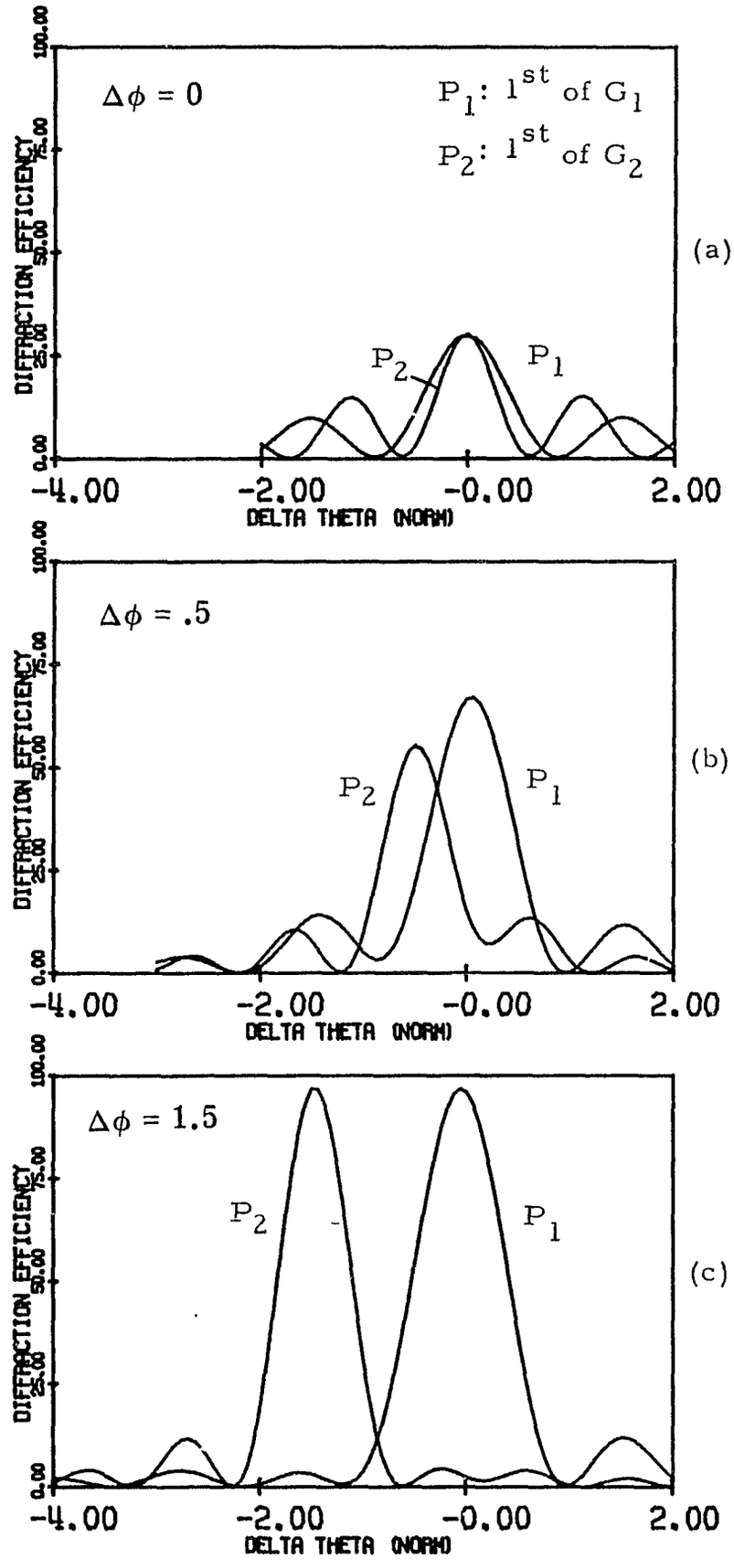


Figure 4-16. Decoupling with Offset: Direct Coupling Mode, $n_1 = n_2$, $\gamma_1 = \gamma_1^o$

geometry, the maximum DE occurs for an angle other than the BA, except for very large offset. If we are only going to readout at the construction angles, there will be no differences between the two geometries as far as the necessary relative offset to decouple the gratings is concerned.

4.3.2 Cross Coupling

We consider cross coupling through the first order of G_1. Therefore, we consider readout angles about θ_2. The computed AS of the cross-coupled order is plotted in Fig. 4-17 for several levels of modulation. The gratings strengths are equal. The results are again quite different from those of the previous geometry (Fig. 4-10). The most obvious difference is the appearance of plateau regions where the DE remains rather uniform.

Figure 4-18 is a plot of the computed AS of the first order of G_1 (P_1) and the cross-coupled order (P_2) for $n_1 = n_2$ and $\gamma_1 = \gamma_1^o$. The normalized offset angle is $\Delta\phi = 0$ (a), .5 (b) and 1.5 (c). The AS of the cross-coupled order is clearly broader than that of the first order. Thus, the mechanism of double diffraction does not inherently lead to a narrow angular response. As the gratings are offset, the DE of P_2 maximizes at the second BA of the two-grating combination and P_1 at its BA. For an offset of 1.5 (Fig. 4-18c), the first order has returned to its single grating result. The general comments made for the previous incoherent geometry with respect to the relative effect the two readout modes have upon decreasing the DE of G_1, are true here also.

4.4 Coherent Superposition Construction

We now consider the construction shown in Fig. 4-19 in which three plane waves are allowed to interfere simultaneously. The

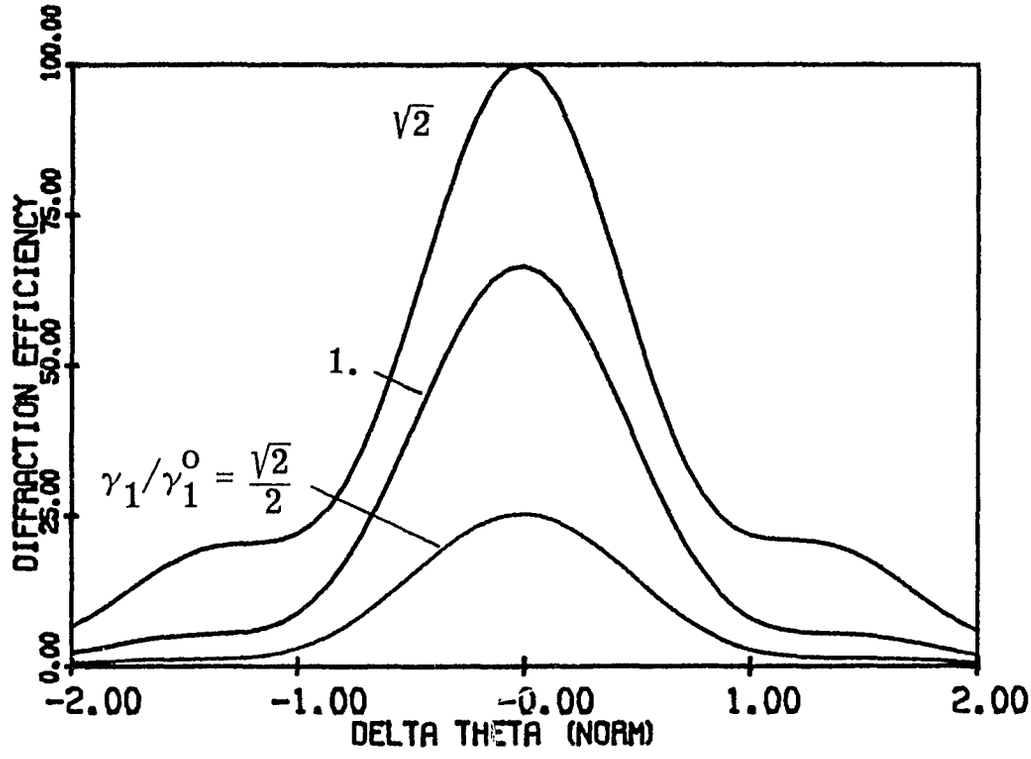


Figure 4-17. Angular Selectivity of Cross-Coupled Order, $n_1 = n_2$

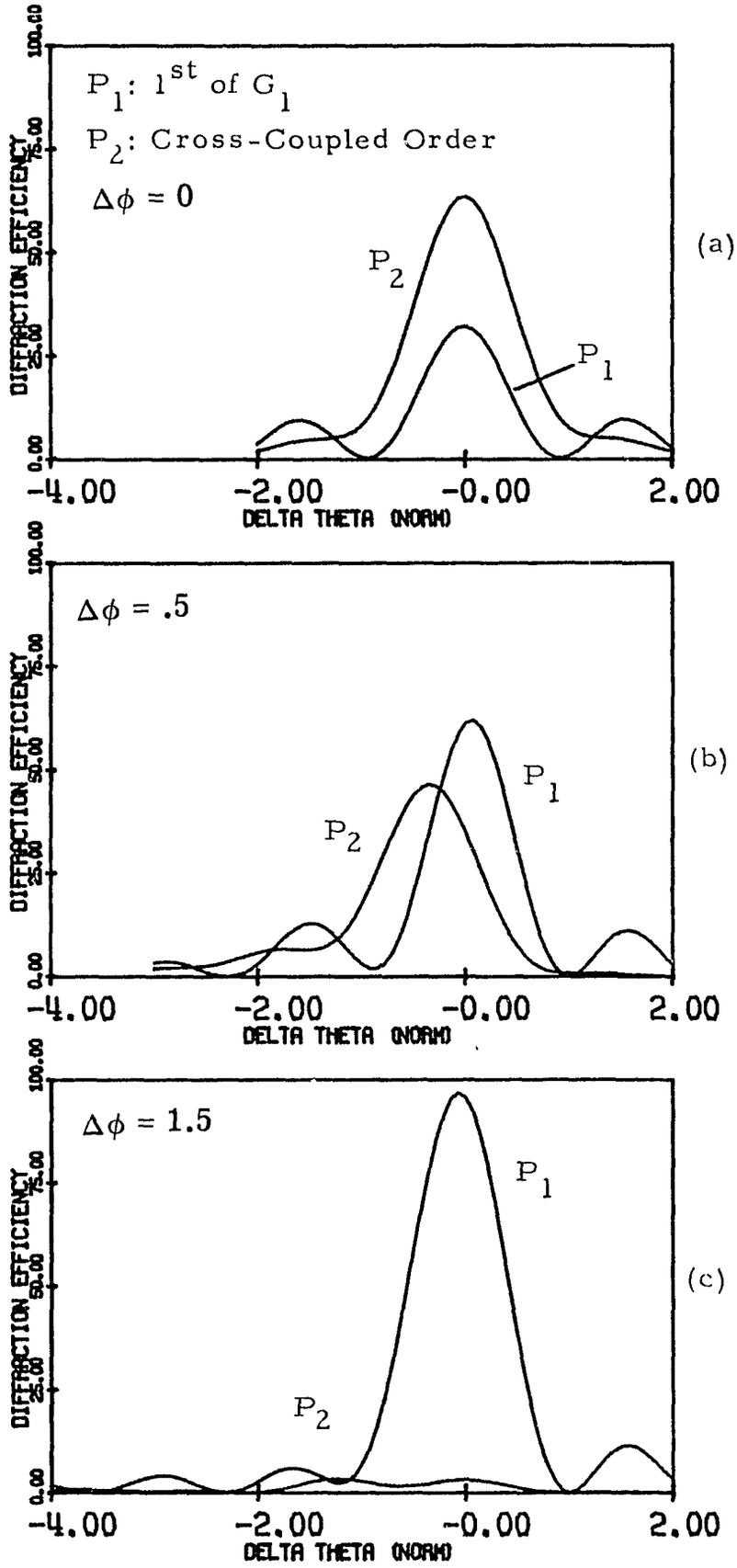


Figure 4-18. Decoupling with Offset: Cross-Coupling Mode, $n_1 = n_2$, $\gamma_1 = \gamma_1^o$

developed plate contains three fringe structures that are strongly coupled. The grating due to R_1 and S_1 is G_1, R_1 and S_2 is G_2, and S_1 and S_2 is G_3. The grating G_j has index modulation n_j. Note that: $f_3 = f_1 + f_2$ and $\phi_3 = \phi_1 + \phi_2$. There are still only two significant diffracted orders. The distinction between the two incoherent constructions is lost, however, because of the addition of the sum grating, f_3. We again assume that the Q factors of the individual gratings are large. This coherent superposition has the advantage that there is less bias buildup of the film during construction than in the incoherent case. Thus, one should be able to achieve higher index modulation in this case before the film sensitivity saturates.

There are still two distinct readout modes: readout angles near the center construction angle and readout near either of the outer construction angles. The former corresponds to the direct-coupling readout mode of the first incoherent construction geometry and the latter to the cross-coupling mode. Of course, this terminology is no longer meaningful. The sum grating component means that each of the orders is coupled to the other two. Nevertheless, this nomenclature allows clear identification of the readout modes and will be used. The diagrams for readout in the two cases are shown in Fig. 4-20. The corresponding differential dispersion curves are qualitatively the same as in the first incoherent addition geometry for $\Delta\phi = 0$ (Figs. 4-3a and 4-8a). Note that in this geometry, there is no means for angularly decoupling the gratings.

Because of the third grating component, the coupling matrix has no nonzero elements. In the direct-coupling case, the diffracted waves P_1 and P_2 (generated by gratings G_1 and G_2, respectively) are coupled by the sum grating G_3 (Fig. 4-20a). Therefore, the matrix elements that connect these waves are no longer zero. For

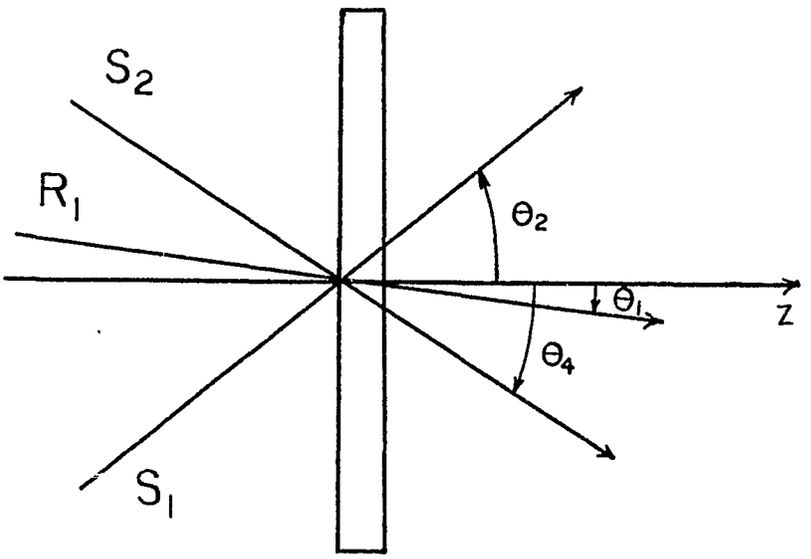


Figure 4-19. Coherent Superposition

(a) Readout about center angle (b) Readout about outer angle

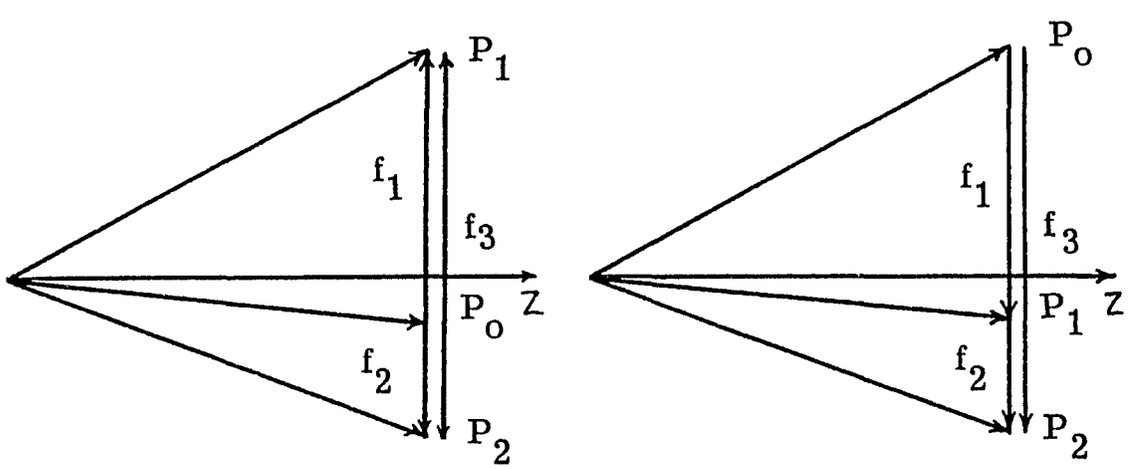


Figure 4-20. Readout Modes for Coherently Added Gratings

the direct-coupling case, we must add to the coupling matrix of Eq. 4.9 the elements

$$H_{23} = i\frac{\delta_3}{c_2} e^{i\Phi_2} \qquad 4.28$$

$$H_{32} = i\frac{\delta_3}{c_1} e^{i\Phi_1} \qquad 4.29$$

where $\delta_3 = \pi n_3 \Delta z/\lambda$ and the Φ_j are given in Eqs. 4.10 and 4.11.

In the cross-coupling mode (Fig. 4-20b), the sum grating directly diffracts P_o into P_2. The coupling matrix of Eq. 4-17 is modified for the coherent superposition by

$$H_{12} = i\frac{\delta_3}{c_2} e^{i\Phi_1} \qquad 4.30$$

$$H_{21} = i\frac{\delta_3}{c_o} \qquad 4.31$$

with δ_3 as above and Φ_1 given by Eq. 4.20. Note that in both cases, the sum frequency grating has the same effect as the nonlinearity generated component in the single grating case. However, here it can be much stronger because we are not relying upon the nonlinear response of the film.

Again, we can immediately use the general results from the Appendix for diagonalizing the coupling matrix and doing the necessary matrix multiplication. (Indeed, this multiple grating structure requires the most general 3 × 3 coupling matrix considered in the Appendix.) The DE of the diffracted orders P_1 and P_2 for the two readout modes are given by Eqs. A.25 and A.26 with the grating strength and differential dispersion parameters given by Eqs. 4.12 - 4.15 and Eqs. 4.23 - 4.25 for the direct and cross-coupling modes,

respectively. In addition, $\gamma_3 = \pi n_3 D/\lambda(c_o c_1)^{1/2}$ for the former case and $\gamma_2 = \pi n_3 D/\lambda(c_o c_2)^{1/2}$ for the latter.

In the special case of readout at any of the construction angles, $\Phi_1 = \Phi_2 = 0$ and for equal grating strengths, the expressions reduce to

$$DE_1 = DE_2 \cong \frac{4}{9} \sin^2 (3\pi n_1 D/2\lambda c_o) \qquad 4.32$$

where the approximate equality results from the simplifying assumption, $c_o = c_1 = c_2$, in the grating strength terms. The above result applies to either readout mode. For equal index modulation, each of the diffracted orders must be equal because there is no distinction between the modes of coupling because of the sum grating component. Note, that in this case, approximately 12% of the light is not diffracted, regardless of the strength of modulation. Another interesting result is that adding a grating frequency component that directly diffracts energy into an order which would otherwise receive energy only by double diffraction, drastically reduces the maximum obtainable DE of that order from 100% (Eq. 4.27) to 44% (Eq. 4.32). This order can be made 100% efficient in the coherent case only by having unequal index modulations.

The angular selectivity curves for the two readout modes are quite different because of the different angular dependence of the dispersion terms in the two cases. To show representative results, we evaluate and plot the DE of the two diffracted orders for the parameters used in the example of the first incoherent construction geometry. In Fig. 4-21, we plot the angular selectivity of P_1 and P_2 for the direct-coupling (a) and cross-coupling (b) modes. In Fig. 4-21a, $\Delta\theta = 0$ corresponds to θ_1 and in Fig. 4-21b $\Delta\theta = 0$ is θ_2. We use $\gamma_1 = \gamma_2 = \gamma_3 = .7\ \gamma_1^o$. The most striking feature of the AS for readout about the center angle is that the maxima for each of the

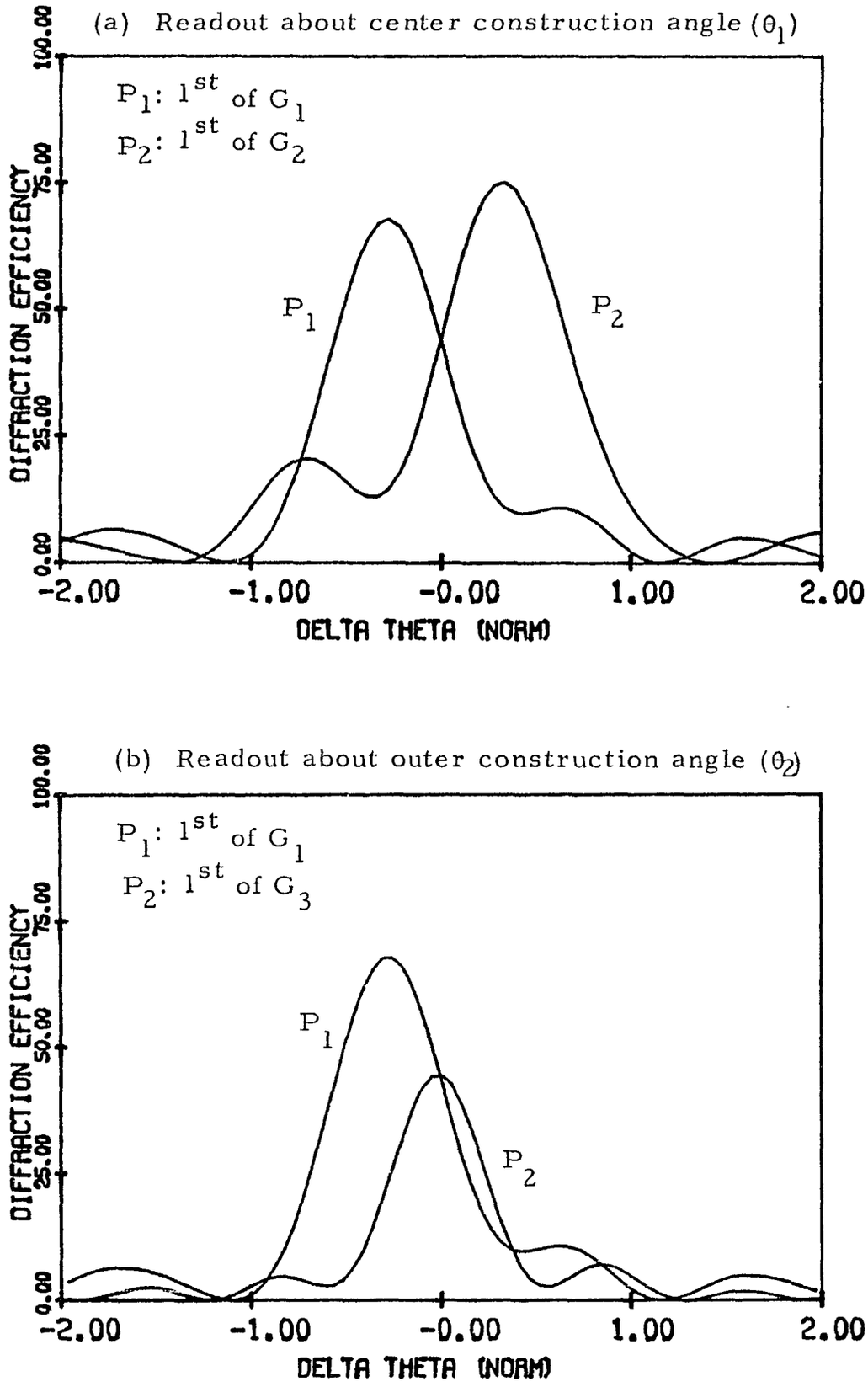


Figure 4-21. Angular Selectivity for Coherently Added Gratings, $\gamma_1 = \gamma_2 = \gamma_3 = \frac{\sqrt{2}}{2}\gamma_1^o$

diffracted orders occur for readout angles off the common construction angle. However, each curve is single peaked so that the two maxima do not overlap as in the incoherent case (for no offset). Thus, the individual gratings can each be more than 50% for a particular angular readout region. The result is that the gratings tend to be somewhat angularly decoupled by the extra sum grating component. This is true even for low modulation. If one is only interested in reading out at the construction angle, there is no gain. But for other angles, one diffracted order can be made rather strong. The curves are also typically narrower than in the case of the incoherent superposition. The maxima of each grating are pushed (in angle) away from the other BA of that grating.

The order that corresponds to the cross-coupled wave in the first incoherent geometry still has its maximum DE for readout at the BA (Fig. 4-21b). It also has noticeable sidelobes and slight asymmetry. At this modulation, this order is much less significant than for the incoherent construction. However, the first order of G_1 maximizes off the BA as in the direct-coupling case. Again, the first order AS of G_1 for each of the two readout modes is essentially the same. Computed results indicate that for $n_1 = n_2$, a ratio of n_3/n_1 less than .1 is necessary to make the coherent results go over to the incoherent ones. This is a useful result because one might expose with a coherent superposition for convenience, but want the system to act like an incoherent addition (38). This can be done by controlling the relative amplitude of the construction beams.

4.5 Experiments

We have performed several experiments with gratings holographically constructed in dichromated gelatin film to verify the results of the above analysis. A schematic drawing of the three-beam

experimental set-up is shown in Fig. 4-22. The components and their functions are the same as described for the two-beam set-up in Chapter 3. As usual, when making holograms, the entire apparatus was placed on a granite slab that floats on air, to isolate the system from ground vibrations. In addition, the apparatus was enclosed in a cabinet during exposure to eliminate air currents. These steps are necessary to eliminate motion during the exposure that would wash out the fringes and reduce or destroy the resulting index modulation. (These steps were also taken in the construction of the single gratings in the last chapter.) Again the pathlengths were made equal to within 1 cm.

4.5.1 Incoherent Superposition

Extensive experiments were performed to verify quantitatively the analytical results predicted for the first incoherent construction geometry discussed. The procedure (see Fig. 4-22) was to block one beam, say S_2, and expose the film plate (sensitized in a 5% solution of ammonium dichromate) to the interference pattern of R_1 and S_1. Then, S_1 was blocked and the grating constructed by R_1 and S_2 was recorded on the same area of the plate. The result, after the standard development, was two (approximately) sinusoidal gratings superimposed throughout the depth of the emulsion. The beam diameters were less than 2 cm, so several sets of double gratings could be made on the same 4" × 5" plate by simply translating the plate after the double exposure was made. For the case where an offset $\Delta\phi$ between the two gratings was desired, the plate was rotated $\pm \Delta\phi/2$ between the two exposures.

For the incoherent superposition, there is the question of how the film responds to the double exposure, independent of the subsequent question of propagation in the coupled-grating system. For

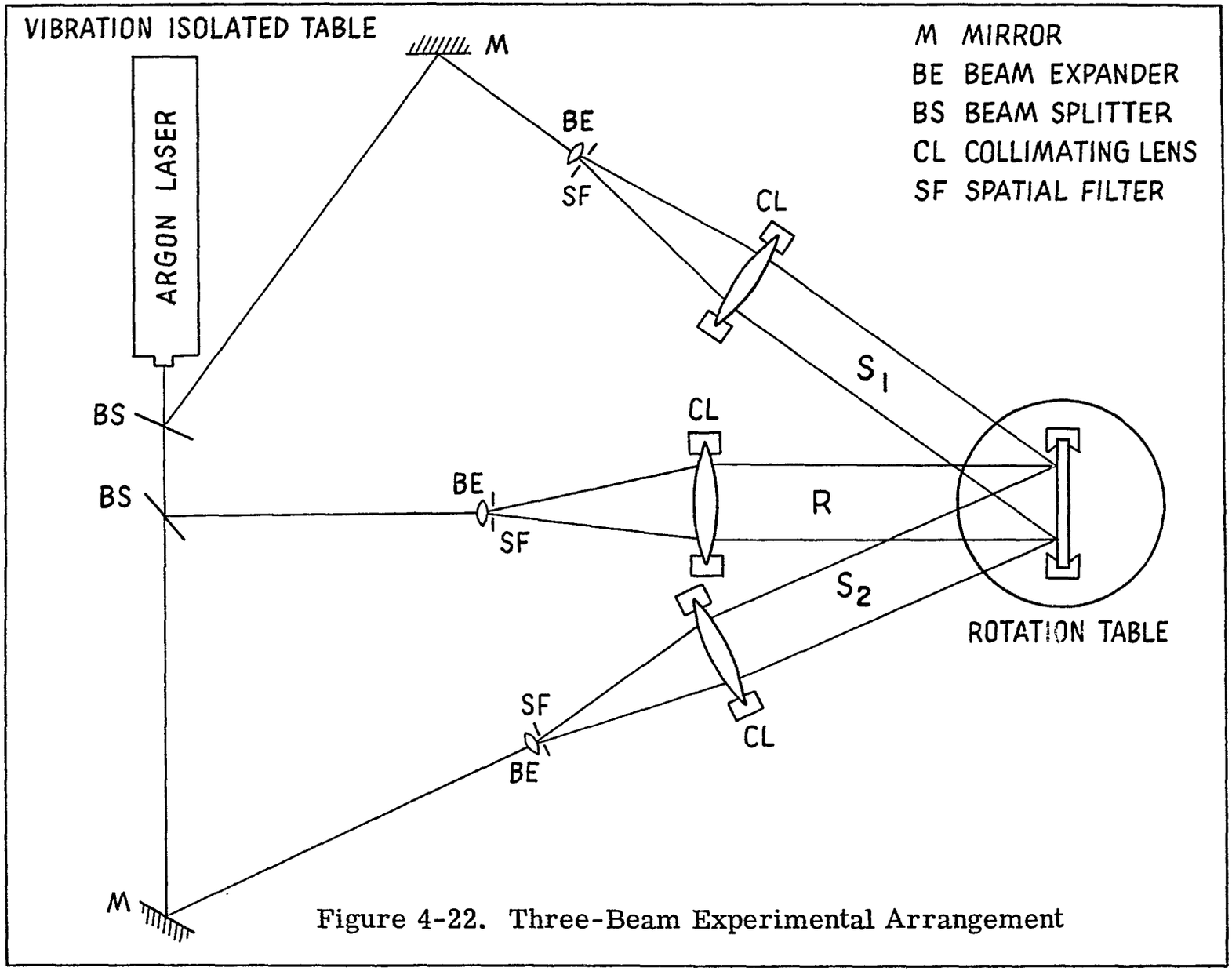


Figure 4-22. Three-Beam Experimental Arrangement

the analysis we have assumed two sinusoidal gratings of arbitrary index modulation. To gain insight into the response of dichromated gelatin film under double exposure conditions, double gratings at various exposure levels were made with $\Delta\phi$ sufficiently large that there was no coupling between the two gratings. With respect to propagation, each grating acts like a single grating. However, because of the film response, a different exposure per grating was required to produce a particular index modulation than would be necessary if only a single exposure was made. The gratings were independently readout at their first BAs and Eq. 2.45 was used to determine the index modulation of each grating from its measured DE. There was essentially no dependence upon the order of exposure; the film responds to the total integrated exposure without distinction to which grating was recorded first. This is true for typical exposures. For extremely high exposures, exposure-induced absorption changes during construction decreases the effective intensity of the second set of construction beams relative to the first, which results in the second grating being somewhat weaker than the first. Even for lower exposures, one grating (G_2) was typically slightly weaker, independent of the order of exposure. This apparently resulted because of the reduced fringe contrast due to small pathlength differences between R_1 and S_1 (Fig. 4-22). These effects could be adequately compensated for by adjusting the exposure times to produce gratings of approximately equal index modulation.

We also found that to obtain the same index modulation as for the single exposure case, the exposure per grating had to be approximately doubled. This is due to bias buildup of the film. In general, the necessary compensation for bias buildup depends upon the number of exposures, level of modulation desired and the sensitizer concentration (32). The number of incoherent additions that can be

made with given individual index modulations is limited by film saturation.

For the high exposures required to obtain significant index modulation under double exposure conditions, film saturation causes the film to respond nonlinearly. As mentioned earlier, the higher harmonic grating components created are unimportant for first-order readout as long as the individual gratings are thick and no construction angle corresponds to a second BA of the other grating. However, the nonlinearity does cause the first order index modulations of each grating to increase much more slowly with exposure (see the single grating case, Fig. 3-13). Thus, long exposure times are required and extra caution must be taken to avoid movement due to ground vibrations.

A problem encountered in attempting to make gratings with no offset is that emulsion swelling due to the development process, tilts the fringe planes. Because of the opposite sign of the slope angles for the two gratings, this tilt introduces an effective offset between the BAs of the two gratings even if they were made with a common construction beam. This same fringe tilt occurs for single grating construction also (although it is minimal if the fringes are perpendicular to the plate), but the only consequence is that the BA is slightly different from the construction angle. The effect can be reduced by baking the developed plate to eliminate the absorbed moisture that causes swelling. However, this also reduces the index modulation (48). Instead, the effect of fringe tilt was compensated for by offsetting the gratings in the opposite sense before exposing. Because the degree of tilt depends upon the exposure level, some experimentation was required to determine the correct compensation.

The internal angles of the construction beams were: $\theta_1 = \theta_3 = -2.^{o}$, $\theta_2 = 19.6^{o}$ and $\theta_4 = -18.6^{o}$. Again, $n_o = 1.52$, $\lambda = .488\ \mu m$ and $D \cong 16\ \mu m$. The grating spatial frequencies were, therefore, $f_1 = 1150$ 1/mm and $f_2 = 890$ 1/mm ($Q \cong 45$ and 25, respectively). The readout angles for the experimental angular selectivity curves have been converted to their internal values.

To verify the possibility of 100% cross coupling, double gratings were constructed with $n_1 \cong n_2$ and in such a way that after processing $\Delta\phi = 0$. Several sets of double gratings were constructed sequentially on the plate at increasing exposure levels. After development, the plate was returned to the plate holder (Fig. 4-22) and readout at θ_2 (beams R_1 and S_2 were blocked). Figure 4-23 is a plot of the experimentally measured DE of the zero, first (of G_1) and cross-coupled orders versus the exposure per grating. Reflection losses are eliminated by normalizing the intensity of each order by the total transmitted intensity. The results clearly demonstrate that for proper modulation, 100% of the transmitted light is diffracted into the cross-coupled order. Because of the nonlinear response, n_1 and n_2 are not linearly proportional to the total exposure. Therefore, the experimental curves are of somewhat different shape than the theoretical results in Fig. 4-9.

The AS curves for this incoherent construction were determined experimentally for varying degrees of offset. Quantitative comparison with the theoretical results were made. The readout angle was varied by simply rotating the plate slightly from its construction position. For the direct-coupling readout mode, beam R_1 was used; S_1 was used for the cross-coupling case. Experimentally measured angular selectivity results for three double gratings with similar index modulation but varying offset are shown in Figs. 4-24 and 4-25 for the direct and cross-coupling readout modes,

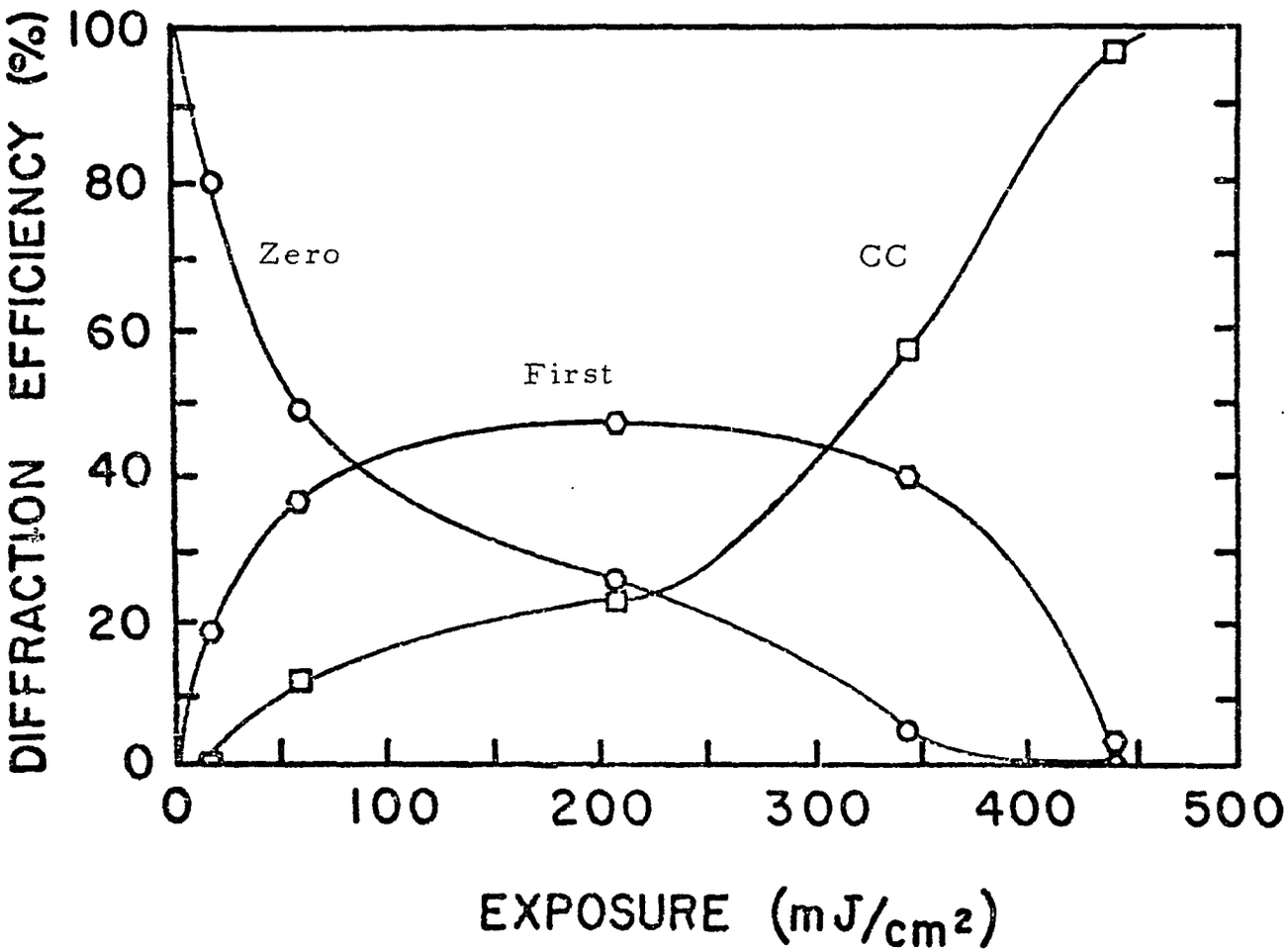


Figure 4-23. Experimental DE for Readout at Noncommon BA, $\Delta\phi = 0$

respectively. The same letter for each figure corresponds to the same double-grating structure. In all cases, the symbols represent the experimental data points and the solid line the corresponding theoretically predicted values.

We could not independently measure the parameters n_1, n_2 and $\Delta\phi$. For the theoretical curves, these parameters were estimated from knowledge of the film index modulation properties under double exposure conditions. The parameters were then varied slightly to give a good fit to the direct-coupling results for each of the three structures. The same values were then, of course, used for the theoretical curves for the cross-coupling results that corresponded to the same structure. No extensive curve fitting was attempted. The values of the parameters used are given on the curves. The values given are actual, not normalized values. The single grating index modulation required to make either grating 100% efficient at its BA is $\cong .015$. The single grating half-width of G_1 is $\cong 2.6^{\circ}$. The value of $\Delta\theta$ on the plots does not correspond to either BA. It is a convenient angle of reference, approximately half way between the two BAs. The modulation level is such that the first orders are maximized; the cross-coupled order is rather low at this level (see Fig. 4-23).

In Fig. 4-24a, the offset between the two gratings is quite small; the coupling is strong and each grating is limited to a maximum of 50%. In Fig. 4-24b, the offset is increased (and changed in sign) and the gratings begin to decouple; the lower frequency grating doing so more rapidly even though it has a slightly lower index modulation. Note that the slight asymmetry of the DE of G_2 as well as the larger asymmetry of that of G_1 are both predicted by the theoretical results. The results of Fig. 4-24c are for an offset such that the gratings are essentially decoupled. The

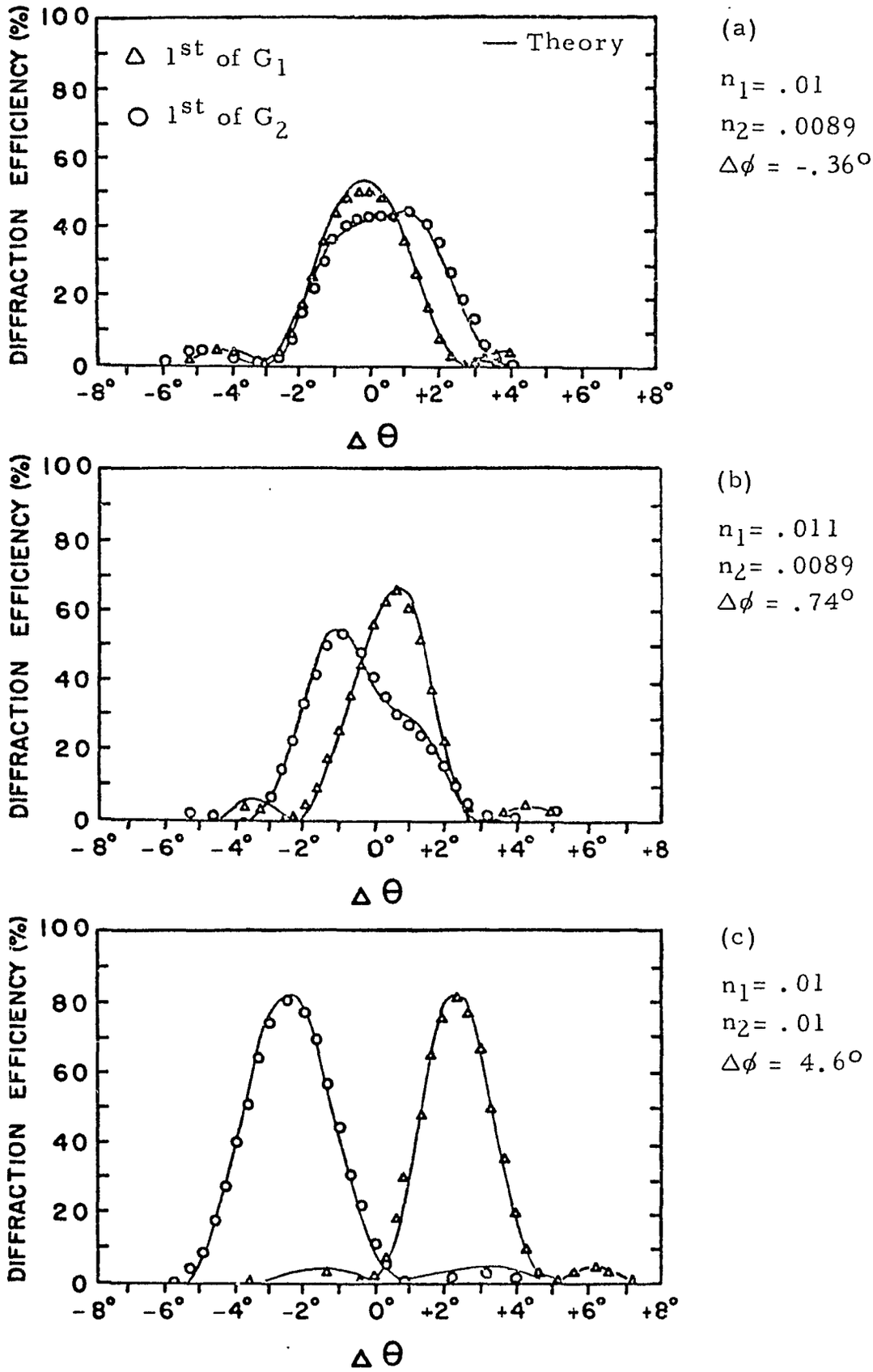


Figure 4-24. Comparison of Experimental and Theoretical Angular Selectivity for Direct-Coupling Readout: Variable $\Delta\phi$

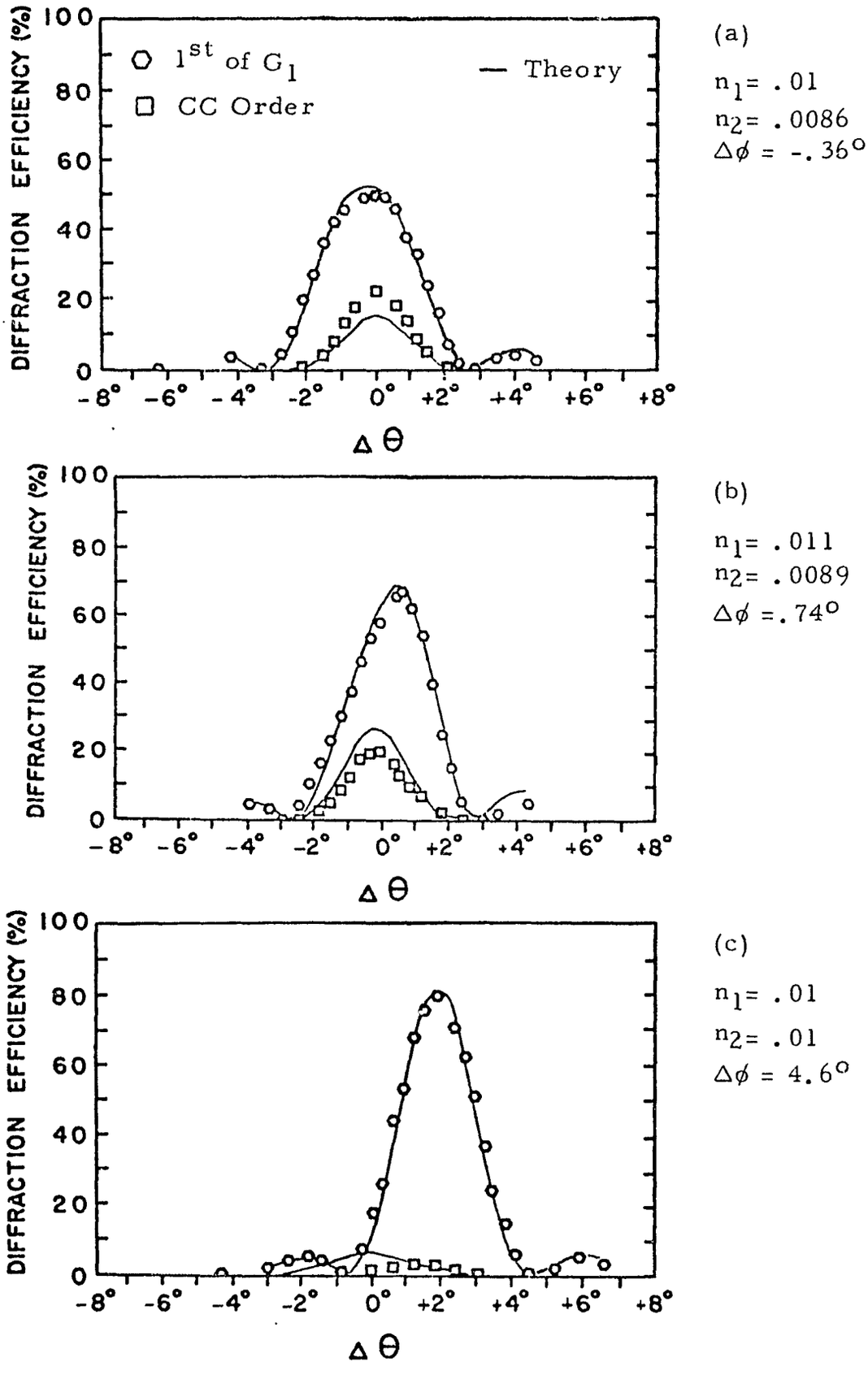


Figure 4-25. Comparison of Experimental and Theoretical Angular Selectivity for Cross-Coupling Readout: Variable $\Delta\phi$

difference in the grating frequencies is evident in the different widths of the curves. The individual index modulations are somewhat less than .015, so the gratings are not 100% efficient at their BAs in spite of the fact that they are decoupled. Because of fringe tilt, due to emulsion swelling, it is not possible to state directly that the maximum DE of each grating does not occur at its BA (construction angle). However, for small offset, the difference in the angles for which each grating has maximum DE is clearly larger than the determined value of $\Delta\phi$.

The decoupling for the cross-coupling readout mode (Fig. 4-25) is very similar. The angular selectivity of the cross-coupled order is clearly sharper than that of the first. Note, that the AS of the first order of G_1 is essentially the same for the two readout modes despite the large differences of the DE of the other diffracted order in the two cases. As suggested, therefore, the decoupling is no more rapid for this readout mode. For large offset (Fig. 4-25c), the cross-coupled order is negligibly small.

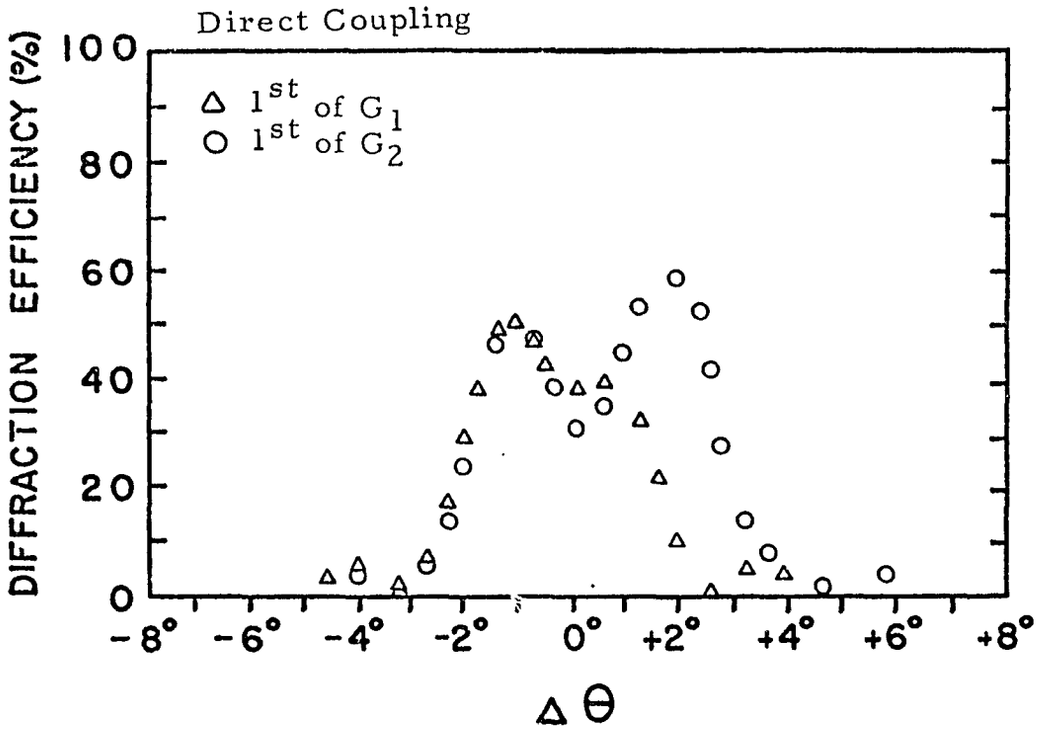
In general, the comparison between experiment and theory as demonstrated in Figs. 4-24 and 4-25 is quite good. The agreement is especially good in the case of direct coupling, of course, because this is the case that was used to determine exactly the parameters n_1, n_2 and $\Delta\phi$. However, the values of these parameters used in the theoretical curves to give good fit were well within the experimental uncertainty of their values estimated from our knowledge of the index modulation versus exposure and fringe tilt due to development. Also, considering the coupling between the gratings, it is significant that these parameters give good agreement with the DE of both of the diffracted waves in the direct-coupling case. The small discrepancies in the cross-coupled order are probably due to a slightly incorrect choice of the index modulation, because as

Fig. 4-23 shows, the DE of the cross-coupled order changes rapidly with modulation in the region of index modulation used in the experiments. The first order changes much more slowly. The measured sidelobes are typically slightly lower than predicted. This results because the index modulation is not constant but decreases somewhat with depth because of attenuation of the exposing beams during construction (16). Nevertheless, the agreement is quite good.

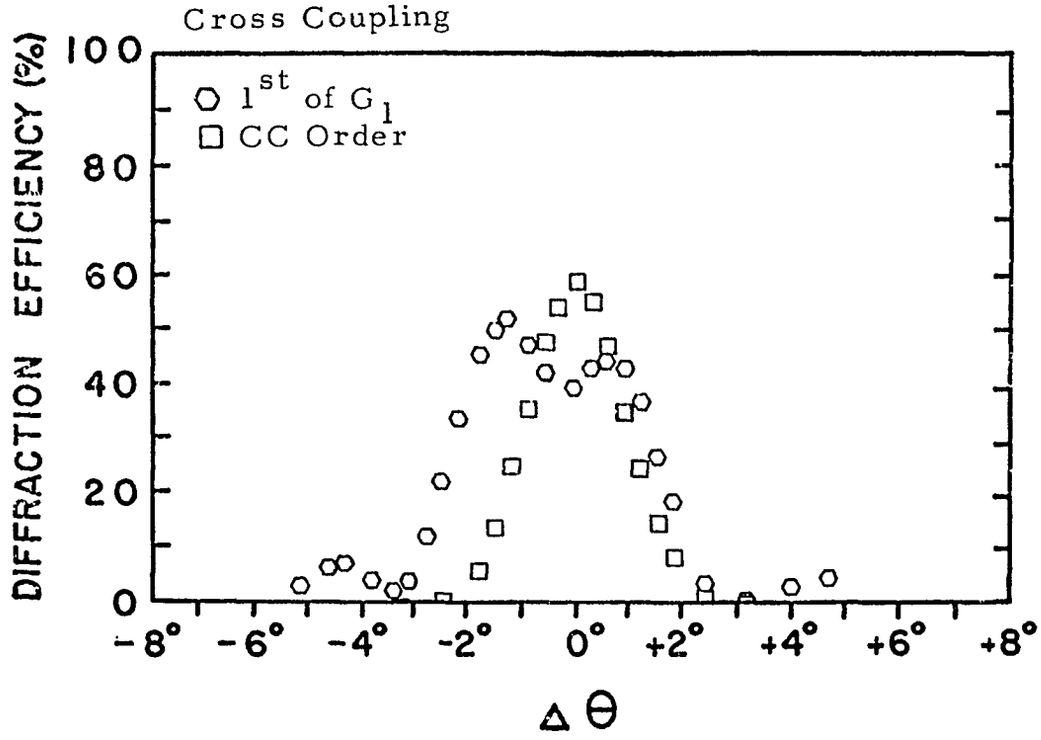
The experimental AS for a double grating made at a higher level of modulation (higher exposure) is shown in Fig. 4-26. The index modulation of G_1 is $\cong .017$, which is greater than the necessary single grating modulation to achieve 100% DE. The double grating was constructed so as to have no offset after development; however, there is a small residual offset. In the direct-coupling case (Fig. 4-26a), the AS of each of the diffracted orders is a double peaked curve with the maximum DE occurring off the common construction angle. The asymmetry is due to the residual offset. At this higher modulation level, the cross-coupled order (Fig. 4-26b) is stronger than the first order. Also, the former displays no sidelobes, as predicted.

4.5.2 Coherent Superposition

Three-grating structures made by simultaneously interferring the three beams of the apparatus in Fig. 4-22 were also constructed. Unfortunately, the fringe tilt induced by swelling can not be compensated for in this case and baking the developed plates did not completely return the fringe planes to their pre-development positions. However, most of the tilt was eliminated which allows qualitative comparison with the theory. The construction parameters were the same as in the previous section. Representative plots of the experimentally measured AS for readout about the center construction angle (θ_1) and about one of the outer angles (θ_2), are



(a)



(b)

Figure 4-26. Experimental Angular Selectivity for High Modulation, $n_1 \cong n_2 \cong .017$ and $\Delta\phi = 0$

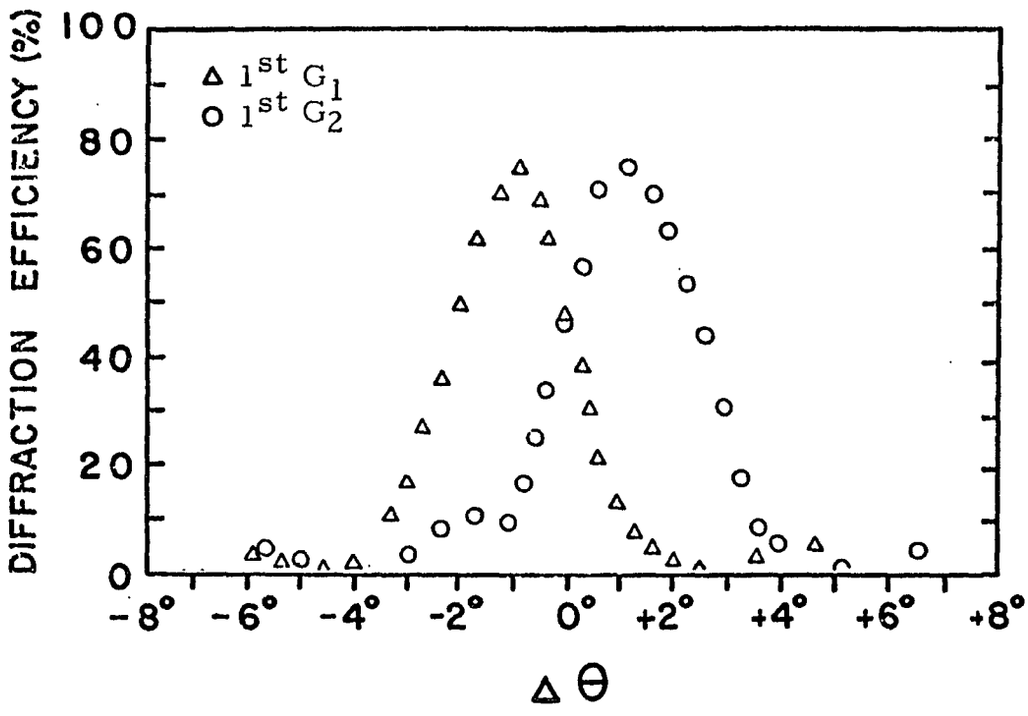
shown in Figs. 4-27a and 4-27b, respectively. Each of the three gratings has approximately the same index modulation, ≅.01. The addition of the sum frequency grating does, indeed, tend to decouple the gratings as each first order DE maximizes in opposite directions off the center construction angle (Fig. 4-27a). The sign of the angular difference from the common construction angle for which this occurs is as predicted (see Fig. 4-21). The AS curves are somewhat sharper than for the case of incoherent addition.

For readout about θ_2, the diffracted order that is only the result of double diffraction in the incoherentgeometry (P_2) is rather weak here even though there is a grating component (G_3) that connects it directly to the readout wave. Also, this order maximizes at the construction angle and displays measurable sidelobes.

The advantage of the coherent addition over the incoherent addition, with respect to bias buildup of the film, was demonstrated by the experiments. A lower total exposure (by a factor of ≅2) was required to produce three coherently added gratings at a particular index modulation then was necessary to make two incoherently added gratings of similar modulation. Because the film response ultimately saturates (see Fig. 3-13), we can achieve a higher maximum index modulation of the gratings by a coherent superposition.

Thus, the experimental results verify the predicted differences between the incoherent and coherent additions. In particular, the interesting fact that the sum frequency grating acts to partially decouple the gratings for readout near the center construction angle has been demonstrated. Also interesting is the suppression of the order that is referred to as the cross-coupled order in the incoherent case. Other experiments also confirm the differences between the properties of incoherently and coherently added gratings as predicted by the analytical results derived here (49).

(a) Readout about center construction angle



(b) Readout about outer construction angle

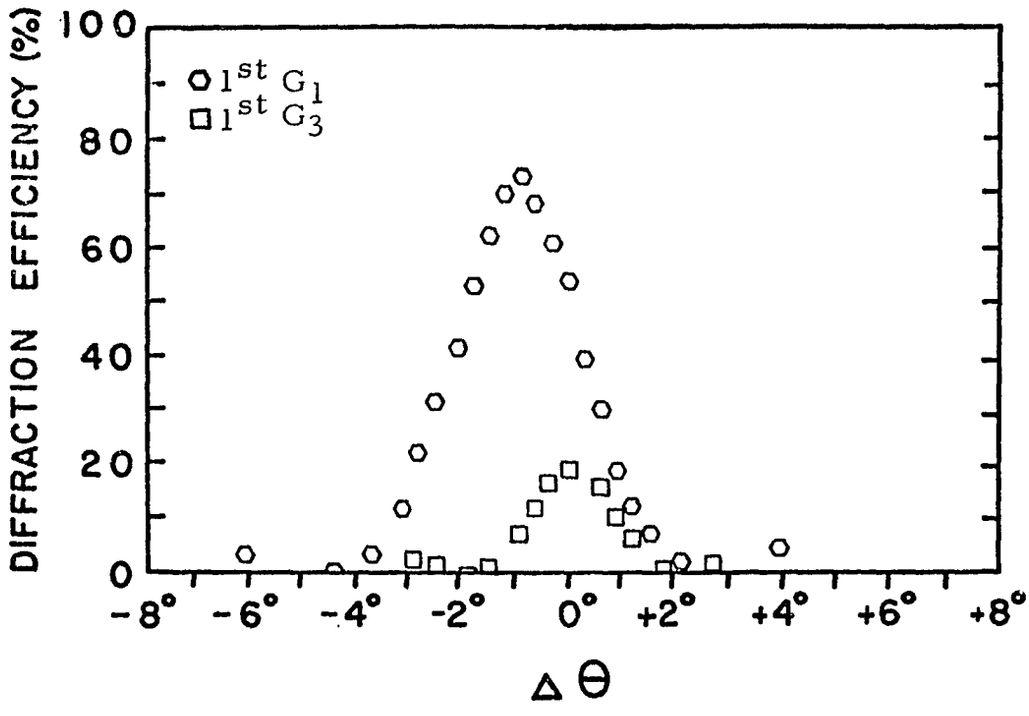


Figure 4-27. Experimental Angular Selectivity for Coherent Superposition, $n_1 \cong n_2 \cong n_3 \cong .01$

4.6 Summary and Conclusions

The method of thin-grating decomposition has been used to analyze the basic coupling mechanisms between multiple gratings recorded with an equal or almost equal construction angle in the same thick phase material. A general three-wave analysis has been performed (Appendix) to derive analytical expressions for the efficiency of the diffracted orders of two incoherently added gratings of arbitrary relative offset and of the three-grating coherent superposition. The results are valid for arbitrary readout angles near the BAs. We predicted and experimentally verified the possibility of 100% cross-coupling of light between two incoherently added gratings for readout at the noncommon BA. We further showed that this phenomenon can be understood as second-order readout of the two-grating system where the differential dispersion of the intermediate step can be made zero by using a common construction beam. Therefore, cross-coupling is a very strong mechanism despite the fact that it is a second-order process. In one of the incoherent geometries, the cross-coupled order has negligible sidelobes.

We have shown that a great deal of insight into the AS properties of strongly-coupled double gratings can be gained by examining the angular dependence of the differential dispersion of the diffracted orders. The two gratings are coupled by virtue of the dependence of the dispersion terms, ξ_1 and ξ_2, upon the readout angle. The individual dispersion terms, as well as their sums and relative values are important in determining the angular selectivity for varying degrees of coupling. These, in turn, depend upon the relative grating frequencies, the offset angle and the type of incoherent construction geometry used. There are interesting and rather unexpected differences in the AS results for the two incoherent addition

geometries. We have also shown that the mechanism of cross-coupling is as important as direct-coupling. For readout at one of the BAs (and equal index modulation of the two gratings), we have shown that the decoupling that results from offset depends only upon the magnitude of the differential dispersion of the non-Bragg order and the modulation level. It is independent of the type of incoherent addition and the readout mode. The necessary offset to achieve decoupling depends upon the modulation level. Decoupling proceeds initially quite rapidly with offset but the approach to a completely decoupled system is asymptotic. For moderately coupled gratings, the first order DE may or may not maximize at the BAs, depending upon the type of incoherent addition. The cross-coupled order maximizes at the second-order BA of the two-grating system in both cases. An interesting result with respect to Bragg-angle multiplexing applications is that nearly decoupled double gratings have AS mainlobes that are narrowed in the angular region of interaction. The consequence is that less angular offset is required to decouple the gratings than would be expected on the basis of single grating theory. This results in a higher possible packing density.

The results for coherently superimposed gratings show that the addition of the sum frequency grating acts to partially decouple the two lower frequency gratings. The readout angles of maximum DE do not correspond to the common construction angle. Thus, at the construction angle, there is no real gain. In fact, for equal modulations, a minimum of 12% of the transmitted light remains undiffracted.

Extensive experiments with multiple gratings interferometrically constructed in dichromated gelatin film have been performed. The results are in good agreement with the theoretical results.

We have analyzed the coupling between two gratings (and three in the coherent case). For this case, we can obtain analytical results that are reasonable to interpret. These results provide insight into the basic coupling phenomena. The method of TGD can be used to analyze an arbitrary number of strongly coupled gratings; however, because more orders are important, the results must, in general, be obtained by numerically performing the matrix multiplication. For example, we can show that in triple incoherent additions, the triple diffraction process can also be 100% efficient. For most applications, although several incoherent additions are made, the construction is such that only nearest neighbor coupling is important. The results derived here can be applied in such cases. Also, although we have treated plane wave gratings, the results can be qualitatively applied to incoherent additions of more complicated holograms.

CHAPTER 5

PROPAGATION IN NONUNIFORMLY MODULATED THICK GRATINGS

We have seen that the DE of a thick grating is strongly dependent upon the readout angle. In applications such as Bragg-angle multiplexing, a very narrow AS is desirable. However, there are applications, for example, the construction of holographic optical elements, where a more uniform, broad response is required. In this chapter, we use the method of TGD to investigate the effect of a nonuniform index modulation upon the AS response of a thick grating with the aim of shaping or apodizing the response in a desired way. A review of previous work is given. For low DE, such that the zero order is not strongly depleted, we show that the DE at angles off the BA is related to the depth dependent index modulation by a Fourier transform (FT) relation. This relationship breaks down at high DE levels, but serves as a guide to useful apodization functions. Because we want to broaden and increase the uniformity of the response, we consider an index modulation that varies as a sinc function in depth. We also analyze the case of a lateral fringe shift at some intermediate distance in the grating and show that it gives considerable broadening. Although, for practical reasons, we have not constructed any apodized gratings, we present experimental results to show that the grating interferometer (27) can be used to construct gratings with the desired index modulation profiles.

5.1 Background

We consider a single thick phase grating with unslanted fringes in which the index modulation is depth dependent, $n_1(z)$. Leith, et al.,

have shown that the relative amplitude of the first order for readout angles off the BA is related to $n_1(z)$ by a FT relation. This is valid provided that the zero order is essentially unchanged as it propagates through the grating, which implies low DE (16). We will give a derivation of this result using TGD. Cohen and Gorden have found similar results for acoustic gratings with nonuniform modulation (50). They also performed some interesting experiments to demonstrate this result. Kermisch has derived the expression for the DE of a thick grating with a slowly decreasing exponential index modulation (51). His analysis includes the effect of depletion of the zero order. The most likely nonuniform case, an exponential decay of n_1 results from attenuation of the recording beams during construction. The most noticeable effect upon the AS for this case is that the zeros are washed out. Kermisch also showed that for a thick grating with arbitrary index profile, the DE for readout at the BA is given by (51)

$$\mathrm{DE}\,(\theta_B) = \sin^2\left(\frac{\pi}{\lambda c_o}\int_o^D n_1(z)\,dz\right). \qquad 5.1$$

In this case, the only difference from the uniform grating (Eq. 2.45) is that $n_1 D$ is replaced by $\int_o^D n_1(z)\,dz$. For arbitrary readout angles, however, the functional form of n_1, and not just its integral, is important. Uchida has also analyzed the case of an exponentially varying index modulation using a coupled-wave analysis (52). Unfortunately, although it is amenable to solution and commonly encountered, the exponential profile does not give useful apodization.

Recently, Kogelnik has analyzed the wavelength selectivity of reflection gratings that have a slowly varying modulation or fringe spacing (53). His intent was to determine profiles that cause

suppression of the high sidelobes characteristic of reflection gratings (30% for modulation such that the DE is 100% at the BA). Such suppression is important in applications of wavelength rejection filters for optical waveguides (54). He shows that the coupled-wave equations can be written as a single nonlinear Riccati equation which must be evaluated numerically for an arbitrary index profile. He also points out useful scaling laws. He finds that a quadratic convex index profile reduces the sidelobe level considerably. As shown in the last chapter, the double diffraction process can also be useful for suppressing sidelobes.

5.2 Application of TGD to Nonuniform Gratings

The method of TGD can be used to numerically calculate the DE for gratings with arbitrary longitudinal index modulation by assuming the modulation to be constant over a thin grating slab. We are interested in broadening and making more uniform the angular response while maintaining the DE at a high level. We, therefore, generally want to consider gratings that are only marginally thick. Because the same means by which the angular response of the first order is increased, also reduces the Bragg suppression of other orders, it is often necessary to include at least the conjugate first and second orders in the numerical calculations. Since there is no known solution to the inverse problem (except for low DE) and in general, we must calculate the response numerically, we make no attempt to determine the optimum index profile. Our intention is to demonstrate the possibility of usefully apodizing the response of thick gratings and to describe an experimental method by which the required index can be realized.

5.2.1 Fourier Transform Relation for Low DE

The FT relation between the angular dependence of DE and $n_1(z)$ for low DE can be shown as follows. We assume that only the 0 and -1 orders are important. The coupling matrix for the m^{th} thin grating is

$$\underset{\sim}{m}^{H} = \begin{bmatrix} e^{-i\Phi} & i\frac{\delta(m)}{c_1} \\ i\frac{\delta(m)}{c_o} e^{-i\Phi} & 1 \end{bmatrix} \tag{5.2}$$

where $\Phi = 2\pi n_o/\lambda \Delta z(\cos \theta_1 - \cos \theta_o)$ and $\delta(m) = \pi n_1(m \Delta z)\Delta z/\lambda$. We assume unslanted fringes and the common phase factor outside the coupling matrix is dropped. We now assume that the depletion of the zero order is negligible and the amplitude of the first order is thus small. In this case, the amplitude of the first order after the N^{th} slab can be written as

$$A_1(N) = i\frac{\delta(N)}{c_o} e^{-iN\Phi} + A_1(N - 1)$$

$$= i \sum_{m=1}^{N} \frac{\delta(m)}{c_o} e^{-im\Phi} \tag{5.3}$$

where $A_o(0) = 1$. If we now let $N \to \infty$, $\Delta z \to 0$, $N\Delta z = D$, Eq. 5.3 becomes

$$A_1(D, \Delta\theta) = \frac{i\pi}{\lambda c_o}\int_o^D n_1(z) e^{-i2\pi f \Delta\theta z} dz \tag{5.4}$$

We have used the approximation of Φ for small angular deviation from the Bragg angle corresponding to wavelength λ (Eq. 2.36).

Equation 5.4 demonstrates the simple FT relation between the angular dependence of the first-order DE and the depth dependence of the index modulation scaled by the grating frequency. For a uniform index over finite thickness D, the result is a sinc function angular dependence. Note that when the results of Eq. 5.4 are valid, the inverse problem is also solved.

The above results can be anticipated by intuitive arguments. If the zero order remains essentially constant in amplitude, the diffracted component from each plane is proportional to $n_1(z)$. The relative phase of the contribution from the z plane depends upon the dispersion between this component and those from other planes, which depends upon the readout angle and grating frequency, as well as upon z. The total effect is found by simply summing the contributions as indicated in Eq. 5.4. Note that this FT relation implies that the AS will be symmetric about the BA for any real index profile. As the DE is increased, the zero order is no longer constant and the contribution from each plane depends upon the magnitude of A_0 as well as upon n_1. The FT relation is no longer valid. The problem becomes considerably more difficult and for arbitrary index profiles, the matrix multiplication must be performed numerically.

5.2.2 Sinc Function Modulation Profile

For low DE, Eq. 5.4 indicates that an index modulation profile

$$n_1(z) = \text{sinc}\,[\alpha(z - D/2)] \qquad 5.5$$

where sinc (y) = sin (πy)/πy, should increase the uniformity of the angular response. The FT of sinc(y) is

$$\mathrm{FT}\{\mathrm{sinc}(y)\} = \begin{cases} 1 & |f_y| \leq 1/2 \\ 0 & \text{otherwise} \end{cases} \qquad 5.6$$

where f_y is the transform variable. However, a completely uniform response would require an infinitely thick emulsion. A sketch of a truncated sinc function is shown in Fig. 5-1. Note that negative values of n_1 correspond physically to a 1/2 period shift in the grating fringes.

To determine whether a sinc function index profile gives appreciable gain in angular response uniformity at high DE also, we calculate the results numerically for some illustrative examples. Before discussing the results, several comments must be made. To assess the improvement that results from apodization, we compare the AS to that of a uniform grating. For a uniform grating, the width of the AS curve is inversely proportional to D and f and the DE at the BA depends upon $n_1 D$. If we can achieve a higher n_1, we can decrease D and thereby achieve a broader response while maintaining the same level of DE. This remains valid provided that the grating can still be considered thick. In fact, we can also increase the width by about 50%, by modulating to the second DE peak ($\gamma = 3\pi/2$ in Eq. 2.45). Thus, as a practical matter, the width (to the first cutoff) is limited by the maximum achievable n_1. We compare the angular response of an apodized grating to that of a uniform grating with the condition that the maximum index modulation of the former be no greater than the constant modulation for the latter. The comparison must also be made at the same level of DE. Because the DE at the BA depends upon the integrated index, the total thickness of the apodized grating (for example, for the sinc function case where n_1 becomes negative) must be much greater than that of the uniform case. This, in turn, can be

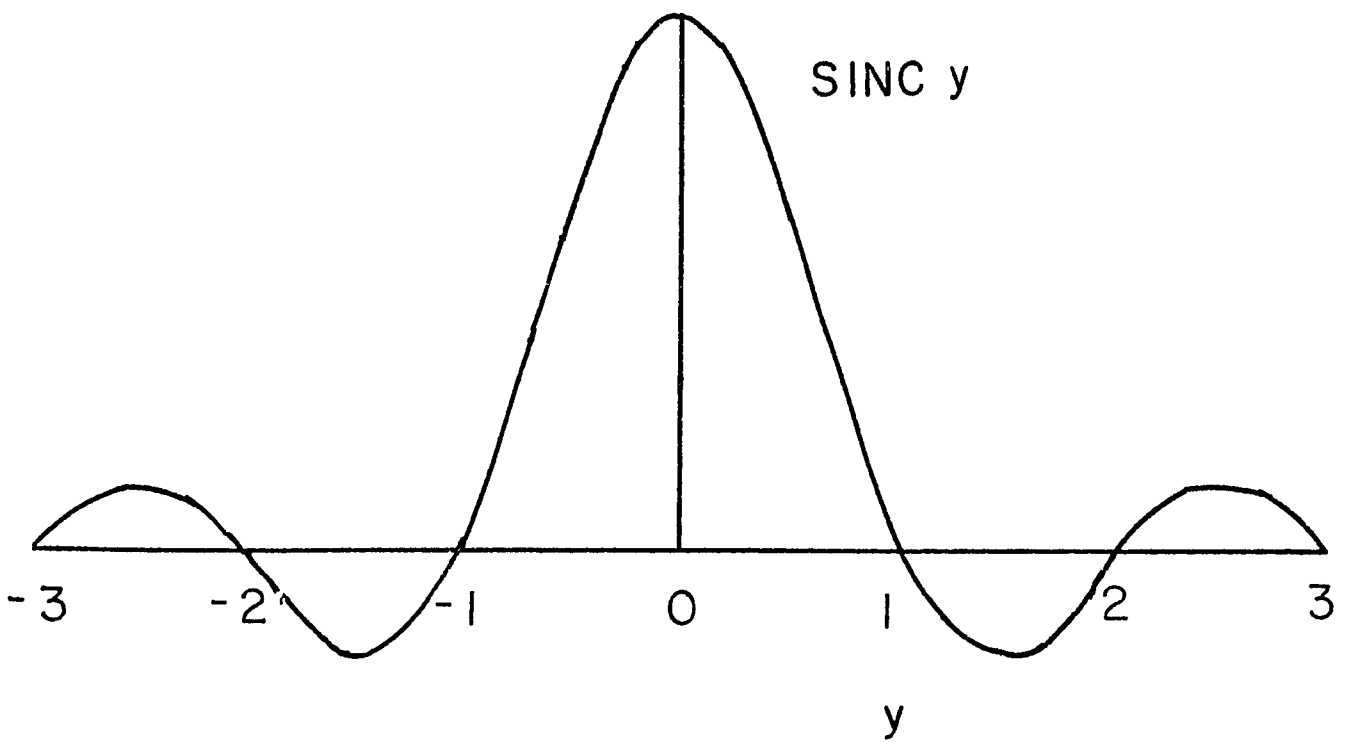
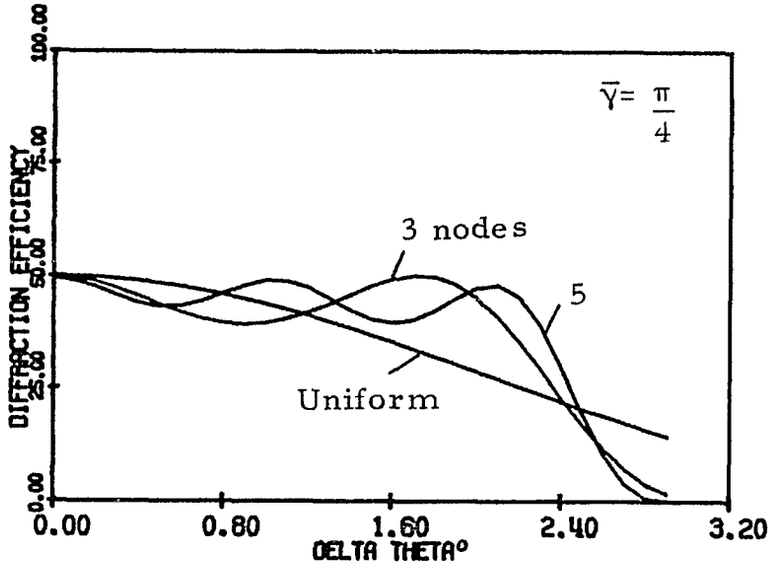


Figure 5-1. Sinc Function

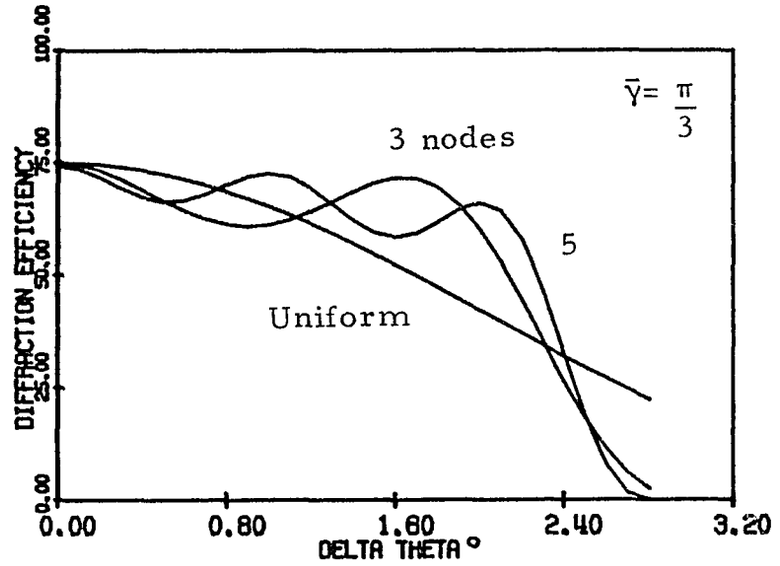
expected to cause a narrowing of the AS. Nevertheless, this is the only realistic way to assess the gain of apodization over what could be achieved for the same maximum index modulation with a uniform grating.

The calculated AS results for a grating with a sinc function modulation dependence are shown in Fig. 5-2. As a reasonable maximum n_1 (for dichromated gelatin, see Fig. 3-13), we use $n_1 \lesssim .03$. For the uniform case, we take D = 8 μm. The grating frequency used was f = 1400 1/mm giving Q $\cong$ 32. The results were calculated for truncated sinc functions with three and five nodes on either side of the center peak. The thicknesses required in these cases were 45 μm and 76 μm, respectively. The results are given for three levels of modulation, $\bar{\gamma} = \frac{\pi}{\lambda\sqrt{c_o c_1}} \int_o^D n_1(z)\,dz$. The AS is symmetrical in $\Delta\theta = \theta_o - \theta_B$. (We would not expect drastic departure from the symmetric response predicted for low DE by the FT relation.)

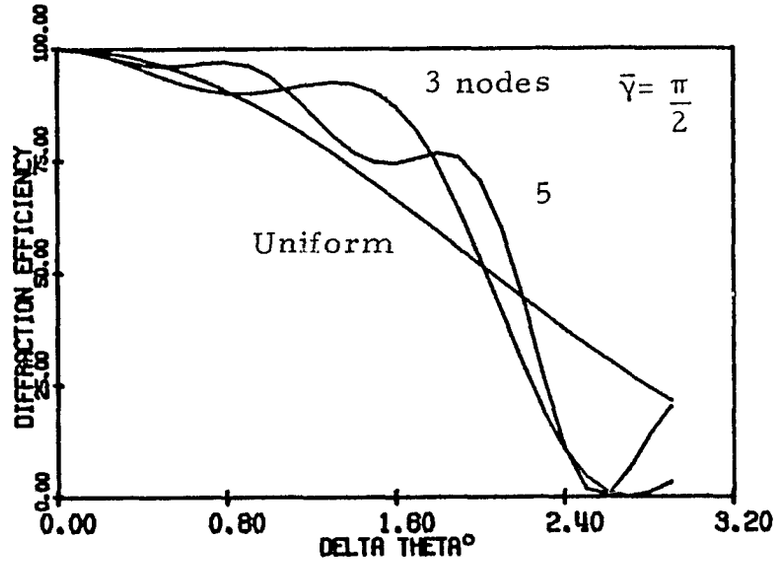
The results show that considerable gain over the uniform case can be obtained for given DE levels in each of the three cases. For example, for $\bar{\gamma} = \pi/2$ (Fig. 5-2c), the angular width for which the DE exceeds 90% is about a factor of 2 greater for the grating apodized with 3 nodes. Note that in this case, the more truncated sinc function gives the better result. Also, the sidelobe for the sinc function with 5 nodes is quite high. For the lowest modulation level (Fig. 5-2a), the approximate FT relation is partially evident. As more nodes of the sinc function are included, the response becomes more uniform by having more ripples with less variation. In all cases, however, the angle for which the first-order DE becomes zero is significantly smaller than for the uniform grating. This occurs because to obtain the correct integrated index, the mainlobe of



(a)



(b)



(c)

Figure 5-2. Angular Response for Sinc Function Index Modulation Profile

the sinc function must be about twice as wide as the uniform grating thickness. Thus, a decrease in the angular width for lower DE is sacrificed to achieve an increase in width and uniformity at the higher DE levels (for a given modulation level). This is usually a reasonable tradeoff.

5.2.3 Fringe Shift

Much of the gain from the sinc function profile results from the fringe shift that corresponds to negative values of n_1. The case of an abrupt shift in the fringes at some intermediate thickness can be treated analytically. The situation is depicted in Fig. 5-3, where the fringes are shifted by d' after thickness D_1. The relative phase shift of the fringes is, $\Delta = 2\pi d'/d$, where $d = 1/f$. Although such an abrupt shift would be difficult to realize, useful insight into the effect of apodization can be gained by analyzing this, perhaps, rather idealized case.

We can find the first-order DE for readout near the first BA for the grating shown in Fig. 5-3 by a straightforward, but tedious, extension of the results of the last section of Chapter 2. We assume that only the zero and first orders are important. The amplitude vector of the light field that exists from the grating is

$$\underset{\sim}{A}(N) = \underset{\sim}{H}_1^{N_2}\, \underset{\sim}{H}_2^{N_1} \begin{bmatrix} 1 \\ \\ 0 \end{bmatrix} \qquad 5.7$$

where $N_2 = D_2/\Delta z$ and $N_1 = D_1/\Delta z$. The matrix $\underset{\sim}{H}_1$ is identical to that given in Eq. 2.29. In $\underset{\sim}{H}_2$, δ is replaced by $\delta\, e^{i\Delta}$. We ignore possible back reflections caused by the shift. The effect that the shift has upon the suppression of the other orders can be examined by including them and doing the matrix multiplication numerically.

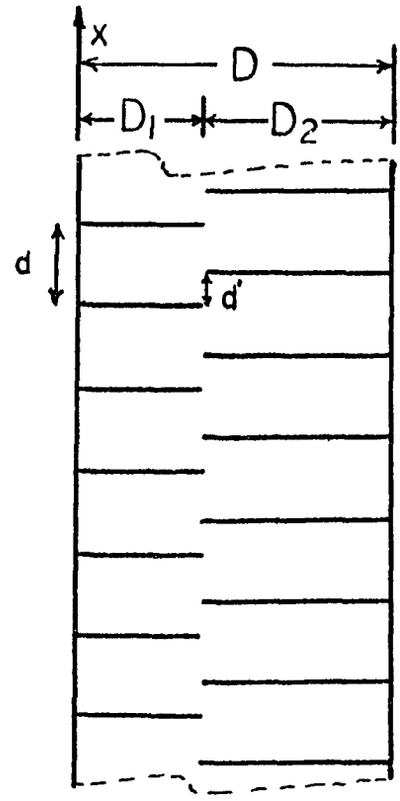


Figure 5-3. Fringe Shift

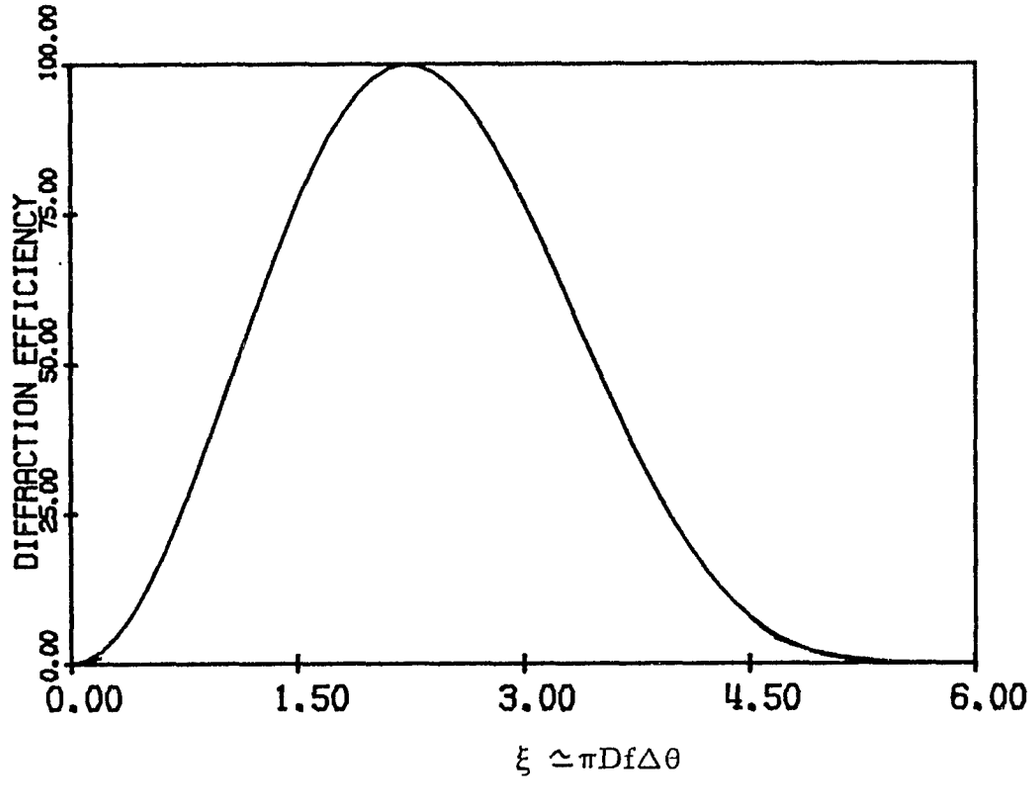


Figure 5-4. Angular Response for π Fringe Shift at Center of Grating

We have determined the result for an arbitrary shift. However, the expression simplifies considerably for $\Delta = \pi$, and we present only this result. For a π fringe shift after thickness D_1, the first order DE for total thickness D is

$$DE = \frac{1}{1 + (\xi/\gamma)^2} \sin^2 \left\{ \left(\frac{D_2 - D_1}{D} \right) (\xi^2 + \gamma^2)^{1/2} \right\} + \frac{4\gamma^2\xi^2}{(\xi^2 + \gamma^2)^2}$$

$$\sin^2 \left[\frac{D_1}{D} (\xi^2 + \gamma^2)^{1/2} \right] \sin^2 \left[\frac{D_2}{D} (\xi^2 + \gamma^2)^{1/2} \right] \qquad 5.8$$

where $\gamma = \pi n_1 D/(c_o c_1)^{1/2}$ and $\xi = \frac{2\pi n_o}{\lambda} D(\cos \theta_1 - \cos \theta_o)$, are the grating strength and dispersion terms that correspond to the total thickness D. At the BA, the DE depends upon the integrated index, $n_1(D_2 - D_1)$. The second term of Eq. 5.8 contributes only for non-Bragg angles. It maximizes for $\gamma = \xi$ and for D_1 and D_2 such that the argument of the two sine terms are $n\pi/2$. For $D_2 = D_1$, Eq. 5.8 becomes (for $\Delta\theta = \theta_o - \theta_B << 1$, $\xi \cong \pi D f \Delta\theta$)

$$DE = \frac{4\gamma^2\xi^2}{(\xi^2 + \gamma^2)^2} \sin^4 \frac{1}{2}(\gamma^2 + \xi^2)^{1/2} \qquad 5.9$$

which is zero at the BA. However, for readout angles (there will be one on either side of the BA) such that $\xi = \pi/\sqrt{2}$ and $\gamma = \pi/\sqrt{2}$, the DE is 100%. The shift moves the maximum DE off the BA. This case is shown in Fig. 5-4. With respect to $\Delta\theta$, results are symmetrical. A similar peaking for symmetric angles off the BA occurs for over-modulated uniform gratings, although not with 100% DE.

We generally want to maintain the DE at the BA; therefore, a shift half way through the grating is not desirable. To compare Eq. 5.8 with the uniform result (with the same DE at the BA and same index), it is convenient to express the grating strength and differential dispersion in terms of the difference thickness. This is

the thickness required of a uniform grating to obtain the same BA efficiency. We define

$$D_d = D_2 - D_1 \qquad (D_2 > D_1) \tag{5.10}$$

$$r = D_1/(D_2 + D_1) \tag{5.11}$$

$$\gamma' = \gamma D_d/D \tag{5.12}$$

$$\xi' = \xi D_d/D \tag{5.13}$$

Then Eq. 5.8 becomes

$$DE = \frac{1}{1 + (\xi'/\gamma')^2} \sin^2 (\xi'^2 + \gamma'^2)^{1/2} + \frac{4\gamma'^2\xi'^2}{(\xi'^2 + \gamma'^2)^2}$$
$$\sin^2 \left[\left(\frac{r}{1 - 2r}\right)(\xi'^2 + \gamma'^2)^{1/2}\right] \sin^2 \left[\left(\frac{1 - r}{1 - 2r}\right)(\xi'^2 + \gamma'^2)^{1/2}\right] \tag{5.14}$$

Expressed in this form, Eq. 5.14 shows very clearly that there is real broadening of the AS over what could be obtained from a uniform grating with the same n_1 and DE at the BA. Indeed, the first term above is just that result (compare with Eq. 2.45) for a uniform grating of thickness D_d. The second term shows the gain that is obtained for angles off the BA. This is a true gain at no cost in maximum index required and with no loss at the lower DE levels as in the case of the sinc function profile.

In Fig. 5-5, we plot the results of Eq. 5.14 for several modulation levels, γ'. Note, as mentioned, that the result for the uniform grating (r = 0) is always the lower bound for the apodized cases. There is considerable broadening. In particular, for $\gamma' = \pi/2$, there is a factor of about 2 gain in width above the 60% DE level for r = .3. Unfortunately, there is not a good gain in uniformity. This could possibly be achieved by using multiple shifts.

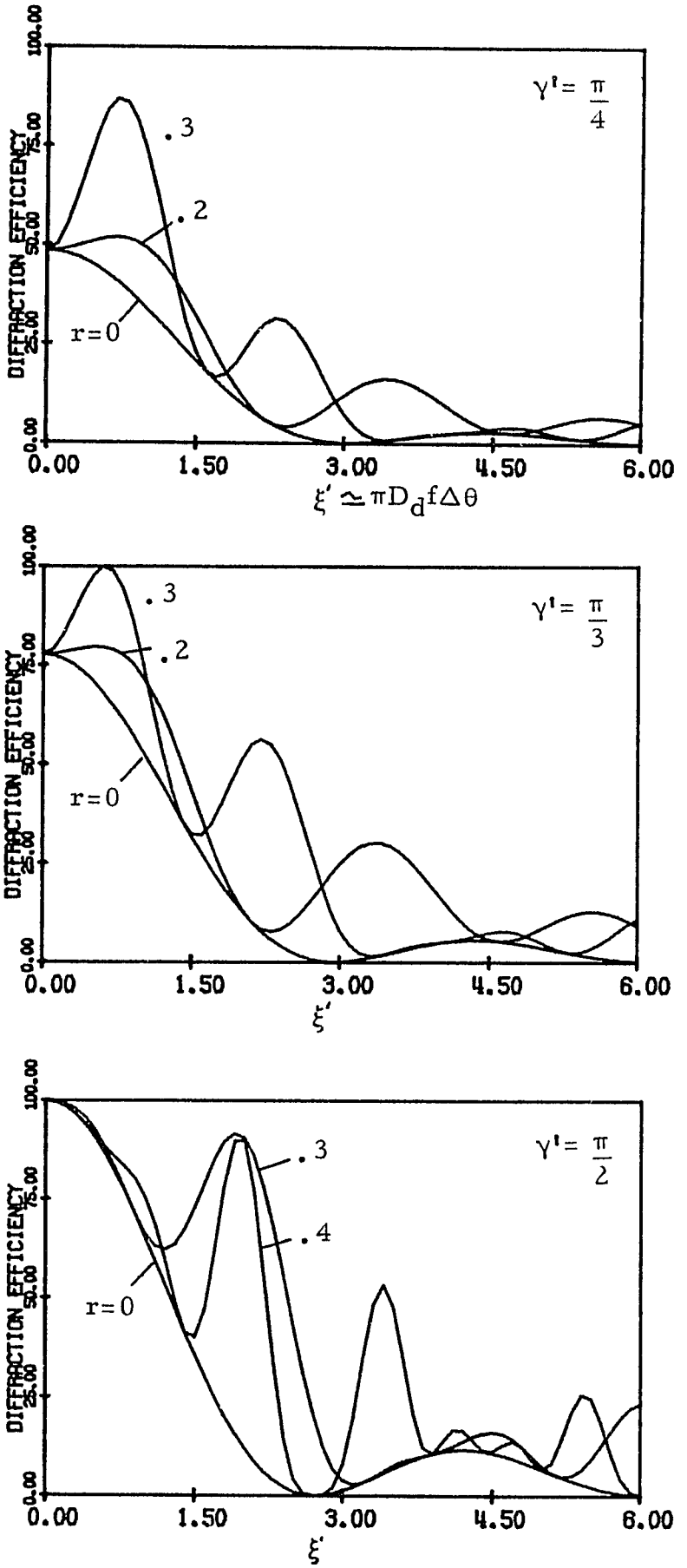


Figure 5-5. Angular Response for π Fringe Shift

We might expect that the perturbation introduced by fringe shift that causes broadening of the first-order response will also decrease the suppression of other orders. This effect has been examined briefly by including higher and conjugate orders and doing the matrix multiplication numerically. We found that it is necessary that both the Q factor of the smaller of D_1 and D_2, as well as that corresponding to the difference thickness D_d be large ($\tilde{>}20$) to suppress other orders. The suppression is not as good as the uniform grating with the same Q (for D_d), especially at angles off the BA where the apodized grating has a much greater response than the uniform grating. Thus, any analysis to optimize the enhancement of apodization must include higher orders. Of course, if higher orders are not undesirable for other reasons, there may still be gain over the uniform case if the generation of these orders is at the expense of the zero rather than the first order.

5.3 Construction of Gratings with Required Index Profiles

The above analysis would be rather fruitless if there was no possible method for making gratings with such unusual index modulation variations. Fortunately, in the case of a sinc function, the grating interferometer (27, 55) under spatially incoherent illumination can, in principle, perform this task.

5.3.1 Grating Interferometer

The grating interferometer (GI) is configured much like the Mach-Zehnder except that it uses gratings as the beam splitter and beam combiner elements. A schematic drawing of a typical arrangement is shown in Fig. 5-6. All the gratings have the same spatial frequency f along the x direction. For simplicity, we can assume that the gratings are thin. We assume that their grating lines are perfectly aligned and the gratings are parallel. Furthermore, we

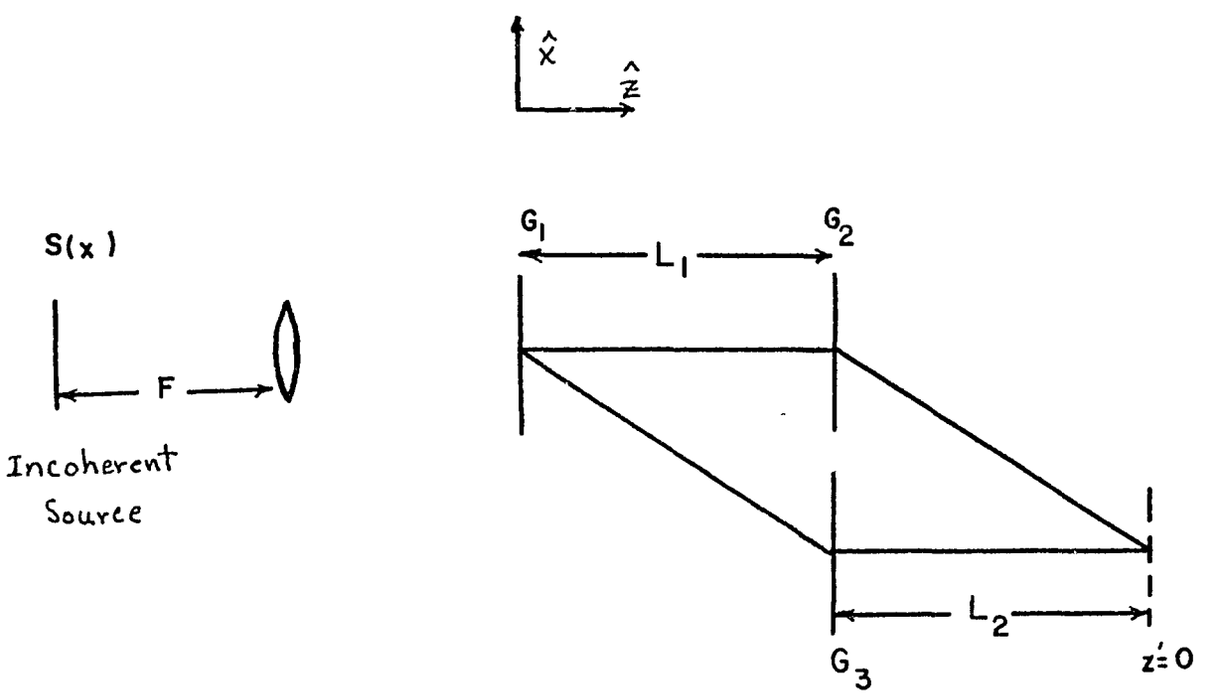


Figure 5-6. Grating Interferometer

consider only one lateral dimension. The incoherent light source (Fig. 5-6) is in the front focal plane of the collimating lens. The light incident upon G_1 is split into several orders. The zero order propagates to G_2 whose -1 order is diffracted toward the area of interest. The -1 of G_1 is diffracted toward G_3; the +1 order of this grating is allowed to interfere with the beam from G_2 to form fringes with spatial frequency f. All other orders are unimportant and are not shown. The perfectly aligned GI, even when illuminated with completely incoherent light, produces arbitrarily many fringes of perfect contrast in the z plane where $L_1 = L_2$. This is called the plane of localization. Perfect white light fringes can be formed in this plane with a flashlight. This is, of course, not possible with a Mach-Zehnder. Indeed, we can show that this useful feature of the GI results from the unique manner with which a grating deflects a beam. At planes off the plane of localization, the contrast of the fringes is reduced.

To use the GI to construct apodized gratings, it is only necessary that the source be spatially incoherent. A standard method for obtaining such a source is to pass a laser beam, expanded by an objective lens, through a spinning diffuser. There is no fixed phase relationship between the light transmitted by different points of the diffuser, so the light is spatially incoherent. The degree of spatial coherence is decreased by making the effective source (diffuser area illuminated) larger. For a spatially incoherent source distribution of intensity $S(x_s)$, we can show that the intensity of the interference at the plane z' (measured relative to the plane of localization) is (27, 55)

$$I(x, z') = I_o(1 + M(z') \cos 2\pi fx) \qquad 5.15$$

where

$$M(z') = \frac{1}{I_o} \int_{-\infty}^{\infty} S(x_s) \exp\left(-i \frac{2\pi f z' x_s}{F}\right) dx_s \qquad 5.16$$

and F is the focal length of the collimating lens. The fringe contrast M(z') in depth is given by the FT of the source intensity profile. A physical explanation of the GI's role in generating the above result can be made in the following way. According to the van Cittert-Zernike theorem (56), the mutual coherence function in a plane parallel to an incoherent source is given by the FT of the source intensity distribution, scaled by the distance between the planes. The mutual coherence between two laterally separated points is a measure of the contrast of the fringes that would be formed if light from these two points were allowed to interfere. The GI essentially transforms the lateral dependence of the mutual coherence of the light incident upon G_1 into the longitudinal contrast modulation of the fringes formed by the interferometer. There is a one-to-one relation between z' and the lateral separation between two points on the entrance plane (G_1) from which light arrives at z' via the two paths of the interferometer. In the plane $z' = 0$, at every x point the interference is between two light waves that have been derived from the same point on G_1. Therefore, the fringes formed have unity contrast. (We assume that the interferred beams are equal in amplitude.) For $z' \neq 0$, the fringe contrast is reduced because the fringes in this plane result from the interference between light that originated at points on G_1 laterally separated proportionately to z'. The proportionality depends upon the grating frequency.

For $S(x_s)$, uniform over the lateral extent W and zero elsewhere,

$$M(z') = \text{sinc}\,(fWz'/F) \qquad 5.17$$

If we center the photo-sensitive emulsion at $z' = 0$, the depth dependence of the exposure will be given by the sinc function, including laterally shifted fringes for negative values of M. If we further assume that the film response is linear, then a thick grating with the desired index modulation profile can be achieved

The FT relation between $S(x_s)$ and $n_1(z')$ for gratings constructed by this method together with that between $n_1(z')$ and $DE(\theta_o - \theta_B)$ for low DE readout, suggests an interesting new method for making holograms of self-luminous incoherent objects. A thick grating made by the above method for an arbitrary source distribution is essentially a hologram of the source in which the information (the FT of the intensity distribution) is encoded as the longitudinal rather than lateral modulation of the fringes. The readout process is linear, so rather than readout sequentially with the plane waves at different angles, we could simply illuminate the developed modulated grating with a bundle of plane waves (spherical wave). The angular and thus spatial distribution of the diffracted light (for low DE) will be the FT of $n_1(z')$. Because the FT is its own inverse except for inversion of coordinates, the diffracted amplitude distribution will reconstruct the source distribution $S(x_s)$.

5.3.2 Experiments

We now present experimental results to demonstrate that the GI can be used to realize a sinc function modulation of the fringe contrast. It was not practical to obtain sufficient localization to make apodized gratings in the relatively thin emulsions with which the previous experiments were performed. However, the feasibility of the technique is verified. The GI configuration shown in Fig. 5-6 was used where the incoherent source was a slit, aligned parallel to the grating lines, that was illuminated by an expanded

He-Ne laser beam whose spatial coherence was destroyed by a rotating diffuser. The gratings were thin, bleached gratings. The focal length of the collimating lens was 39 cm and $L_1 \cong 70$ cm. The system was roughly aligned under coherent illumination and the source coherence gradually reduced (by increasing the source size) to find the plane of localization. The frequency of the fringes formed is the same as that of the gratings of the interferometer. To make the fringes viewable, a fourth grating with the same frequency was placed in the observation plane to produce Moire fringes (beat fringes caused by slight misalignment of this grating with respect to the fringes formed by the GI). The Moire fringes have a much lower frequency.

The fringe contrast was measured using a 50 μm probe connected by fiber optic link to a photomultiplier tube. The probe was mounted inside a microscope eyepiece that was attached to a precision lateral translator. The fringe contrast or visibility is determined by measuring the maximum and minimum intensities of the interference pattern

$$FV = \frac{I_{max} - I_{min}}{I_{max} + I_{min}}. \qquad 5.18$$

The final grating and the detector were placed on a translation mount to vary z'. It is difficult to make the two beams equal in amplitude. Thus, the measured FV was normalized by its value in the plane of localization.

A typical plot of the measured FV versus z' is shown in Fig. 5-7. Note that the FV is defined as the magnitude of the contrast (Eq. 5.18). In fact, the fringes do experience the required contrast reversal (1/2 fringe shift) when the FV zeroes and increases.

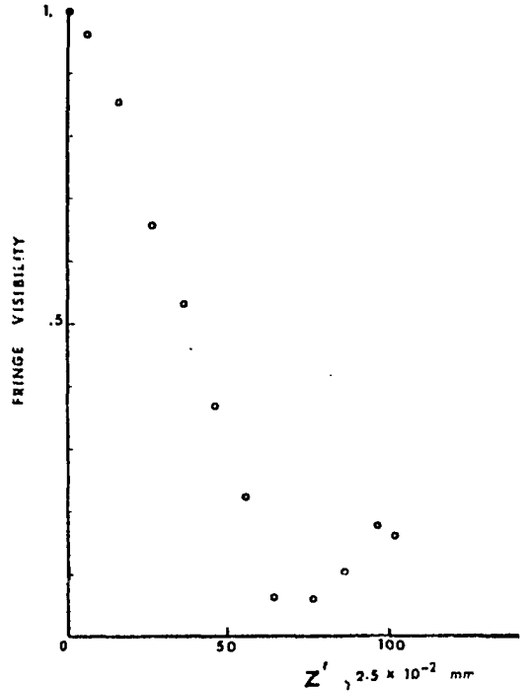


Figure 5-7. Fringe Visibility Versus z', W = 1 mm, f = 330 1/mm

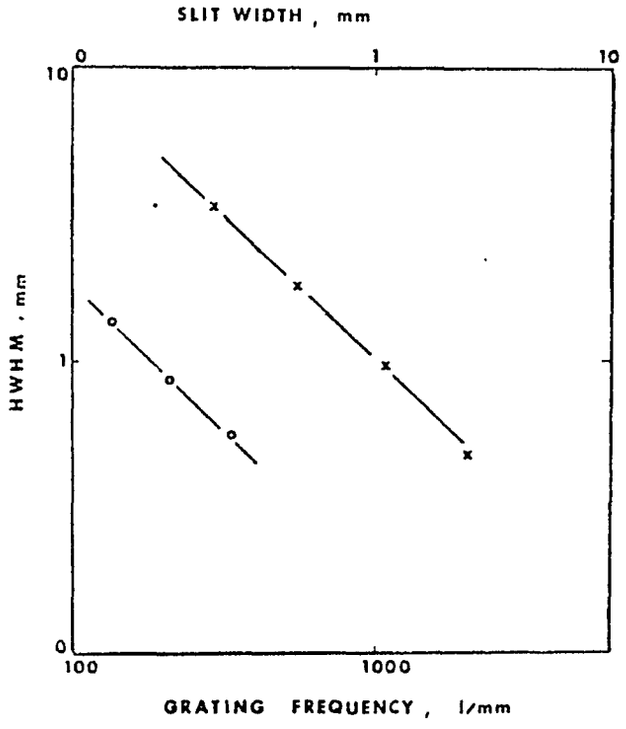


Figure 5-8. HWHM of Fringe Visibility Curves: vs f(o) for W = 2 mm; vs W(x) for f = 330 1/mm

The scaling of the fringe localization with f and W as predicted by Eq. 5.17, was also verified experimentally. For a fixed W, the FV versus z' curves were determined for GIs with different grating frequencies f. The half-width at half-maximum (HWHM) for each case was determined. Also, for a GI with fixed f, the HWHM of the FV versus z' that results for various slit widths, W, was found. In both cases, the focal length (F) of the collimating lens was fixed. The results, plotted in Fig. 5-8, demonstrate the linear dependence of the fringe localization upon both f and W as predicted by Eq. 5.17.

The degree of localization for the above results was not very great due to the relatively low grating frequencies and slit widths used. However, according to the scaling of the localization with f and W as indicated in Eq. 5.17 and shown by the experimental results, the width of the mainlobe should be able to be decreased considerably for reasonable values of f, F and W.

5.4 Summary and Conclusions

In this chapter, we have investigated the effect of a depth dependent index modulation upon the AS of a thick grating. The method of TGD can be used to calculate the angular response of the DE for an arbitrary index modulation profile. For low DE, the angular dependence of the DE is given simply by the FT of $n_1(z)$. We have examined the apodization achieved by a sinc profile and by an abrupt fringe shift. The former causes significant increase in the uniformity and angular width of the response at high DE levels. The width at cutoff is significantly less than for the comparable uniform grating. A 1/2 period fringe shift gives an increase in the DE over the uniform case for all levels. It does not increase the uniformity of the response, however.

We have proposed that the GI be used to construct apodized gratings. Any symmetrical index modulation profile can be generated, although there are practical problems encountered in achieving localization in relatively thin emulsions. We have also shown that the complementary FT relations for grating construction by the GI and subsequent readout, suggest an interesting new method of doing incoherent holography. We have performed experiments to demonstrate the feasibility of making apodized grating with the GI.

Other work on the GI, including an analysis and experiments of the effects of rotation misalignment upon the fringe contrast, has been performed (27) but is not included here. We have also holographically constructed gratings that are free from the inherent phase error due to substrate irregularities (57, 58). The procedure is to include the unique correction factor in the constructed fringe pattern so that the grating is self-correcting. Using these methods, high-quality gratings for the GI can be made with inexpensive substrates.

CHAPTER 6
SUMMARY AND CONCLUSIONS

In this thesis, we have developed the theory of thin-grating decomposition to investigate several topics of optical propagation in holographic gratings including secord-order readout of thick gratings, the properties of strongly-coupled multiple gratings and the effect of a nonuniform index modulation profile upon apodizing the angular response. For the first two topics, a general three-wave analysis has been performed to derive expressions for the efficiency of the two diffracted orders. Experimental results from gratings constructed in dichromated gelatin have generally been in very good agreement with the derived results. Specific concluding remarks are given at the end of each chapter. Here we comment on some of our more interesting results, point out areas of applications and suggest areas of further research.

For second-order readout, we discovered a higher-order phase condition between the intermediate waves of the double-diffraction process. As a consequence, the transition between the thin and the thick regimes is oscillatory. Although we have not examined higher order readout, we expect this effect to become even more pronounced in such cases. In practical applications and for materials that are not strongly nonlinear, this phase condition indicates the preferred grating parameters to produce a strong second order. For readout at the second BA, the predicted strong grating frequency dependence of DE_2, has been verified experimentally.

The study of strongly-coupled gratings has yielded many interesting discoveries including: the importance of cross coupling,

unexpected differences between the AS results for the different incoherent construction geometries, the DEs may maximize at readout angles different from their BAs, the necessary offset angle to decouple two gratings is almost a factor of two smaller than would be expected and the sum grating in the coherent addition acts to partially decouple the other two gratings. We have shown that the strong cross-coupling in double gratings is a special case of second-order readout where the intermediate dispersion is also zero. For double gratings, the sum and relative values, as well as the individual values, of the diffracted orders' dispersion terms are important. We have determined the angular offset between BAs to decouple the two gratings. At the BA, the decoupling that results from offset is independent of construction type or readout mode. Again, experimental results agree well with the theory.

The analysis of coupled double gratings should be useful in the design of systems for optical data storage in thick materials. Though generally undesired, the phenomenon of cross coupling may be useful for sidelobe suppression. The coherent addition is not weakened by film bias buildup and has an AS that could be useful in beam deflection applications.

The results of the analysis of nonuniformly modulated gratings have shown that significant improvement in the width and uniformity of the angular response can be obtained. In particular, a sinc function modulation profile yields very useful apodization even at high DE levels. We have also noted that one must recognize that apodization may also diminish Bragg suppression of other orders. The grating interferometer offers an interesting method of making gratings with a sinc function profile.

In addition to the new results that we have obtained, we believe that the method of TGD is a useful, physical approach to

understanding optical propagation in periodic holographic structures. Indeed, TGD has been successfully used by others in our laboratory to study guiding in thick gratings (59, 60).

For areas of further research, we recommend construction of apodized gratings in very thick (1 mm) materials , including an attempt to demonstrate the method of incoherent holography mentioned; studies of multiple diffraction phenomenon in reflection gratings and an extended study (most likely numerical) of intermediately thick gratings to determine the tradeoffs between maximum DE and width of the AS.

APPENDIX

GENERAL THREE-WAVE ANALYSIS

In Chapters 3 and 4, we are required to perform

$$\underset{\sim}{A}(N) = \underset{\sim}{H}^{N}\begin{bmatrix}1\\0\\0\end{bmatrix} \qquad \text{A.1}$$

in the limit $N \to \infty, \Delta z \to 0$ such that $N\Delta z = D$, where $\underset{\sim}{H}$ is a 3×3 unitary matrix that describes the coupling between three plane waves over a thin slab of thickness Δz. The form of the coupling matrix depends upon the grating construction and the coupling mechanism that is important for the readout mode of interest. The functional dependence of the phase terms (differential dispersion) also depend upon these factors. To avoid needless mathematical duplication, we perform the above matrix multiplication for the most general 3×3 coupling matrix to find the diffraction efficiency of the two diffracted orders. The results can then be directly applied to second-order readout of single gratings in Chapter 3 and to the incoherently and coherently superimposed gratings described in Chapter 4, by making the appropriate correspondence of terms. We follow the procedure discussed in Chapter 3.

The most general 3×3 coupling matrix can be written as

$$\underset{\sim}{H} = \begin{bmatrix} 1 & i\frac{\delta_1'}{c_1}e^{i\Phi_1} & i\frac{\delta_2'}{c_2}e^{i\Phi_2} \\ i\frac{\delta_1'}{c_o} & e^{i\Phi_1} & i\frac{\delta_3'}{c_2}e^{i\Phi_2} \\ i\frac{\delta_2'}{c_o} & i\frac{\delta_3'}{c_1}e^{i\Phi_1} & e^{i\Phi_2} \end{bmatrix} \qquad \text{A.2}$$

The matrix must be symmetric in amplitude; Φ_1 and Φ_2 are the differential dispersion terms associated with the two diffracted orders. They depend upon the grating frequencies, construction geometry and readout angle. The δ_j' and Φ_j are proportional to Δz, the thin grating thickness. The c_j are the direction cosines of the waves.

To raise the coupling matrix to the N^{th} power, we transform to the diagonal representation. The diagonal elements of the $\underset{\sim}{H}$ in this basis are its eigenvalues σ_j that satisfy the matrix equation

$$\det (\underset{\sim}{H} - \sigma_j \underset{\sim}{I}) = 0 \qquad \text{A.3}$$

We define $\psi_j = -i(1 - \sigma_j)$. The eigenvalues are then $\sigma_j = 1 - i\psi_j \cong e^{-i\psi_j}$. The eigenvalue problem becomes that of finding ψ_j such that

$$\psi_j^3 + p'\psi_j^2 + q'\psi_j + r' = 0 \qquad \text{A.4}$$

where

$$p' = \Phi_1 + \Phi_2 \qquad \text{A.5}$$

$$q' = \Phi_1\Phi_2 - \frac{\delta_2'^2}{c_o c_2} - \frac{\delta_1'^2}{c_o c_1} - \frac{\delta_3'^2}{c_1 c_2} \qquad \text{A.6}$$

$$r' = \frac{2\delta_1'\delta_2'\delta_3'}{c_o c_1 c_2} - \frac{\delta_2'^2\Phi_1}{c_o c_2} - \frac{\delta_1'^2\Phi_2}{c_o c_1} \qquad \text{A.7}$$

We have made a first order expansion of $e^{-i\Phi_j}$ and have kept only first-order terms in Δz.

The solutions of A.4 are

$$\psi_o' = 2\left(-\frac{a'}{3}\right)^{1/2} \cos \Omega' - \frac{p'}{3} \qquad \text{A.8}$$

$$\psi_1' = 2\left(-\frac{a'}{3}\right)^{1/2} \cos\left(\Omega' + \frac{2\pi}{3}\right) - \frac{p'}{3} \qquad \text{A.9}$$

$$\psi_2' = 2\left(\frac{-a'}{3}\right)^{1/2} \cos\left(\Omega' + \frac{4\pi}{3}\right) - \frac{p'}{3} \qquad \text{A.10}$$

where

$$a' = \frac{1}{3}(3q' - p'^2) \qquad \text{A.11}$$

$$b' = \frac{1}{27}(2p'^3 - 9p'q' + 27r') \qquad \text{A.12}$$

$$\Omega' = \cos^{-1}\left[(-b'/2)\Big/\left(-\frac{a'^3}{27}\right)^{1/2}\right]. \qquad \text{A.13}$$

The associated eigenvectors that are the basis vectors in the diagonal representation satisfy the matrix equation

$$(\underset{\sim}{H} - \sigma_j \underset{\sim}{I})E_j = 0. \qquad \text{A.14}$$

They can be written in terms of the original basis vectors as

$$\begin{bmatrix} E_o \\ E_1 \\ E_2 \end{bmatrix} = \begin{bmatrix} 1 & \mu_o & \nu_o \\ 1 & \mu_1 & \nu_1 \\ 1 & \mu_2 & \nu_2 \end{bmatrix} \begin{bmatrix} A_o \\ A_1 \\ A_2 \end{bmatrix} \qquad \text{A.15}$$

where the form of the μ and ν will be given shortly. In the diagonal representation, the matrix multiplication of A.1 is

$$\underset{\sim}{E}(N) = \begin{bmatrix} e^{-iN\psi_o'} \\ e^{-iN\psi_1'} \\ e^{-iN\psi_2'} \end{bmatrix} \qquad \text{A.16}$$

because from A.15, the initial condition in the $\underset{\sim}{E}$ representation is

$$\underset{\sim}{E}(o) = \begin{bmatrix} 1 \\ 1 \\ 1 \end{bmatrix}. \qquad \text{A.17}$$

To find $\underset{\sim}{A}(N)$, we invert A.15. Keeping in mind that $N\Delta z = D$, the emulsion thickness, we define the total grating strengths and differential dispersion terms

$$\gamma_1 = \frac{N\delta_1'}{\sqrt{c_o c_1}} \qquad \text{A.18}$$

$$\gamma_2 = \frac{N\delta_2'}{\sqrt{c_o c_2}} \qquad \text{A.19}$$

$$\gamma_3 = \frac{N\delta_3'}{\sqrt{c_1 c_2}} \qquad \text{A.20}$$

$$\xi_j = \frac{N\Phi_j}{2} \qquad j = 1, 2 \qquad \text{A.21}$$

It is tedious but necessary to also define

$$p = Np' = 2(\xi_1 + \xi_2) \qquad \text{A.22}$$

$$q = Nq' = 4\xi_1\xi_2 - \gamma_1^2 - \gamma_2^2 - \gamma_3^2 \qquad \text{A.23}$$

$$r = Nr' = 2\gamma_1\gamma_2\gamma_3 - 2\gamma_2^2\xi_1 - 2\gamma_1^2\xi_2 \qquad \text{A.24}$$

Unprimed values of a, b, Ω and the ψ_j are then defined in terms of the unprimed p, q and r as before. We then invert A.15 to find $\underset{\sim}{A}(N)$ in terms of $\underset{\sim}{E}(N)$. The second and third components of $\underset{\sim}{A}$ correspond to the amplitudes of the diffracted orders. The diffraction efficiencies of these orders can be written as

$$DE_1 = \frac{1}{R}\Big\{\nu_{12}^2 + \nu_{20}^2 + \nu_{01}^2 + 2\nu_{12}\nu_{20}\cos(\psi_o - \psi_1) + 2\nu_{12}\nu_{01}\cos(\psi_o - \psi_2) + 2\nu_{20}\nu_{01}\cos(\psi_1 - \psi_2)\Big\} \quad \text{A.25}$$

DE_2 = same as A.25 with $\nu_{ij} \rightarrow \mu_{ij}$ A.26

where

$$\nu_{ij} = \nu_i - \nu_j \quad \text{A.27}$$

$$\mu_{ij} = \mu_i - \mu_j \quad \text{A.28}$$

$$R = \mu_o\nu_{12} + \mu_1\nu_{20} + \mu_2\nu_{01} \quad \text{A.29}$$

and

$$\mu_j = -\frac{(\gamma_3\psi_j - \gamma_1\gamma_2)}{\gamma_1\gamma_3 - \gamma_2(\psi_j + 2\xi_1)} \quad \text{A.30}$$

$$\nu_j = \begin{cases} \frac{1}{\gamma_3}\left[-\gamma_1 + \frac{(\psi_j + 2\xi_1)(\gamma_3\psi_j - \gamma_1\gamma_2)}{\gamma_1\gamma_3 - \gamma_2(\psi_j + 2\xi_1)}\right] & \gamma_3 \neq 0 \quad \text{A.31} \\ -\frac{\gamma_2}{(\psi_j + 2\xi_2)} & \gamma_3 = 0 \quad \text{A.32} \end{cases}$$

Special Cases

There are several cases for which the general results above can be considerably simplified.

Incoherent Direct Coupling, with $\Phi_1 = \Phi_2$

This case corresponds to the readout angle for which the dispersion between the zero and each of the first orders is the same (see differential dispersion curves, Figs. 3-1 and 4-3). In this special case, the eigenvalues are simply

$$\psi'_o = -\Phi \qquad \text{A.33}$$

$$\psi'_{1,2} = \frac{-\Phi \pm \left(\Phi^2 + 4\left(\delta'^2_1/c_o c_1 + \delta'^2_2/c_o c_2\right)\right)^{1/2}}{2} \qquad \text{A.34}$$

where $\Phi_1 = \Phi_2 = \Phi$. Note, in fact, that for this special case, there is a singularity in the general expressions for μ_j and ν_j. This is really not a problem. When evaluating the general expressions, we simply avoid this one readout angle. However, we also avoid the problem by expressing the eigenvectors as

$$\begin{bmatrix} E_o \\ E_1 \\ E_2 \end{bmatrix} = \begin{bmatrix} o & 1 & -\frac{\delta'_1}{\delta'_2}\frac{c_2}{c_1} \\ 1 & \mu_1 & \nu_1 \\ 1 & \mu_2 & \nu_2 \end{bmatrix} \begin{bmatrix} A_o \\ A_1 \\ A_2 \end{bmatrix} \qquad \text{A.35}$$

where $\mu_j = \frac{-\delta'_1}{c_o(\psi'_j + \Phi)}$, $\nu_j = \frac{-\delta'_2}{c_o(\psi'_j + \Phi)}$ $j = 1, 2$. Note that the initial condition in the $\underset{\sim}{E}$ basis is $\underset{\sim}{E}(o) = \begin{bmatrix} o \\ 1 \\ 1 \end{bmatrix}$. The expressions for the DEs of the two first orders become

$$DE_j = \frac{\gamma_j^2}{\left(\gamma_1^2 + \gamma_2^2 + \xi^2\right)} \sin^2\left(\gamma_1^2 + \gamma_2^2 + \xi^2\right)^{1/2}, \qquad j = 1, 2 \qquad \text{A.36}$$

The terms are given by Eqs. A.18, A.19 and A.21. In the special case where $\Phi_1 = \Phi_2 = 0$ (this corresponds to readout at the common BA of two gratings made with no offset) this reduces to

$$DE_j = \frac{\gamma_j^2}{\left(\gamma_1^2 + \gamma_2^2\right)} \sin^2 \left(\gamma_1^2 + \gamma_2^2\right)^{1/2}, \qquad j = 1, 2 \qquad \text{A.37}$$

Incoherent Cross Coupling with $\Phi_1 = \Phi_2 = 0$

This special case corresponds to readout at the noncommon BA for two incoherently added gratings with no offset. The eigenvalues become

$$\psi'_o = 0 \qquad \text{A.38}$$

$$\psi'_{1,2} = \pm \left(\delta_3'^2 / c_1 c_2 + \delta_1'^2 / c_o c_1\right)^{1/2} \qquad \text{A.39}$$

The general results of Eqs. A.23 and A.24 then reduce to

$$DE_1 = \frac{\gamma_1^2}{\left(\gamma_1^2 + \gamma_3^2\right)} \sin^2 \left(\gamma_1^2 + \gamma_3^2\right)^{1/2} \qquad \text{A.40}$$

$$DE_2 = \frac{4\gamma_1^2\gamma_3^2}{\left(\gamma_1^2 + \gamma_3^2\right)} \sin^4 \frac{1}{2}\left(\gamma_1^2 + \gamma_3^2\right)^{1/2} \qquad \text{A.41}$$

Coherent, Equal Grating Strengths, $\Phi_1 = \Phi_2 = 0$

This special case corresponds to readout at any of the construction angles of a three grating structure in which each grating has the same modulation (which we could expect to be the case if the construction beams are of equal amplitude). The general results reduce to

$$DE_1 = DE_2 \cong \frac{4}{9} \sin^2 \frac{3}{2}\gamma \qquad \text{A.42}$$

where $\gamma = \pi n_1/\lambda \cos \theta_o$ and we assume for simplification that, with respect to the grating strength parameters, $\cos \theta_o = \cos \theta_1 = \cos \theta_2$.

REFERENCES

1. E.N. Leith and J. Upatnieks, J. Opt. Soc. Am. 52, 1123 (1962).
2. E.N. Leith and J. Upatnieks, J. Opt. Soc. Am. 53, 1377 (1963).
3. E.N. Leith and J. Upatnieks, J. Opt. Soc. Am. 54, 1295 (1964).
4. T.A. Shankoff, Appl. Opt. 7, 2101 (1968).
5. R.K. Curran and T.A. Shankoff, Appl. Opt. 9, 1651 (1970).
6. L.H. Lin, Appl. Opt. 8, 963 (1969).
7. W.S. Colburn and K.A. Haines, Appl. Opt. 10, 1636 (1971).
8. B.L. Booth, Appl. Opt. 11, 2994 (1972).
9. B.L. Booth, Appl. Opt. 14, 593 (1975).
10. J.J. Amodei and D.L. Staebler, RCA Review 33, 71 (1972).
11. J. Upatnieks and C. Leonard, Appl. Opt. 8, 85 (1969).
12. J. Upatnieks and C. Leonard, IBM J. Res. Devel. 24, 527 (1970).
13. H. Kogelnik, Bell Syst. Tech. J. 48, 2909 (1969).
14. R. Alferness, Appl. Phys. 7, 29 (1975).
15. R. Alferness and S.K. Case, J. Opt. Soc. Am. 65, 730 (1975).
16. E.N. Leith, A. Kozma, J. Upatnieks, J. Marks and N. Massey, Appl. Opt. 5, 1303 (1966).
17. C.B. Burckhardt, J. Opt. Soc. Am. 56, 1502 (1966).
18. M. Bergstein and D. Kermisch, Proceedings of Symposium on Modern Optics, (Brooklyn Poly. Press, New York, 1967), 655.
19. M. Chang and N. George, Appl. Opt. 9, 713 (1970).
20. F.G. Kaspar, J. Opt. Soc. Am. 63, 37 (1973).
21. A.A. Friesem, "Three Dimensional Recording Media in Holography," Ph.D. thesis (University of Michigan, 1968).
22. W.H. Zachariasen, Theory of X-Ray Diffraction in Crystals (Wiley, New York, 1945).
23. B. Batterman and H. Cole, Rev. Mod. Phys. 36, 681 (1964).
24. M. Born and E. Wolf, Principles of Optics (2nd ed., Pergamon Press, New York, 1964), Chapter 12.

25. Edward J. Saccocio, J. Appl. Phys. 38, 3994 (1967).

26. E.N. Leith and B.J. Chang, Appl. Opt. 3, 1957 (1973).

27. B.J. Chang, R. Alferness and E.N. Leith, Appl. Opt. 14, 1592 (1975).

28. R.G. Zech, Ph.D. thesis (University of Michigan, 1974); Univ. Microfilms order No. 74-25-369.

29. J.W. Goodman, Introduction to Fourier Optics (McGraw-Hill, New York, 1968), p. 49.

30. Ibid., p. 54.

31. G.L. Fillmore and R.F. Tynan, J. Opt. Soc. Am. 61, 199 (1971).

32. S.K. Case and R. Alferness, Appl. Phys. 10, 41 (1976).

33. A. Yariv, Introduction to Optical Electronics (Holt, Rinehart and Winston, Inc., 1971), p. 189.

34. R. Alferness, Opt. Commun. 15, 209 (1975).

35. W.J. Tomlinson, E.A. Chandross, H.P. Weber and G.D. Aumiller, Appl. Opt. 15, 534 (1976).

36. R. Alferness, J. Opt. Soc. Am., 66, 353 (1976).

37. A. Kozma, G.W. Jull and K.O. Hill, Appl. Opt. 9, 721 (1970).

38. R.A. Baugh, Ph.D. thesis (Stanford University, 1969); Univ. Microfilms order No. 70-10-422.

39. S.F. Su and T.K. Gaylord, J. Opt. Soc. Am. 65, 59 (1975).

40. W.S. Colburn, R.G. Zech and L.M. Ralston, Holographic Optical Elements, Tech. Rep. AFAL-TR-72-409 (1973).

41. M. Chang, Appl. Opt. 10, 2550 (1971).

42. A more accurate value can be found by including the second order (at the first Bragg angle) and using the general results of the Appendix.

43. P.J. van Heerden, Appl. Opt. 2, 393 (1963).

44. K.S. Pennington and L.H. Lin, Appl. Phys. Letts. 7, 56 (1965).

45. E.N. Leith and J. Upatnieks, J. Opt. Soc. Am. 57, 699 (1967).

46. D. Meyerhofer, RCA Review 33, 111 (1972).

47. S.K. Case, J. Opt. Soc. Am. 65, 724 (1975).

48. S.K. Case, Ph.D thesis (University of Michigan, 1976).

49. B.J. Chang, private communication.

50. M.G. Cohen and E.I. Gordon, Bell Syst. Tech. J. 44, 693 (1965).

51. D. Kermisch, J. Opt. Soc. Am. 59, 1409 (1969).

52. N. Uchida, J. Opt. Soc. Am. 63, 280 (1973).

53. H. Kogelnik, Bell Syst. Tech. J. 55, 109 (1976).

54. D.C. Flanders, H. Kogelnik, R.V. Schmidt and C.V. Shank, Appl. Phys. Letts. 24, 194 (1974).

55. B.J. Chang, Ph.D. thesis (The University of Michigan, 1974).

56. Born and Wolf, p. 521.

57. E.N. Leith, R. Alferness and S. Case, Opt. Commun. 11, 204 (1974).

58. R. Alferness, Opt. Commun. 12, 152 (1974).

59. E.N. Leith, G. Kung, R. Alferness and B. Hansche, Opt. Commun. 14, 229 (1975).

60. G. Kung and E.N. Leith, Appl. Opt. 14, 2614 (1975).